HSV-1- and MVA-mediated NLRP1 inflammasome inhibition

Dissertation der Fakultät für Biologie

der Ludwig-Maximilians-Universität München

Inga Szymańska

München, 2023

Diese Dissertation wurde angefertigt
unter der Leitung von Prof. Dr. Veit Hornung
am Genzentrum
der Ludwig-Maximilians-Universität München

Ersgutachter/in:	Prof. Dr. Heinrich Leonhardt
Zweitgutachter/in:	Prof. Dr. Veit Hornung
Tag der Abgabe:	04.12.2023
Tag der mündlichen Prüfung:	02.05.2024

EIDESSTATTLICHE RKLÄRUNG

Ich versichere hier mit an Eides statt, dass meine Dissertation selbständig und ohne unerlaubte Hilfsmittel angefertigt worden ist.
Die vorliegende Dissertation wurde weder ganz noch teilweise einer anderen Prüfungskommission vorgelegt.
Ich habe noch zu keinem früheren Zeitpunkt versucht, eine Dissertation einzureichen oder an einer Doktorprüfung teilzunehmen.

München, den 23.11.2023

Inga Szymańska

Table of Contents

1. Introduction

1.1 The immune system

Humans encounter multiple microorganisms throughout their lifetime. Many are harmless or form a commensal bond with the host, colonizing the skin or the gut. Harmful microorganisms, on the other hand, can disturb homeostasis and cause damage to the host; such organisms include pathogenic bacteria, fungi, viruses, and parasites, and the human immune system has evolved to detect and clear them. To do this effectively, it has to distinguish self and innocuous microorganisms from harmful pathogens (1).

The immune system consists of two branches: innate and adaptive. Innate immunity is initiated within minutes after a pathogen encounter and is unspecific. It includes anatomical barriers, such as skin, and physiological barriers, such as pH, complement system, and innate immune cells (2). Those cells recognize conserved pathogen-associated molecular patterns (PAMPs) via a repertoire of germline-encoded pattern recognition receptors (PRRs); this allows the recognition of a wide array of pathogens with a limited number of receptors (1,2). Examples of PAMPs include lipopolysaccharide (LPS), which is a part of the membrane of Gram-negative bacteria, or lipoteichoic acid (LTA), a part of the cell wall of Gram-positive bacteria (2,3). In addition, PRRs can detect molecules released by cells in response to stress or damage called damage-associated molecular patterns (DAMPs); examples include ATP or the nuclear protein HMGB1 (4). The cells of the adaptive branch of the immune system include T-cells and B-cells. Unlike the innate cells, they express a diverse repertoire of antigen-specific receptors termed T- and B-cell receptors (TCRs and BCRs, respectively). Those receptors are not germline-encoded but generated in the process of random recombination of DNA segments that encode the antigen-binding site of the receptor. Adaptive immune response develops

longer than the innate, over several days or weeks; however, it establishes memory, which allows a faster response upon repeated pathogen encounters (2,5).

Most immune cells develop in the bone marrow from common myeloid or lymphoid progenitors. The common myeloid progenitor gives rise to the cells of the innate immune system, which include granulocytes (neutrophils, eosinophils, and basophils), mast cells, monocytes, and macrophages (1). Some tissue-resident macrophages, such as microglia or Kupffer cells, are generated from the yolk sack during embryonic development, while others derive from monocytes circulating in the blood (1). The common lymphoid progenitor gives rise to the cells of the adaptive immune system, T-and B-cells, and the innate immune system, including innate lymphoid cells and natural killer (NK) cells (1). Dendritic cells (DCs), which link the innate and adaptive immune responses, originate from myeloid and lymphoid lineages (1,6).

1.2 The immune response

Anatomical barriers, such as skin, gut, and lung epithelia, are the first line of defense against pathogens (2). Epithelial cells form a tight barrier that prevents microbes from penetrating. In addition, the low pH of the skin and competing microbiome slows down pathogen growth. Mucosal membranes, such as in the airways, clear pathogens by trapping them in mucus and expelling them using cilia (2). Furthermore, epithelial cells express PRRs and secrete cytokines and antimicrobial peptides to alert other epithelial and immune cells and kill invading microbes (7,8).

Immune cells, primarily macrophages, detect pathogens that overcome the anatomical barriers. Upon pathogen encounter, macrophages become activated and secrete cytokines to alert other immune cells, stimulate their division, and upregulate the expression of adhesion molecules on immune and epithelial cells to facilitate cell recruitment (5). The first cells to arrive at the site of infection are neutrophils, a subset of granulocytes that are very efficient in pathogen phagocytosis and killing (5). Like all granulocytes, neutrophils have cytoplasmic granules containing toxic proteins and enzymes, which they fuse with phagosomes, killing the phagocytosed pathogens (5).

Eosinophils, another subset of granulocytes, play a role in immunity against parasites, which are too large for phagocytosis. Instead, eosinophils bind to the pathogen and release their granules on its surface (1,5). NK cells are critical in antitumor and antiviral immunity; they recognize cancer and virus-infected cells and induce their apoptosis by releasing perforins and granzymes (5). Another immune mechanism against pathogens is the complement system; it consists of serum proteins activated in a cascade, leading to the formation of a membrane attack complex and pathogen lysis. Furthermore, the complement can opsonize pathogens to increase the efficiency of phagocytosis (1,5).

Another type of immune cell recruited to the site of infection are DCs, antigen-presenting cells (APCs) that initiate the adaptive immune response (2,5). DCs phagocytose pathogens, degrade them, and display pathogen-derived peptides on the MHC receptors, presented to antigen-specific T-cells. There are two classes of MHC receptors: class I, expressed by all nucleated cells, and class II, expressed by APCs (2,5). MHC I receptors present peptides derived from proteins that are endogenously expressed, e.g., in virus-infected or cancer cells. MHC II receptors present exogenous peptides derived from phagocytosed and processed material (5). For effective activation of T cells, DCs need to be activated by stimulation of PRRs or by inflammatory mediators produced by other cells, which leads to upregulation of co-stimulatory molecules (1). This mechanism prevents innocuous molecules from inducing an immune response. DCs are known as ‘professional APCs’ as they express high amounts of co-stimulatory molecules and are the most efficient inducers of adaptive immune response. Activated DCs migrate to lymph nodes, looking for antigen-specific T-cells (1,2).

T-cells can reside in the lymph nodes or circulate in the bloodstream and lymphatic system, which increases the chances of antigen encounter (5). There are two principal populations of T-cells, depending on the expression of the surface markers, CD8 or CD4. CD8+ T-cells, also known as cytotoxic T-cells, recognize antigens bound to MHC I molecules. They play a role in the immune response against viral infections and cancer (5). CD4+ T-cells, known as T helper (Th) cells, recognize antigens displayed on MHC II molecules; they orchestrate the immune response and activate B-cells (5). Encounter

with an APC carrying a specific antigen leads to Th cell proliferation and differentiation into different subsets, depending on the cytokine milieu (2,5).

B-cells are responsible for antibody-mediated immunity; upon encountering the antigen, they differentiate into antibody-secreting plasma cells (5). This response can be independent of T-cells or T-cell-dependent when the antigen recognized by the surface BCR is internalized, loaded onto an MHC molecule, and presented to an antigen-specific T-cell (5). Upon antigen recognition, the T-cell induces B-cell proliferation and differentiation into a plasma cell (1,5). Antibodies secreted by plasma cells serve several functions: they opsonize pathogens, which facilitates their phagocytosis and complement recruitment, and neutralize toxins and viruses (2). After clearing the infection, most activated lymphocytes die, but some remain as memory cells, which initiate the response more rapidly upon subsequent antigen encounters (2).

1.3 The innate immune system

Innate immune cells and certain non-immune cells, such as epithelial cells (e.g., keratinocytes) or fibroblasts, detect pathogens using PRRs and are crucial at the early stages of infection. PRR activation causes the release of cytokines, chemokines, type I interferons (IFNs), and antimicrobial peptides, resulting in inflammation, which manifests in redness, swelling, heat, and pain (9–11). Those signs are caused by increased vascular permeability, which leads to the leakage of plasma and increased recruitment of immune cells (10,11).

1.3.1 Pattern recognition receptors

The term pattern recognition receptor (PRR) was first coined by Charles Janaway (12). Based on the observation that efficient T cell priming and activation required an adjuvant, he suggested that immune cells encode receptors that play a role in the discrimination of self from non-self. He proposed that those receptors, named PRRs, are evolutionarily conserved and present in organisms with primitive immune systems that do not have antigen-specific cells. Janeway postulated that PRRs are activated by pathogen-associated molecular patterns (PAMPs), which he defined as molecules that

are shared by many pathogens, are not present in the host, and are a product of complex processes that would require multiple mutations to alter. He further suggested that activation of PRRs is critical for T cell activation, which prevents the generation of specific immune responses against innocuous peptides. As an example of PAMP, he proposed lipopolysaccharide (LPS), a membrane component of Gram-negative bacteria. LPS fulfills Janeway's criteria for PAMPs: it is shared by a large group of bacteria, is not produced by human cells, and cannot be easily modified as its synthesis is a multi-step process (13). Toll-like receptors (TLRs) were the first receptors to have the characteristics of PRRs described by Janaway (14). The Toll receptor was identified in Drosophila as crucial for anti-fungal immune responses (15). Subsequently, Medzhitov et al. identified a human Toll homolog as a receptor that can drive NF-kB activation and, thus, co-stimulatory molecule expression (16). Finally, Bruce Beutler's group uncovered that LPS detection is governed by a gene locus that encodes for murine Toll-like receptor 4 (17). Together, these lines of investigation established TLRs as members of the previously postulated PRR system. Today, ten members of the human TLR family are known (14). Other PRR families include RIG-I-like receptors (RLRs), NOD-like receptors (NLRs), C-type lectin receptors (CLRs), AIM2-like receptors (ALRs), and cGAS-STING axis (3,18). In most cases, PRR activation leads to transcriptional upregulation of genes involved in immune response, driven by three major transcription factors: NF-kB, AP-1, and IRF (14). A subset of PRRs does not cause the activation of transcription factors but triggers the assembly of a protein complex called the inflammasome. Activation of an inflammasome leads to maturation and release of pro-inflammatory cytokines, such as IL-1β and IL-18, and in most cases also to pyroptotic cell death (Broz & Dixit, 2016).

TLRs are transmembrane proteins residing on the cell surface or inside endosomes. The cell surface TLRs are primarily responsible for sensing components of bacterial cells, whereas endosomal TLRs detect nucleic acids (14). TLRs residing on the cell surface include TLR1, 2, 4, 5, and 6. TLR2 forms a heterodimer either with TLR1 to detect triacylated lipoproteins or with TLR6 to detect diacylated lipoproteins. TLR4 recognizes LPS, and TLR5 senses flagellin (14). Endosomal TLRs include TLR3, 7, 8, and 9. TLR3 is activated by double-stranded RNA (dsRNA), TLR7 and TLR8 by degradation products of single-stranded RNA (ssRNA), and TLR9 by non-methylated CpG-rich DNA (14,20). The

ligand for TLR10 has not been identified (14). Upon activation, TLRs dimerize and engage downstream signaling pathways, culminating in activation of the previously-mentioned transcription factors. Most TLRs signal through the adaptor protein MyD88, leading to the recruitment and activation of IRAK kinases and TRAF6, an E3 ubiquitin ligase; this triggers the activation of TBK1 and IKK kinases and induction of NF-kB and AP-1 transcription factors (14,21). TLR3 is an exception and signals through the adaptor protein TRIF, whereas TLR4 signals through TRIF and MyD88. TRIF-dependent signaling also activates the kinase TBK1, as well as NF-kB and AP-1 transcription factors (14). In addition, TRIF induces the transcription factor IRF3 (14). A group of endosomal TLRs, TLR7-9, also activates the adaptor molecule TASL, which is responsible for the activation of IRF5, another member of the IRF transcription factor family (22). CLRs are transmembrane receptors expressed at the cell surface that bind carbohydrates, for example, fungal β-glucan. Examples of CLR family members include dectin-1 and dectin-2 (21); activation of these receptors leads to NF-kB induction (23).

RLRs are cytoplasmic receptors responsible for sensing dsRNA produced, for example, during viral infections (24). This family consists of RIG-I and MDA5 receptors, which signal through the mitochondrial-antiviral signaling protein (MAVS); the third family member, LGP2, is thought to regulate the other RLRs (24). Upon ligand binding, RIG-I and MDA5 oligomerize and interact with MAVS localized at the mitochondria; the signaling cascade leads to TBK1 activation and induction of NF-kB, AP-1, and IRF3 transcription factors. (24).

NLRs are another family of cytoplasmic receptors that detect numerous stimuli. Its members include NOD1 and NOD2 receptors, which sense the components of bacterial cells, and inflammasome-forming proteins, such as NLRP3, described in more detail in the following sections (21,25). NOD1 and NOD2 both recognize peptidoglycan, a cell wall component of most bacteria; NOD1 detects γ-D-glutamyl-mesodiaminopimelic acid, and NOD2 phosphorylated muramyl dipeptide (21,26). Ligand binding causes receptor oligomerization and activation of a signaling cascade, leading to NF-kB and AP-1 activation (27).

cGAS-STING axis is responsible for immune response to cytoplasmic dsDNA (18,28). Upon binding dsDNA, the protein cyclic GMP-AMP synthase (cGAS) produces the second messenger molecule, cyclic GMP-AMP (cGAMP); this molecule is sensed by STING localized at the endoplasmic reticulum (ER) (28). cGAMP binding causes STING oligomerization and translocation to Golgi (28). Similarly to MAVS and TRIF, STING activates the kinase TBK1 and the transcription factor IRF3. In addition, NF-kB and MAPK pathways are activated (28). Cytoplasmic dsDNA is also detected by a member of the ALR family, AIM2, an inflammasome-forming sensor, described in more detail in the following sections.

1.3.2 Effects of PRR activation

The response mediated by different PRRs depends on which transcription factor is activated in the downstream signaling pathway. NF-kB and AP-1 activate the expression of chemokines and pro-inflammatory cytokines such as TNFα, IL-1β, or IL-6. Locally, those cytokines induce T-cell differentiation, activate B-cells, and increase vascular permeability (1,29,30). TNFα can cause necroptosis, a form of programmed cell death, which leads to the release of DAMPs and further exacerbates inflammation (31). The IRF family of transcription factors primarily drives the expression and secretion of type I interferons involved in antiviral response (21). Activation of the interferon receptor induces the expression of proteins that interfere with different stages of viral infection; examples include oligoadenylate synthase (OAS), RNase L, and protein kinase R (PKR), which inhibit viral protein expression. PKR is a dsRNA-dependent protein kinase; it phosphorylates the eukaryotic translation initiation factor 2 (eIF2α), suppressing translation (32). OAS also detects dsRNA and, in response, produces 2'-5'-linked oligoadenylates, which activate RNase L (18). Active RNase L, in turn, degrades cytoplasmic RNA (18).

1.4 Inflammasome signaling

Inflammasome is a cytosolic complex composed of a sensor molecule, adaptor protein ASC, and caspase-1. The subset of PRRs that form an inflammasome includes members of the NLR family (e.g., NLRP1 and NLRP3), AIM2, CARD8, and pyrin (19,33). Some

inflammasome receptors, like NAIP-NLRC4, bind their ligand directly; others, like NLRP3, sense perturbations in cell homeostasis caused by a pathogen. Upon stimulus sensing, the receptor molecule oligomerizes and - in most cases - recruits ASC, which forms filaments; subsequent recruitment of caspase-1 results in its proximity-induced cleavage and activation (19). Active caspase-1 matures the pro-inflammatory cytokines - IL-1β and IL-18 - and cleaves the protein GSDMD (Fig. 1.1). The N-terminal fragment of GSDMD forms pores at the cell membrane, leading to pyroptosis, a form of programmed cell death (19).

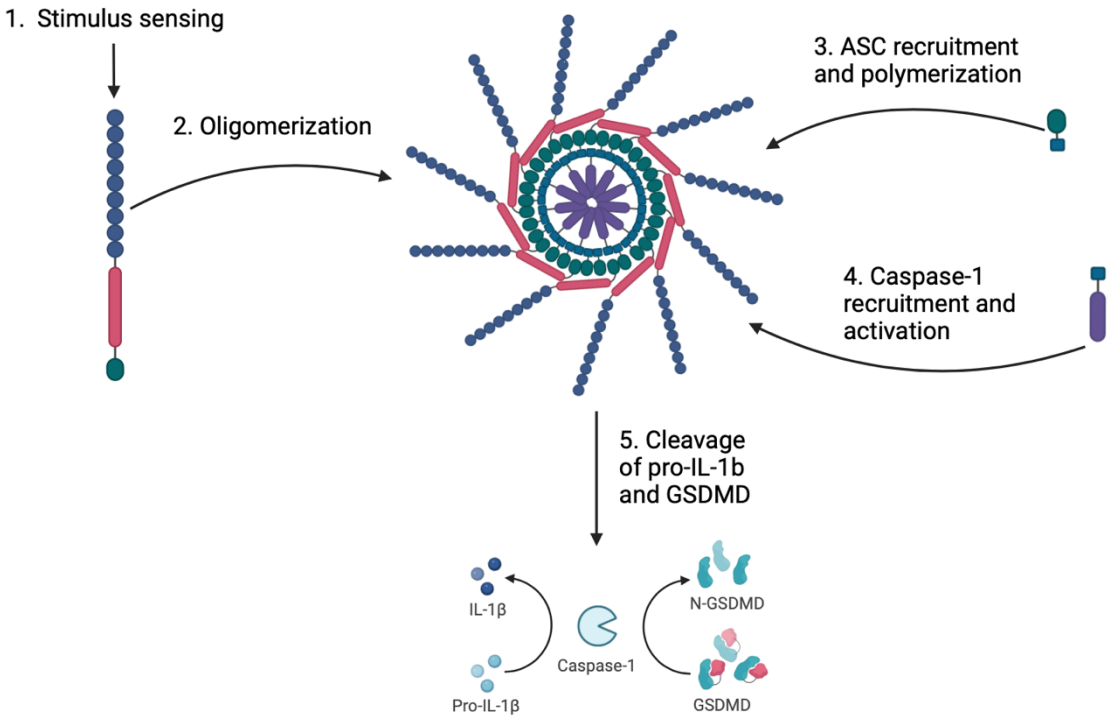

Fig. 1.1 An overview of inflammasome signaling. Upon stimulus sensing (1) the sensor molecule oligomerizes (2) and recruits ASC, which polymerizes (3). Caspase-1 is recruited to ASC filaments and activated (4). Active caspase-1 matures IL-1β and cleaves GSDMD (5).

1.4.1 Inflammasome sensors

NLRP1, a member of the NLR family, was the first sensor molecule reported to form inflammasome and cleave caspase-1 and IL-1β *in vitro* (34). Its ligands remained unknown for a long time, and today it is known to be activated by multiple stimuli, including inhibition of dipeptidyl peptidase 9 (DPP9), viral proteases, double-stranded RNA, and ribotoxic stress response (35,36). NLRP3 is another member of the NLR family

that forms an inflammasome. Similarly to NLRP1, it responds to multiple activators, including the ionophore Nigericin, ATP, particulate matter such as silica, and small molecules targeting mitochondria, imiquimod, and CL097 (19,37). Most of those stimuli induce potassium efflux from the cells (38). Mechanistically, potassium efflux and other NLRP3-activating stimuli cause the *trans*-Golgi network (TGN) dispersal and recruitment of NLRP3 to dispersed TGN (39). In addition, activation of NLRP3 inflammasome requires a priming step. Priming involves the activation of other PRRs or cytokine receptors and is thought to serve two functions: transcriptional upregulation and induction of post-translational modification of NLRP3 (40). NAIP-NLRC4 inflammasome is triggered by components of bacterial cells. NAIP binds ligands directly and initiates oligomerization of NLRC4 and inflammasome assembly. The mouse genome encodes several NAIP proteins, each sensing a different ligand. NAIP1 and NAIP2 detect needle and rod subunit of type 3 secretion system (T3SS), respectively, and NAIP5 and NAIP6 detect flagellin (41,42). The human genome encodes only one functional NAIP protein; it recognizes all of the mentioned stimuli (43). CARD8 inflammasome is activated by inhibition of DPP9 and cleavage by viral proteases (33,44). AIM2 inflammasome detects dsDNA released into the cytosol during infection with bacteria such as *Francisella tularensis* and *Listeria monocytogenes* or viruses such as Vaccinia virus (19,45). Upon dsDNA binding to its HIN200 domain, AIM2 engages ASC via the pyrin domain, leading to inflammasome assembly (19,45). Pyrin inflammasome is activated by blocking Rho GTPase by bacterial toxins, such as TcdB produced by *Clostridium difficile* (46). NLRP6 forms an ASC-dependent inflammasome in response to multiple PAMPs, including LPS, LTA, and dsRNA (47).

In addition, there were reports of other less well-studied members of the NLR family forming an inflammasome. NLRP7 was published to assemble an inflammasome upon lipopeptide recognition and to be a negative regulator of inflammasome activation (48). NLRP10 is expressed by differentiated keratinocytes and is activated by compounds that induce mitochondrial damage; however, the mechanism or relevance in defense against pathogens is unknown (49).

Inflammasomes are critical in pathogen clearance, but aberrant activation can lead to excessive inflammation and auto-inflammatory diseases. Multiple mutations of different inflammasome sensors are known to cause genetic disorders. For example, mutations in NLRP3 cause familial cold autoinflammatory syndrome and Muckle-Wells syndrome (50), mutations in pyrin cause Familial Mediterranean Fever syndrome (51), and mutations in NLRP1 cause skin disorders (52).

1.4.2 Caspase-1 recruitment and activation

Caspases are a family of cysteine proteases subdivided into three main groups: inflammatory, apoptotic initiator, and apoptotic effector caspases (53). Caspase-1, -4, and -5 belong to the inflammatory caspases. The initiator group includes caspase-8, -9, and -10, and the apoptotic effector group caspase-3, -6, and -7. Additionally, the human genome encodes caspase-2 and -14, whose functions are not well defined, and caspase-12, expressed by a small portion of the human population (53). Caspases consist of an N-terminal caspase recruitment domain (CARD) or death effector domain (DED) and a C-terminal catalytic domain (53). The catalytic domain includes a large and a small subunit called p20 and p10, respectively. Caspases are expressed as inactive zymogens and require activation, usually by cleavage. The inflammatory and apoptotic initiator caspases undergo proximity-induced autocleavage, whereas the apoptotic effector caspases are cleaved by initiator caspases. An active caspase forms a heterotetramer consisting of two p10 and two p20 subunits (53).

Inflammasome sensor molecule oligomerization causes caspase-1 recruitment to the inflammasome complex; in most cases, this complex also contains the adaptor protein ASC (apoptosis-associated speck-like protein containing CARD), which consists of a pyrin domain (PYD) and a CARD (19). Most inflammasome sensors have an N-terminal PYD, which interacts with the PYD of ASC (19). Upon recruitment to the sensor molecule, ASC polymerizes and forms PYD filaments with the CARD on the outside. Caspase-1 contains an N-terminal CARD, which is recruited to the CARD of ASC, leading to the formation of caspase-1 filaments (54). This results in proximity-induced activation of caspase-1, which involves cleavage of the linker regions between p20 and p10 and CARD and p20 (53,55). The catalytic subunits - p10 and p20 - form an active heterotetramer, which

matures the pro-inflammatory cytokines IL-1β and IL-18 (53,55). It also cleaves the pore-forming protein GSDMD, which leads to pyroptosis. (53,56). In addition, caspase-1 cleaves the apoptotic effector caspases, caspase-3 and -7 (57).

Several inflammasome sensors engage ASC via CARD instead of PYD. One example is NLRC4, which contains an N-terminal CARD. Usually, the NLRC4 inflammasome uses ASC, but it can also recruit and activate caspase-1 directly. This mode of activation results in cell death; however, the cytokine cleavage is less efficient (58,59). Human NLRP1 also recruits ASC via CARD-CARD interaction, yet it is unable to activate caspase-1 in the absence of ASC (60); this contrasts with murine Nlrp1b, which can form an inflammasome both with and without ASC (58). CARD8 protein also contains a CARD, but it does not engage ASC. Instead, it activates caspase-1 directly, usually resulting in cell death without IL-1β release (61). Initially, direct recruitment of caspase-1 to the inflammasome was thought to not result in caspase-1 cleavage; however, a recent report demonstrated that murine Nlrp1b and CARD8 lead to caspase-1 processing, although at lower levels than when mediated by ASC (62).

1.4.3 GSDMD and pyroptosis

In most cases, inflammasome activation results in pyroptosis, a pro-inflammatory form of cell death mediated by the protein GSDMD (56). GSDMD consists of N- and C-terminal fragments separated by a linker region. The N-terminal fragment can form pores at the cell membrane; it binds to phosphoinositides found on the inner leaflet of the plasma membrane but does not bind to the outer leaflet. Consequently, the pores form only on the inside of a cell (63). Under homeostatic conditions, the binding of the C-terminal fragment prevents the N-terminus from forming pores. Active caspase-1 cleaves the linker region at Asp275, releasing the inhibition (56,64). In addition, caspase-3, activated by caspase-1, can cleave GSDMD at Asp87; this cleavage generates an N-terminal fragment unable to form pores, thus preventing pyroptosis (57).

One of the functions of GSDMD pores is cytokine release; mature IL-1β can pass through the pores before pyroptosis induction (65,66). Over time, the formation of GSDMD pores leads to membrane ballooning and rupture. This loss of membrane integrity may

not be a passive event and was reported to be dependent on the protein NINJ1 (67). While living cells can release IL-1β, as in the case of the alternative inflammasome, pyroptosis leads to the release of other molecules, including HMGB1, lactate dehydrogenase (LDH), IL-1α or ATP (53,68).

1.4.4 Interleukin-1β and interleukin-18

Interleukin-1β (IL-1β), IL-18, and IL-1α belong to the interleukin-1 family of cytokines. IL-1 was the first discovered interleukin. It was initially called leukocytic pyrogen as it was secreted by monocytes after infection with *Staphylococci* and could induce fever in rabbits (69). Today, it is known to play a role in inflammation and exhibit a pleiotropic effect on multiple organs. Aberrant IL-1β release contributes to the pathogenesis of many autoinflammatory diseases and cancer (30).

IL-1β is expressed primarily by hematopoietic cells upon stimulation of PRRs or cytokine receptors, such as the TNFα receptor or IL-1 receptor (30); human keratinocytes express it constitutively (70). IL-1β is expressed in an inactive form as pro-IL-1β and requires maturation by cleavage, which generates an active 17 kDa fragment. The cleavage is usually performed by caspase-1 following inflammasome assembly (71). IL-1β has no signal peptide and does not follow the conventional Golgi-dependent secretion route (71); instead, GSDMD mediates its release during inflammasome activation (56,65).

IL-1β signals through cell surface receptor IL1-R1, which, in turn, recruits the co-receptor IL-1R3. Dimerization of the two receptors brings two intracellular TIR domains closer, activating the NF-kB transcription factor via the MyD88-dependent pathway (30). IL-1β has multiple effects on both local and systemic levels. It is a known pyrogen that induces fever by activating the hypothalamus-pituitary-adrenal axis (72). It increases the release of prostaglandin E2 (PGE2), activating the sympathetic nervous system and inducing noradrenaline secretion. Noradrenaline raises the body temperature by increasing brown fat metabolism, which produces heat, and vasoconstriction, which prevents heat loss (72). The beneficial effects of fever include reduction of replication of pathogens and increased neutrophil recruitment and activation (72). IL-1β also contributes to acute phase response in the liver and induction

of expression of acute phase proteins (APPs). An example of APP is C-reactive protein (CRP), which binds to bacterial and fungal cell walls and activates the complement cascade (1). Locally, IL-1β leads to the upregulation of adhesion molecules and chemokines on the surface of epithelial cells, which enhances leukocyte infiltration (30). In addition, IL-1 increases the lifespan of macrophages and neutrophils and contributes, in conjunction with IL-23, to the polarization of T-cells and innate lymphoid cells into IL-17 and IL-22-producing cells (30).

IL-18, similarly to IL-1β, is expressed as an inactive precursor and requires processing by caspase-1 into an active 17 kDa molecule; in contrast to IL-1β, its expression is constitutive (71). IL-18 binds to the receptor IL-1R5, which forms a complex with the co-receptor IL-1R7, activating the NF-kB pathway via MyD88. In the presence of IL-15 or IL-12, which induce IL-1R7 expression, IL-18 promotes IFNγ production by T-cells, NK cells, and innate lymphoid cells; because of that, initially, it was known as IFNγ-inducing factor (30). IL-18 also contributes to Th1 differentiation in conjunction with IL-12 (73). Additionally, it shares some of the effects of IL-1β, such as induction of adhesion molecules and chemokines expression (71).

Because of its contribution to disease pathology, treatments of certain inflammatory diseases target the IL-1β signaling pathway. An example of such a drug is Anakinra, a recombinant IL-1 receptor antagonist (IL-1Ra) that mimics the endogenous IL-1Ra and blocks the IL-1β receptor (74). Another example is Canakinumab, a monoclonal antibody against IL-1β, found to reduce inflammation and cardiovascular events in patients with atherosclerotic disease in the CANTOS trial (75). In addition, patients treated with Canakinumab for atherosclerosis had a lower incidence of lung cancer, underlining the role of IL-1β and inflammation in carcinogenesis (76).

1.5 The NLRP1 inflammasome

Although NLRP1 is expressed by humans and mice, there are considerable differences in the expression pattern, structure, and activation mechanism. In humans, NLRP1 is mainly expressed by epithelial cells, such as keratinocytes or lung epithelia, whereas

murine Nlrp1b is expressed by macrophages (52). Humans only have one NLRP1 protein, whereas mice have several paralogs. In the commonly used inbred mouse strain C57BL/6, three Nlrp1 paralogs have been characterized: Nlrp1a, Nlrp1b, and Nlrp1c (19,77). In other mouse strains, Nlrp1d, Nlrp1e, and Nlrp1f were identified (35,78). In addition to the paralog variety, Nlrp1b is highly polymorphic, and only certain alleles were shown to form an inflammasome (35,79). Human NLRP1 consists of an N-terminal PYD domain, followed by a disordered region, NACHT, LRR, FIIND, and a C-terminal CARD (Fig. 1.2, Zhong et al., 2016); murine Nlrp1b has a similar domain architecture but lacks the N-terminal PYD (Fig. 1.2, Sandstrom et al., 2019). Both human NLRP1 and murine Nlrp1b undergo constitutive autocleavage at the FIIND domain, which contains two subdomains, ZU5 and UPA; the cleavage generates an N-terminal (NT) fragment consisting of PYD, NACHT, LRR, and ZU5 and a C-terminal (CT) fragment composed of UPA and CARD (81); this processing is necessary for NLRP1-mediated IL-1β maturation, although the two termini remain non-covalently associated (80,82,83). The PYD of human NLRP1 was initially thought to be inhibitory, as mutations in PYD and LRR cause constitutive NLRP1 activation (52); however, replacing PYD with a fluorescent protein does not activate the inflammasome, so the more likely function of PYD is the stabilization of the N-terminal fragment (Robinson et al., 2022).

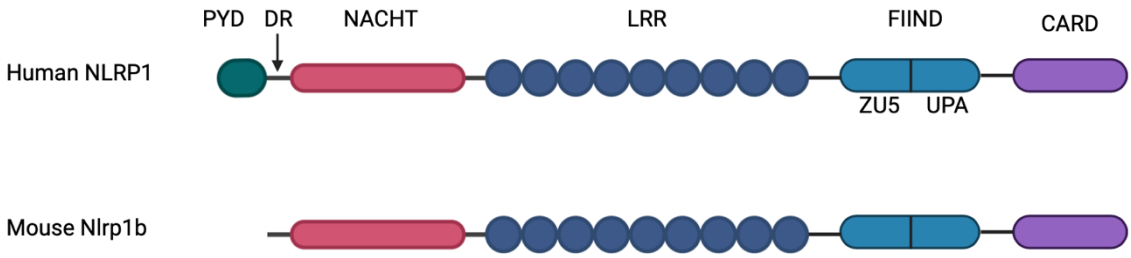

Fig. 1.2 Domain organization of human NLRP1 and mouse Nlrp1b (adapted from (35)).

The NLRP1 inflammasome assembly is mediated by the UPA-CARD of the CT fragment. There are two proposed mechanisms of CT oligomerization; one is that it forms a helical filament composed of CARD dimers, where one molecule forms a core, and the other forms the outer layer with flexibly linked UPA likely forming oligomers on the outside

(Hollingsworth et al., 2021); the other theory is that the filament consists of a CARD core and UPA rings on the outside (85). While CARD can form filaments and recruit ASC by itself, the UPA domain enhances this process. The CARD of NLRP1 interacts with the CARD of ASC but not that of caspase-1, which may be the reason why, in contrast to NLRC4 inflammasome, ASC is necessary for both NLRP1-mediated pyroptosis and IL-1β processing (85).

NLRP1 mutations cause two skin disorders: multiple self-healing palmoplantar carcinoma and familial keratosis lichenoides chronica, characterized by ulcerative skin growths and increased susceptibility to skin cancer (52). NLRP1 dysfunctions are also associated with vitiligo and respiratory papillomas (86,87). Because of its expression pattern, studies on human NLRP1 inflammasome often use primary or immortalized keratinocytes or epithelial cells as a model.

1.5.1 Activation of murine Nlrp1b

The activation mechanism was first uncovered for murine Nlrp1. It was reported that certain alleles of murine Nlrp1b confer susceptibility of mouse macrophages to anthrax lethal factor (LF), a toxin from *Bacillus anthracis*. It was also found that Nlrp1b is responsible for caspase-1 activation upon stimulation with LF (77); subsequently, Vance and colleagues demonstrated that LF directly cleaves Nlrp1b (80); they proposed a 'functional degradation' model in which LF-mediated cleavage of the NT fragment induces its proteasomal degradation, releasing the CT fragment, which forms an inflammasome. In this model, activation of Nlrp1b does not depend on the cleavage of a specific residue but on NT fragment destabilization. Indeed, selective degradation of the N-terminus causes IL-1β maturation (80). Mechanistically, LF-induced degradation of the Nlrp1b NT fragment relies on the N-end rule pathway, which targets proteins with destabilizing residues at the N-terminus for degradation (80,88). In addition, Nlrp1b can be activated by IpaH7.8, an E3 ubiquitin ligase expressed by the bacterium *Shigella flexneri*. IpaH7.8 directly ubiquitinates Nlrp1b, leading to inflammasome activation (80). Ubiquitination of the NT fragment after treatment with LF was never directly shown; nevertheless, inhibition of proteasome prevents Nlrp1b activation by LF.

1.5.2 The role of DPP9 in NLRP1 inflammasome signaling

In 2017, it was reported that Val-boroPro (VbP) - an inhibitor of the serine proteases dipeptidyl peptidase 8 (DPP8) and DPP9 - induced GSDMD-mediated pyroptosis in human and mouse monocytes and macrophages; furthermore, genetic deletion of DPP9 resulted in constitutive pyroptosis (61). It was later discovered that VbP-induced pyroptosis in mouse macrophages is mediated by Nlrp1b (89). Similarly to LF, Nlrp1b inflammasome activation by VbP requires auto-cleavage at FIIND and is blocked by proteasomal inhibition; however, it is not dependent on the N-end rule pathway (88,89). In human cells, VbP-induced pyroptosis was later found to be dependent on another inflammasome sensor, CARD8 (33).

In parallel, independent work by Reversade, Zhong, and colleagues (90) identified DPP9 as an interacting partner of human NLRP1 and CARD8. Currently, DPP9 is known to sequester NLRP1, preventing its activation; this inhibition depends on the interaction of DPP9 with FIIND of NLRP1 and on the catalytic activity of DPP9. Cryo-electron microscopy structures revealed that human NLRP1 and DPP9 form a complex consisting of a DPP9 molecule bound to the FIIND of one full-length and one CT fragment of NLRP1 (Fig. 1.3, Hollingsworth et al., 2021). The UPA domain of the CT fragment inserts into the active site of DPP9, causing a conformational change of DPP9 similar to that caused by the binding of a substrate or an inhibitor. This discovery suggested that VbP displaces the free C-terminus from the active site, causing the accumulation of CT fragments in the cytosol, which leads to inflammasome assembly (Fig. 1.3). Depletion of the FL or NT fragment of NLRP1 also disrupts the C-terminus binding to DPP9, leading to its accumulation (81). The role of DPP9 in NLRP1 inflammasome signaling is underlined by the report that DPP9 deficiency causes an inflammasomopathy, which can be rescued by deletion of NLRP1 or IL-1β (91).

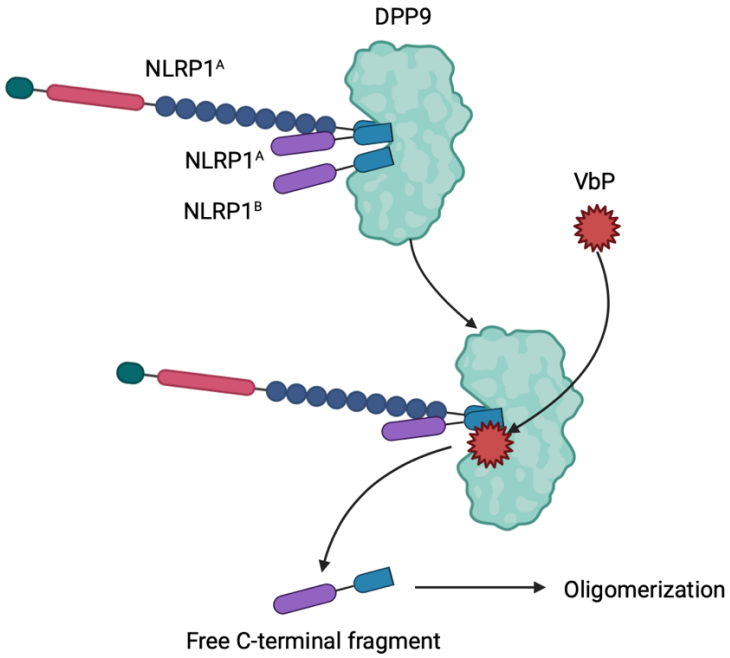

Fig. 1.3 Overview of NLRP1 activation by VbP. The NLRP1-DPP9 complex consists of DPP9, full-length NLRP1 ($NLRP1^{A}$) and C-terminal fragment of NLRP1 ($NLRP1^{B}$). VbP replaces $NLRP1^{B}$ at the DPP9 active site, leading to the release of the free C-terminal fragment and its oligomerization (adapted from (35)).

1.5.3 Activation of human NLRP1 by viral proteases

MDP was the first reported ligand of human NLRP1; however, MDP-induced activation of endogenous NLRP1 in keratinocytes has not been confirmed (92). The first reported pathogen-derived activators of human NLRP1 were rhinoviral 3C proteases (60). The mechanism is different than that of LF-induced mNlrp1b activation, as the NT degradation is not dependent on the N-end rule pathway. Instead, the cleavage after the residue Q130 exposes an N-terminal glycine (G131), which is recognized by the $cullin^{ZER/ZYG11B}$ complex, ubiquitinated, and degraded in the N-glycine degron pathway. As with VbP, NLRP1 activation by 3C proteases is prevented by proteasomal inhibition (60).

An independent study also identified enteroviruses expressing 3C proteases as activators of human NLRP1 inflammasome (93). The authors demonstrated that coxsackievirus and poliovirus cleave NLRP1 at the same residue as rhinoviral 3C proteases. In addition, NLRP1 is activated by a protease from another member of the *Picornaviridae* family, rosavirus 2; however, the cleavage site seems to be different than that of enteroviral proteases (93). NLRP1 in bronchial epithelial cells has also been reported to be activated by 3C-like (3CL) protease from SARS-CoV-2 (94).

1.5.4 Activation of human NLRP1 by dsRNA

Human NLRP1 is activated by the positive-sense single-stranded RNA (ssRNA) virus, Semliki Forest Virus (SFV); however, in contrast to activation by enteroviruses, this process is not mediated by a viral protease but by dsRNA generated during SFV replication (95). This mode of activation is not functional in murine Nlrp1b. Mechanistically, dsRNA binds to NACHT-LRR domains of NLRP1 and thereby results in inflammasome assembly. *In vitro* studies have also shown that dsRNA binding leads to ATP hydrolysis, but a mechanistic understanding of this phenomenon is still lacking. Similarly to other modes of NLRP1 activation, it can be blocked by proteasomal inhibition (95). It is unclear if other factors are needed as dsRNA does not activate reconstituted NLRP1 inflammasome in HEK cells (96).

1.5.5 Activation of human NLRP1 by ribotoxic stress response

Exposure to ultraviolet B (UVB) irradiation is a known cause of sunburn. UVB can induce damage to DNA, cell death, and inflammation and increase the risk of skin cancer (97). UV irradiation activates the MAPK pathway by initiating the ribotoxic stress response (RSR); it causes ribosome collisions, triggering the mitogen-activated protein kinase kinase kinase (MAPKKK) ZAKα, which in turn activates stress-activated protein kinases (SAPKs), p38 and JNK (98). Notably, UVB was also found to trigger NLRP1-dependent IL-1β release in keratinocytes, which are often exposed to UVB (99). Initially, this response was shown to be dependent on the mitogen-activated protein kinase (MAPK) pathway; however, the link between MAPK and NLRP1 remained unclear (100).

In 2022, the mechanism of RSR-mediated NLRP1 activation was elucidated by the work of Zhong and colleagues (36). They found that the N-terminal DR of NLRP1 is constitutively phosphorylated, and treatment with UVB or other RSR-inducing agents such as anisomycin (ANS) or hygromycin leads to its hyperphosphorylation. The NLRP1 DR has ZAKα and p38 phosphorylation sites, and ZAKα deficiency completely abrogates NLRP1 activation by RSR induction. Mutations of serine/threonine residues T178, S179, and T180 abolish inflammasome assembly, suggesting that those residues are the target

of ZAKα or other kinases. The exact roles of the p38 and JNK remain to be clarified, as inhibition or genetic deletion of those kinases have different effects across studies (36,96).

As with other NLRP1 activators, RSR-induced activation depends on the proteasomal function (96). The role of the NLRP1 hyperphosphorylation is unknown, but it can be speculated that it leads to the N-terminal degradation. This activation mode is unique to human NLRP1 as murine Nlrp1b is unresponsive to ANS (36). ZAKα and DR phosphorylation are not required for VbP-induced NLRP1 activation, and the role of ZAKα in dsRNA-mediated NLRP1 activation remains to be elucidated (96,101).

Subsequently, other activators of RSR and p38 were found to trigger NLRP1 inflammasome assembly. Next to SFV, other alphaviruses such as Mayaro virus (MAYV) and Chikungunya virus (CHIKV) activate NLRP1 inflammasome; however, it is not clear if the activation is induced by RSR or by direct binding of dsRNA (96). RSR-mediated NLRP1 activation was also reported for the pathogenic bacteria *Corynebacterium diphtheriae* and *Pseudomonas aeruginosa*. Both bacteria express the exotoxins Diphtheria Toxin and exotoxin A, respectively, which inactivate eucaryotic elongation factor 2 (EEF2), inhibiting protein synthesis (102,103). A widely-used NLRP3 activator, Nigericin, also triggers ZAKα-dependent NLRP1 inflammasome activation in primary human keratinocytes through induction of RSR (100,104). It was also reported that poly(dA:dT) causes NLRP1- and ZAKα-dependent inflammasome assembly in another cell model, N/TERT2G immortalized keratinocytes (105). Those studies underline the importance of the cell model used as Nigericin and poly(dA:dT) do not activate NLRP1 inflammasome in N/TERT-1 keratinocytes or HEK cells expressing inflammasome components (96,104).

1.5.6 Reductive and protein folding stress in NLRP1 signaling

As both human and murine NLRP1 interact with DPP9 under homeostatic conditions, it has been suggested that both inflammasomes evolved to sense one specific danger signal, possibly related to protein folding stress and peptide accumulation (106). DPP9 is a serine protease that cleaves the N-terminal XP peptides (where X denotes any

amino acid); the accumulation of endogenous XP dipeptides inhibits DPP9 (107). XP dipeptides alone do not activate NLRP1; however, they synergize with compounds inducing protein folding stress. Mechanistically, protein folding stress is thought to increase the N-terminal degradation, which, in combination with DPP9 inhibition, leads to inflammasome assembly; additionally, it enhances VbP-mediated IL-1β release (106).

NLRP1 was also reported to sense reductive stress. In detail, the NACHT-LRR region of NLRP1 interacts with the oxidized form of oxidoreductase thioredoxin-1 (TRX1); this interaction is thought to restrain the activation of NLRP1 by increasing the stability of the N-terminus. Consequently, TRX1-deficient cells react more strongly to DPP9 inhibition, although TRX1 deficiency alone does not activate NLRP1 (108). In line with this finding, certain antioxidants that cause reductive stress potentiate VbP-induced NLRP1 activation (109).

1.5.7 Activation of human NLRP1 by Kaposi's sarcoma-associated virus

All NLRP1 activation modes described so far rely on the degradation of the NT fragment and are blocked by proteasomal inhibition. One exception identified so far is the activation by ORF45 of Kaposi's sarcoma-associated virus (KSHV) (110). Mechanistically, ORF45 binds to the DR of the NT fragment of NLRP1, leading to its translocation into the nucleus, which, in turn, frees the C-terminal fragment. The authors also suggested a novel model of NLRP1 inhibition whereby the CT fragment binds to the NLRP1 DR. According to this model, ORF45 binding to DR would displace the CT fragment, leading to its accumulation in the cytosol and oligomerization.

1.6 The CARD8 inflammasome

CARD8 shares many similarities with NLRP1. It consists of an N-terminal DR, followed by FIIND, and a C-terminal CARD but lacks PYD, NACHT, and LRR found in NLRP1 (Fig. 1.4, Sharif et al., 2021). CARD8, similarly to NLRP1, undergoes constitutive autocleavage at FIIND, generating N- and C-terminal fragments that remain non-covalently associated (83). It also interacts with DPP9 and is activated by compounds inhibiting DPP9, such as VbP (33,90). However, despite containing a DR, CARD8 is not activated by ribotoxic

stress response (36). The expression pattern of CARD8 differs from that of NLRP1; it is expressed in human but not murine cells and mainly by cells of hematopoietic origin (33). CARD8 inflammasome activation was first observed in myeloid cells (61,112); subsequent reports found it can also be activated in resting lymphocytes (113,114).

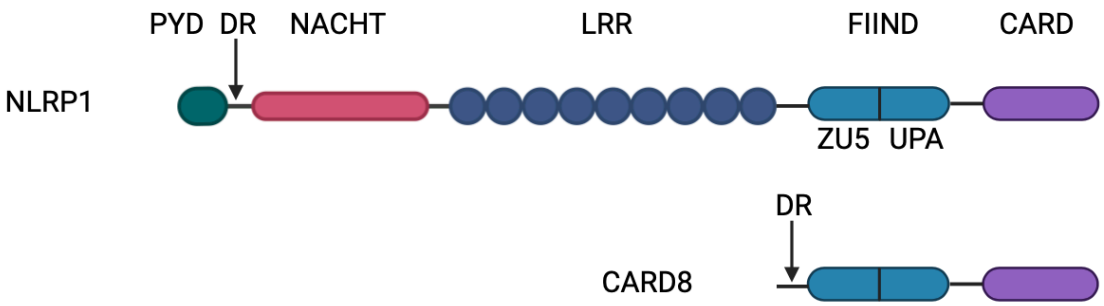

Fig. 1.4 Domain organization of human NLRP1 and CARD8 (adapted from (35)).

Similarly to NLRP1, UPA-CARD of CARD8 forms filaments upon stimulation, with CARD forming the core and UPA likely on the outside (84,85). In contrast to NLRP1 and NLRC4, the CARD of CARD8 is unable to engage ASC and can only interact with caspase-1 (85). As a result, CARD8 inflammasome leads to activation of caspase-1, cleavage of GSDMD, and pyroptosis, but in most cases, does not lead to the release of mature IL-1β (33).

1.6.1 CARD8 inflammasome activation by DPP9 inhibition

CARD8 inflammasome is activated by VbP by a mechanism comparable to NLRP1 activation. CARD8 forms a complex with DPP9, which, similarly to the DPP9-NLRP1 complex, consists of one DPP9 molecule bound to the FIIND of one FL and one CT fragment of CARD8. However, the CT fragment does not interact with the active site of DPP9 but with the region adjacent to the substrate tunnel (111). Unlike NLRP1, VbP does not displace the CT fragment from DPP9. Instead, it is thought to indirectly disrupt the ternary complex formation and induce degradation of the NT fragment. The DR is required for VbP-induced NT degradation and inflammasome activation (115). The

degradation mainly depends on the ubiquitination-independent proteasome pathway, which involves 20s proteasome-mediated degradation of disordered and misfolded proteins, although ubiquitination may also play a role (116).

In contrast to NLRP1, CARD8 is activated by XP dipeptides alone; this can be accomplished by stimulation with exogenous dipeptides or with a compound blocking M24B aminopeptidases. M24B enzymes cleave the N-terminal amino acid with proline in the second position, and their inhibition leads to the accumulation of endogenous XP dipeptides and inhibition of DPP9 activity (107).

1.6.2 CARD8 inflammasome activation by viral proteases

HIV-1 was the first pathogen reported to activate the CARD8 inflammasome (44). It encodes a protease that cleaves the CARD8 protein at the DR, which leads to proteasomal degradation of the NT fragment. However, pre-treatment with non-nucleoside reverse transcriptase inhibitors (NNRTSs) is needed for the protease expression and CARD8 activation. Typically, the protease is only expressed around viral budding, which may protect the latent virus from pyroptosis (44). Later, CARD8 inflammasome was also reported to be activated by enteroviruses and coronaviruses (117,118).

1.6.3 Reductive and protein folding stress in CARD8 signaling

Similarly to NLRP1 signaling, reductive stress and protein folding stress synergize with VbP to enhance CARD8 inflammasome activation. Both are thought to accelerate the NT fragment degradation, although neither leads to inflammasome assembly alone (106,109). Bestatin methyl ester (MeBs), which induces protein folding stress, is an example of a compound that potentiates VbP-induced pyroptosis. Interestingly, MeBs also decreases HIV-1 protease-induced IL-1β release by blocking the N-end rule pathway (44,106).

1.7 Herpes simplex virus 1

Herpes simplex virus 1 (HSV-1) belongs to the *alphaherpesvirinae* subfamily of the *Herpesviridae* family together with HSV-2 and varicella zoster virus (VZV), the causative agent of chickenpox (119). The viral particle consists of an icosahedral capsid enclosing a linear dsDNA genome, tegument, and host-derived envelope. The genome encodes over 80 genes and is approximately 150 kbp long (120). The tegument contains proteins responsible for the transport and release of the viral genome into the nucleus, induction of viral gene expression, immune evasion, and virion assembly (119,121). On the surface of the viral envelope are glycoproteins important for virus entry (119).

HSV-1 is a common pathogen, and according to WHO estimates, 67% of people under 50 are infected (https://www.who.int). HSV-1 is transmitted by skin-to-skin contact and can enter through defects in the skin or mucosal epithelia (122). The infection usually manifests as oral sores, although most infected individuals are asymptomatic (119,122). The virus establishes latent lifelong infection in the ganglia, and upon reactivation, it is transported along the axon into epithelial cells, where it initiates lytic infection, leading to symptoms. In rare cases, HSV-1 infection can cause severe outcomes, such as encephalitis (119,122).

HSV-1 first uses surface glycoproteins to bind to the heparan-sulfate proteoglycans on the target cell. The viral entry is mediated by surface receptors herpes virus entry mediator (HVEM) or nectin-1 or -2 (119). The viral envelope fuses with the cell membrane, releasing the capsid and the tegument proteins into the cytoplasm. With the help of tegument proteins, the capsid is transported into the cell nucleus, where the genome is released, and the expression of viral genes is initiated (119). HSV-1 genes are divided into three groups based on the expression kinetics: immediate early (IE), early, and late (123). The expression of IE genes is stimulated by the tegument protein VP16 and peaks between 3 to 4 hours post-infection (hpi) (123). IE proteins participate in immune evasion and promote the expression of early and late genes; they include infected cell proteins (ICPs) 0, 4, 22, 27, and 47 (119). In most cases, the expression of late genes depends on viral DNA replication (119); inhibition of DNA replication, for example, with the compound Acyclovir, inhibits or strongly decreases their expression

(123). Late genes encode primarily capsid and tegument proteins, membrane glycoproteins, and proteins involved in capsid assembly and egress (120,123).

Several PRRs were suggested to be involved in HSV-1 detection. Virion components and genomic DNA were reported to activate TLR2 and TLR9, respectively (124). HSV-1 was also reported to generate intermediate dsRNA during replication, which activates MDA5-MAVS signaling (125,126). However, it also employs multiple mechanisms to avoid triggering the immune response. Examples of such a mechanism include VP22, which inhibits AIM2 inflammasome, or UL36, reported to de-ubiquitinate TRAF3, a ubiquitin ligase acting downstream of certain PRRs (121,127). Another HSV-1-encoded protein is the E3 ubiquitin ligase ICP0, which was demonstrated to interfere with multiple signaling pathways; for example, it was shown to cause degradation of MyD88 and MAL and inhibition of NF-kB signaling (128).

1.8 Vaccinia virus and modified vaccinia virus Ankara

Vaccinia virus (VACV) is a dsDNA virus belonging to the poxvirus family, which also comprises monkeypox virus (MPXV) and variola virus (VARV), the causative agent of smallpox (122). Modified vaccinia virus Ankara (MVA) is an attenuated VACV strain generated by passaging VACV in chicken embryo fibroblasts over five hundred times (129). As a result, VACV lost large portions of its genome, including immunomodulatory genes, and the ability to replicate in mammalian cells (129). VACV was historically used for protection against smallpox. The practice of inoculation with the virus started in the 18th century; in this procedure - called vaccination - material from blisters of milkmaids infected with cowpox was administered to healthy individuals (130). It was safer than the previously used method, variolation, which involved inoculation with infectious material derived from smallpox patients. While VACV was originally thought to derive from the cowpox virus, it is now known to be more closely related to horsepox, although the original host is unknown. The use of VACV led to the eradication of smallpox, and VACV and MVA are still used for vaccine development and studies of poxvirus biology (130).

Multiple PRRs are involved in the immune response to VACV and MVA; for example, it activates two dsDNA sensors: AIM2 inflammasome, leading to IL-1β release, and cGAS-STING axis, leading to IFN release (45,131). Similarly to HSV-1, VACV was shown to generate dsRNA, which activates MDA5 and IFN response and triggers NLRP1 inflammasome assembly in certain cell lines, possibly through the MAPK signaling pathway (105,132). VACV avoids detection by inhibiting various signaling pathways, such as IFN signaling, apoptosis, and numerous steps downstream of PRR and interleukin receptor activation, preventing the induction of both innate and adaptive immune responses (133). Furthermore, VACV interferes with inflammasome signaling; for example, the protein B13R was shown to inhibit IL-1β processing by caspase-1 (134), whereas another protein, F1L, in addition to its role in inhibiting apoptosis, was reported to inhibit NLRP1 inflammasome (135). However, F1L was mostly studied in a monocytic cell line, and its effect on endogenous NLRP1 remains unclear. Notably, many VACV genes inhibiting immune signaling, such as B13R, are non-functional in the MVA (129).

2. Aim of the work

Humans are regularly exposed to different viruses, including human pathogens. Our immune system developed multiple mechanisms for their detection and clearance; however, viruses also evolved means of avoiding triggering the immune response. Inflammasomes are an example of a potent mechanism employed by the innate immune system to clear pathogens. Activation of an inflammasome can disrupt viral replication by causing cell death before the viral life cycle is complete and alert other immune cells about infection. As an example, an HIV-1 protease was reported to activate CARD8 inflammasome (44); however, this protease is expressed late in the infection, preventing premature pyroptosis.

NLRP1 was the first discovered inflammasome sensor, but the mechanism of its activation was only recently elucidated. It is triggered by DPP9 inhibition, although the physiological relevance of this during an infection is unknown (90). In terms of pathogen-induced assembly, it is activated by viral proteases, dsRNA produced during viral infections, and by ribotoxic stress response and MAPK pathway triggered by viral and bacterial pathogens (36,60,95,96). HSV-1 and VACV are two viruses that are frequently used in the studies of viral immune evasion. Both have been shown to produce dsRNA and activate MAPK, yet they do not activate NLRP1 inflammasome in keratinocytes (95,132,136–138). VACV has been reported to express the protein F1L, which specifically binds to and inhibits human NLRP1 inflammasome (135); however, it is unclear whether this protein inhibits endogenous NLRP1 and, if so, by what mechanism. In addition, it is not known if and how F1L-deficient VACV would activate NLRP1 in keratinocytes. The effect of HSV-1 infection on NLRP1 activation has not been examined so far.

The objective of this study was to verify if VACV and HSV-1 interfere with the activation of endogenous NLRP1 in keratinocytes. Furthermore, we aimed to identify the putative viral-encoded NLRP1 inhibitors and determine if viruses deficient in those proteins activate NLRP1 inflammasome.

3. Materials and methods

3.1 Materials

3.1.1 Plasticware and glassware

The consumables were manufactured by Bioplastics, Biorad, Biozym, Corning, Greiner, Labomedic, Neolab, PerkinElmer, Sarstedt, and VWR.

3.1.2 Cell culture and media supplements

Product	**Provider**
DMEM (high glucose, no glutamine, no calcium)	Thermo Fisher Scientific
DMEM (high glucose)	Thermo Fisher Scientific
Opti-MEM	Thermo Fisher Scientific
Ham's F12 Nutrient Mix	Thermo Fisher Scientific
Penicilin/Streptomycin	Thermo Fisher Scientific
GlutaMAX	Thermo Fisher Scientific
HEPES	Sigma-Aldrich
MEM Non-Essential Amino Acids	Thermo Fisher Scientific
EpiLife™ Defined Growth Supplement (EDGS)	Thermo Fisher Scientific
Bovine Pituitary Extract (BPE)	Thermo Fisher Scientific
Invitrogen™ UltraPure™ 0.5M EDTA, pH 8.0	Thermo Fisher Scientific
Trypsin-EDTA (0.05%), phenol red	Thermo Fisher Scientific
DPBS, no calcium, no magnesium	Thermo Fisher Scientific
Epidermal growth factor (EGF)	MPI of Biochemistry Protein Production Core Facility
Fetal calf serum (FCS)	Thermo Fisher Scientific
Sodium pyruvate	Thermo Fisher Scientific

3.1.3 Reagents and chemicals

Product	**Provider**
Agarose powder	Biozym
Alt-R® CRISPR-Cas9 crRNA XT	IDT Integrated DNA Technologies
Alt-R® CRISPR-Cas9 tracrRNA	IDT Integrated DNA Technologies
Alt-R™ S.p. HiFi Cas9 Nuclease V3	IDT Integrated DNA Technologies

Ampicilin	Carl Roth
Bromophenol blue	Carl Roth
BSA	Carl Roth
$CaCl_2$	Carl Roth
Chloroform	Sigma-Aldrich
cOmplete ™ Protease Inhibitor Coctail	Roche
Crystal Violet	Sigma-Aldrich
DMSO	Carl Roth
DSS	Thermo Fisher Scientific
DTT	Carl Roth
EDTA	Carl Roth
Ethanol	Roth
Formaldehyde	Sigma-Aldrich
GeneRuler 1kb, 100bp	Thermo Fisher Scientific
Glycerol	Carl Roth
Glycine	Carl Roth
HCl	Carl Roth
Immobilon Forte Western HRP substrate	Merck
Isopropanol	Carl Roth
Kanamycin	Carl Roth
KCl	Carl Roth
LB	Carl Roth
LB agar	Carl Roth
Methanol	Sigma-Aldrich
Methyl cellulose, viscosity 1500 cP	Sigma-Aldrich
$MgCl_2$	Carl Roth
Milk	Carl Roth
N-Ethylmaleimide	Sigma-Aldrich
Na_2HPO_4	Carl Roth
NaCl	Carl Roth
P3 Primary Cell 96-well Nucleofector™ Kit	Lonza
PageRuler™ Prestained Protein Ladder	Thermo Fisher Scientific
Phos-tag™ Acrylamide	FUJIFILM Wako Chemicals
PhosSTOP Phosphatase Inhibitor Coctail	Roche
Pierce ECL Western Blotting substrate	Thermo Fisher Scientific
Prestained Protein Marker EDTA free	APExBIO
RNase A	Life Technologies
SDS	Carl Roth
Sybr Safe DNA Gel Stain	Thermo Fisher Scientific
Tris	Carl Roth
Triton X-100	Carl Roth
Tween-20	Carl Roth

3.1.4 Cell culture reagents and stimuli

Reagent	**Provider**
Anisomycin	Biomol
Blasticidin S	Thermo Fisher Scientific
Deoxyribonucleic acid sodium salt from herring testes (HT-DNA)	Sigma-Aldrich
Doxycyclin Hyclate	Sigma-Aldrich
GeneJuice	Merck
Hygromycin	Invivogen
IVT4	Self-made
Lipofectamine 2000	Thermo Fisher Scientific
Nigericin sodium salt	Sigma-Aldrich
Poly(I:C) HMW	Invivogen
Polybrene	Sigma-Aldrich
Puromycin	Carl Roth
Trypan blue	Sigma-Aldrich
Val-boroPro	APExBIO

3.1.5 Kits

Kit	**Provider**
CyQUANT™ LDH Cytotoxicity Assay	Thermo Fisher Scientific
CellTiter-Glo® 2.0 Cell Viability Assay	Promega
Human Total IL-18 DuoSet ELISA	R&D Systems
PureLink Maxi-Prep kit	Qiagen
PureYield Plasmid Miniprep System	Promega
QIAquick gel extraction kit	Qiagen
Streptavidin HRP	BD Bioscience
TMB Substrate Reagent Set	BD Bioscience

3.1.6 Enzymes and enzyme buffers

Product	**Provider**
Restriction enzymes and FastDigest Green Buffer	Thermo Fisher Scientific
Gibson mix; 2x Master mixture containing 2.67 µl 5x ISO buffer (0.5 M Tris-HCl pH 7.5, 50 mM $MgCl_2$, 1 mM dGTP, 1 mM dATP, 1 mM dTTP, 1 mM dCTP, 50 mM DTT, 25% PEG-8000, 5 mM NAD), 0.053 U T5 Exonuclease, 0.33 U Phusion Polymerase, 53.33 U Taq Ligase, H_2O to 10 µl	MPI of Biochemistry Protein Production Core Facility
Phusion polymerase and buffer	Thermo Fisher Scientific

Proteinase K	Carl Roth
Restriction enzymes	Thermo Fisher Scientific
T4 DNA ligase and buffer	Thermo Fisher Scientific

3.1.7 Antibodies

Antibody	**Dilution**	**Supplier**	**Application**
α-dsRNA (J2)	1:400	SCICONS	IF
donkey α-goat IgG HRP	1:2000	Santa Cruz Biotechnology	WB
goat α-mouse IgG Alexa Fluor 488	1:500	BioLegend	IF
goat α-mouse IgG HRP	1:2000	Santa Cruz Biotechnology	WB
goat α-rabit IgG HRP	1:2000	Santa Cruz Biotechnology	WB
α-ASC	1:1000	Adipogen	WB
α-caspase-1	1:1000	Adipogen	WB
α-GSDMD	1:1000	Novusbio	WB
α-ICP0	1:200	Santa Cruz Biotechnology	WB
α-ICP4	1:1000	Santa Cruz Biotechnology	WB
α-IL-1β	1:1000	R&D Systems	WB
α-mNeon	1:1000	ChromoTek	WB
α-NLRP1	1:1000	BioLegend	WB
α-phospho-p38	1:1000	Cell Signalling Technology	WB
α-ZAK	1:2000	Biomol	WB
α-β-Actin HRP	1:1000	Santa Cruz Biotechnology	WB

3.1.8 Buffers and solutions

Buffer	**Recipe**
10x PBS	800 g NaCl, 20 g KCl, 142 g Na_2HPO_4, water to 10 l, pH 7.4
10x TBS	240 g Tris, 880 g NaCl, water to 10 l, pH 7.6
10x Tris-Glycine buffer	290 g Tris, 1440 g glycine, water to 10 l, pH 8.6
2x Laemmli sample buffer	150 mM Tris-HCl pH 6.8, 200 mM DTT, 4% SDS, >0.02% Bromophenol blue, 20% glycerol, water to 100 ml
6x Laemmli sample buffer	1.2 ml 500 mM Tris-HCl pH 6.8, 0.93 g DTT, 1.2 g SDS, 6 mg Bromophenol blue, 4.7 ml glycerol, 2.1 ml water
50x TAE buffer	242 g Tris, 57.1 ml acetic acid, 18.6 g EDTA 2Na-2H_2O, water to 1 l

Direct Lysis Buffer	10 mM Tris pH 7.5, 1 mM $CaCl_2$, 2 mM $MgCl_2$, 1 mM EDTA, 1% Triton X-100, 0.2 mg/ml proteinase K
DISC lysis buffer	30 mM Tris-HCl pH 7.0, 120 mM NaCl, 10% glycerol, 1% Triton X-100
10x Transfer buffer	242.4 g Tris, 1 kg glycine, water to 7 l, pH 8.7
Western blot transfer buffer	200 ml 10x transfer buffer, 400 ml ethanol, 1.4 l water
LB agar	20 g LB, 15 g agar, 1 l water
LB medium	20 g LB, 1 l water
Miniprep buffer P1	50 mM Tris pH 8.0, 10 mM EDTA, 100 µg/ml RNase A
Miniprep buffer P2	200 mM NaOH, 1% SDS
Miniprep buffer N3	4.2 M Guanidinium chloride
Miniprep buffer PE	10 mM Tris pH 7.5, 80% ethanol
PBST (ELISA wash buffer)	1 l 10x PBS, 5ml Tween-20, 9 l water
TBST	1 l 10x TBS, 5ml Tween-20, 9 l water
EDTA-free MES running buffer	50 mM MES, 50 mM Tris, 0.1% SDS

3.1.9 Plasmids

Plasmid	**Application**	**Source**
p103_EGFP-HHV-1-RL2-F2	HEK transfection, cloning	(139)
p103_EGFP-HHV-1-RL2-F2-RFm	HEK transfection	This work
p103_EGFP-HHV-1-RL2-F2-T67A	HEK transfection	This work
p103_EGFP-EGFP-HHV-1-UL26.5	HEK transfection, cloning	(139)
p103_EGFP-HHV-1-UL36A	HEK transfection, cloning	(139)
p103_EGFP-HHV-1-UL36A-C40A	HEK transfection	This work
pCRISPaint-mNeon-PuroR	Cloning	(140)
pFUGW_mNeon_Blast	Cloning	This work
pcDNA3.1_mNeon	HEK transfection	This work
pcDNA3.1_NLS-BFP	HEK transfection, cloning	AG Hornung, sequence in section 9.1
pcDNA3.1_VACV-F1L-codopt	Cloning	This work
pcDNA3.1_YFP-HHV-1-RL2	HEK transfection	This work

pcDNA3.1_YFP-HHV-1-RL2xE	HEK transfection	This work
pCMV_gag-pol	Retrovirus production	AG Hornung
pCMV-VGV-g	Lentivirus and retrovirus production	AG Hornung
pEYFP-ICP0-C3	Cloning	Addgene #134559
pEYFP-ICP0xE-C3	Cloning	Addgene #134561
pFUGW_CARD8_Blast	Lentiviral transduction	(95)
pFUGW_hsNLRP1_Blast	Lentiviral transduction, cloning	(95)
pFUGW_hsNLRP1_Hygro	Lentiviral transduction	(95)
pFUGW_hsNLRP3_Blast	Lentiviral transduction	(95)
pFUGW_hsNLRP1(DR)-mNeon_Blast	Cloning	AG Hornung, sequence in section 9.2
pFUGW_hsNLRP1(PYD-DR)-mNeon_Blast	Lentiviral transduction	This work
pFUGW_NB_Blast	Cloning	AG Hornung
pLI_FLAG-mScarlet_Blast	Lentiviral transduction	AG Hornung, sequence in section 9.3
pLI_FLAG-VACV-F1L-codopt_Blast	HEK transfection	This work (codon-optimized sequence of VACV F1L strain Copenhagen designed with the IDT Codon Optimization Tool, sequence in section 9.4)
pLIP-ICP0	Cloning	(141)
pLI_HHV-1-RL2-MG_Blast	Lentiviral transduction	This work
pLI_HHV-1-RL2-MG-RFm_Blast	Lentiviral transduction	This work
pLI_mNeon_Blast	HEK transfection	This work
pLI_NB_Blast	Cloning	AG Hornung
pMDL/pPRE	Lentivirus production	AG Hornung
pRP_hsPYCARD-mCherry	Retroviral transduction	(95)
pRSV-Rev	Lentivirus production	AG Hornung

3.1.10 Primers

Product	**Template**	**Product**	**Primer 5' -> 3'**	
p103_EGFP-HHV-1-RL2-F2-RFm	p103_EGFP-HHV-1-RL2-F2	C116G fragment 1	Fwd	GGCATGGACGAGCTGTACAAG
			Rev	CACGGCGCCCACGT
		C116G fragment 2	Fwd	GACGTGGGCGCCGT
			Rev	TGGATCCGAGCTCGGTACC
			Fwd	GGCATGGACGAGCTGTACAAG

		C156A fragment 1	Rev	GGCGTTGGCCAGCG
		C156A fragment 2	Fwd	CCGCTGGCCAACGCC
			Rev	TGGATCCGAGCTCGGTACC
p103_EGFP-HHV-1-RL2-F2-T67A	p103_EGFP-HHV-1-RL2-F2	T67A fragment 1	Fwd	GGCATGGACGAGCTGTACAAG
			Rev	AACAGTTCCGCGTCCGTG
		T67A fragment 2	Fwd	GCACGGACGCGGAACTG
			Rev	TGGATCCGAGCTCGGTACC
p103_EGFP-HHV-1-UL36A-C40A	p103_EGFP-HHV-1-UL36A	C40A fragment 1	Fwd	CACTATAGGGAGACCCAAGCTGG
			Rev	GCGCATGGCCGATACCG
		C40A fragment 2	Fwd	CGGTATCGGCCATGCGC
			Rev	ATGGCTCCCGCCCAC
pFUGW_mNeon_Blast	pCRISPaint-mNeon-PuroR	mNeon	Fwd	CAGGTCGACTCTAGTTCGAGCAGC TAGCATGGTGAGCAAGGGCGAGG AG
			Rev	CGCAACCCCAACCCCGGATCTCACT TGTACAGCTCGTCCATGC
pcDNA3.1_mNeon	pFUGW_mNeon_Blast	mNeon	Fwd	CACTATAGGGAGACCCAAGCTGGC TAGCATGGTGAGCAAGGGC
			Rev	CAGAATTCCACCACACTGGACTAGT GGATCCTCACTTGTACAGCTCGTC
pFUGW_hsNLRP1(PYD-DR)-mNeon_Blast	pFUGW_hsNLRP1(DR)-mNeon_Blast	mNeon	Fwd	GCCCCACCACCACCCA
			Rev	CGCAACCCCAACCCCG
	pFUGW_hsNLRP1_Blast	hsNLRP1(PYD-DR)	Fwd	CAGGTCGACTCTAGTTCGAGCA
			Rev	TGGGTGGTGGTGGGG
pLI_FLAG-VACV-F1L-codopt_Blast	pcDNA3.1_VACV-F1L-codopt	FLAG-VACV-F1L PCR 1	Fwd	ATGGATTACAAGGACGACGATGAC AAGGGCGGCGGCAGCATGCTGTCA ATGTTCATG
			Rev	GGATCCTTAACCTATCATATACTTC AGGGTC
		FLAG-VACV-F1L PCR 2	Fwd	CGTCAGATCGCCTGGAGAATTGGC TAGCGCCACCATGGATTACAAGGA CGACGATGACA
			Rev	CGCAACCCCAACCCCGGATCCTTAA CCTATCATATACTTCAGGGTC
pLI_HHV-1-RL2-MG-RFm_Blast	pLI_HHV-1-RL2-MG_Blast	C156A fragment 1	Fwd	CGTCAGATCGCCTGGAGAATTG
			Rev	GCTTGGCATTAGCGAGCGG
		C156A fragment 2	Fwd	CCGCTCGCTAATGCCAAG
			Rev	CGAGGGCCACTTGCCG
		C116G fragment 1	Fwd	CGTCAGATCGCCTGGAGAATTG
			Rev	GTACATACGGCACCAACATCACC
			Fwd	GGTGATGTTGGTGCCGTATGTAC

		C116G fragment 2	Rev	CGAGGGCCACTTGCCG
pLI_mNeon_Blast	pCRISPaint-mNeon-PuroR	mNeon	Fwd	CGTCAGATCGCCTGGAGAATTGGCTAGCATGGTGAGCAAGGGCGAGGAG
			Rev	CGCAACCCCAACCCCGGATCCTCACTTGTACAGCTCGTCCATGCC

3.1.11 Cloning strategy and plasmid description

For all point mutations, primers were designed to span the mutation site. The genes were amplified in two fragments overlapping at the site of the mutation and joined by the Gibson assembly reaction.

Plasmid	**Description**
p103_EGFP-HHV-1-RL2-F2-RFm	First, the C156A mutation was introduced by amplifying RL2-F2 by PCR using the primers and template from section 3.1.10. p103_EGFP-HHV-1-RL2-F2 plasmid was digested with Kpn2I and HindIII enzymes. Two fragments and the vector were joined by Gibson assembly. The resulting construct was amplified by PCR using the primers and template from section 3.1.10 to generate the C116G mutation. Two fragments and the digested vector were joined again by Gibson assembly.
p103_EGFP-HHV-1-RL2-F2-T67A	T67A mutation was introduced by amplifying RL2-F2 by PCR using the primers and template from section 3.1.10. p103_EGFP-HHV-1-RL2-F2 plasmid was digested with Kpn2I and HindIII enzymes. Two fragments and the digested vector were joined by Gibson assembly.
p103_EGFP-HHV-1-UL36A-C40A	C40 mutation was introduced by amplifying UL36A by PCR using the primers and template from section 3.1.10. p103_EGFP-HHV-1-RL2-F2 plasmid was digested with NheI and Pfl23II enzymes. Two fragments and the digested vector were joined by Gibson assembly.
pFUGW_mNeon_Blast	mNeon was amplified by PCR using the primers and template from section 3.1.10. pFUGW_NB_Blast plasmid was digested with NheI and BamHI enzymes. The PCR product and the digested vector were joined by Gibson assembly.
pcDNA3.1_mNeon	mNeon was amplified by PCR using the primers and template from section 3.1.10. pcDNA3.1_NLS-BFP plasmid was digested with NheI and BamHI enzymes. The PCR product and the digested vector were joined by Gibson assembly.
pcDNA3.1_VACV-F1L-codopt	The sequence of VACV F1L from strain Copenhagen was codon-optimized using IDT DNA Codon Optimization Tool

	and ordered as a gBlock. pcDNA3.1_NLS-BFP plasmid was digested with NheI and BamHI enzymes. gBlock and the digested vector were joined by Gibson assembly.
pcDNA3.1_EYFP-HHV-1-RL2	pEYFP-ICP0-C3 plasmid was digested with NheI and BamHI enzymes to generate EYFP-ICP0 fragment. pcDNA3.1_NLS-BFP plasmid was digested with NheI and BamHI enzymes. EYFP-ICP0 and the digested vector were ligated using T4 ligase.
pcDNA3.1_EYFP-HHV-1-RL2xE	pEYFP-ICP0xE-C3 plasmid was digested with NheI and BamHI enzymes to generate EYFP-ICP0xE fragment. pcDNA3.1_NLS-BFP plasmid was digested with NheI and BamHI enzymes. EYFP-ICP0xE and the digested vector were ligated using T4 ligase.
pFUGW_hsNLRP1(PYD-DR)-mNeon_Blast	mNeon and PYD and DR of NLRP1 (amino acids 1-254) were amplified by PCR using the primers and template from section 3.1.10. pFUGW_NB_Blast plasmid was digested with NheI and BamHI enzymes. The PCR products and the digested vector were joined by Gibson assembly.
pLI_FLAG-VACV-F1L-codopt_Blast	VACV-F1L was amplified by PCR using the primers and template from section 3.1.10. During PCR 1, a FLAG tag connected by a linker (GGGS) was added to the N-terminus of F1L. During PCR 2, sequence overlapping the vector sequence was added to the product of PCR 1. pLI_NB_Blast plasmid was digested with NheI and BamHI enzymes. The PCR 2 product and the digested vector were joined by Gibson assembly.
pLI_HHV-1-RL2-MG_Blast	pLIP-ICP0 plasmid was digested with NheI and BamHI enzymes to generate ICP0 fragment. pLI_NB_Blast plasmid was digested with NheI and BamHI enzymes. ICP0 and the digested vector were ligated using T4 ligase.
pLI_HHV-1-RL2-MG-RFm_Blast	First, the C156A mutation was introduced by amplifying RL2-F2 by PCR using the primers and template from section 3.1.10. pLI_HHV-1-RL2-MG_Blast was plasmid digested with NheI and MauBI enzymes. Two fragments and the digested vector were joined by Gibson assembly. The resulting construct was amplified by PCR using the primers and template from section 3.1.10 to generate the C116G mutation. Two fragments and the digested pLI_HHV-1-RL2-MG_Blast were joined again by Gibson assembly.
pLI_mNeon_Blast	mNeon was amplified by PCR using the primers and template from section 3.1.10. pLI_NB_Blast plasmid was digested with NheI and BamHI enzymes. The PCR product and the digested vector were joined by Gibson assembly.
pcDNA3.1_NLS-BFP	TagBFP protein with an N-terminal NLS sequence (PAAKKKKLD).
pLI_FLAG-mScarlet_Blast	mScarlet protein with an N-terminal FLAG tag (DYKDDDDK) connected by a linker (GGGS).

3.1.12 Laboratory equipment

Laboratory equipment	**Manufacturer**
Spark® multimode microplate reader (LDH)	TECAN
4D-Nucleofector (Unit X)	Lonza
BD FACSMelody™ Cell Sorter	BD Biosciences
BD LSRFortessa™ Cell Analyzer	BD Biosciences
Gel Doc XR+ Gel Documentation System	Bio-Rad
DMi8 inverted microscope	Leica
Fusion Fx	Vilber
DMi1 inverted microscope	Leica
BioTek Microplate reader (LDH, ELISA)	Epoch
NanoPhotometer® NP80	IMPLEN
C1000 Touch and T100 Thermal Cyclers	Bio-Rad
Thermomixer comfort	Eppendorf
UVP Crosslinker CL-1000	Analytik Jena
TC20 Automated Cell Counter	Bio-Rad

3.2 Cell culture methods

3.2.1 Cell lines

The following cells were used in the study:

- N/TERT-1 – immortalized human keratinocytes, a gift from J. Rheinwald (142)
- HEK293T – human embryonic kidney cells stably expressing SV40 Large T antigen (Leibniz Institute DSMZ, DSMZ no. ACC 635)
- Vero – cell line derived from the kidney of an adult African green monkey (AG Hornung)
- U2OS – human cell line derived from sarcoma of the tibia, a gift from Lars Dölken (University of Würzburg)

3.2.2 Viruses

HSV-1 strain 17 was a gift from Andreas Pichlmair (Technical University of Munich).

HSV-1 dICP0 strain 17 was a gift from Lars Dölken (University of Würzburg).

WT, dF1L, and dF1Lrev MVA were a gift from Gerd Sutter (University of Munich).

3.2.3 Culture conditions

All cells were cultured at 37°C in 5% CO_2. N/TERT-1 keratinocytes were cultured in 1:1 mix of Ham's F12 nutrient mix and DMEM (high glucose no glutamine, no calcium) supplemented with 1% penicillin/streptomycin, 1% non-essential amino acids, 1% GlutaMAX, 10 mM HEPES, 0.5% EDGS, 25 µg/ml bovine pituitary extract, 0.1 mM $CaCl_2$, and 20 ng/ml epidermal growth factor. HEK293T, U2OS, and Vero cells were cultured in DMEM (high glucose) supplemented with 10% fetal calf serum (heat-inactivated for 1 h at 55°C), 1% penicillin/streptomycin, and 1% sodium pyruvate. For passaging of adherent cells, they were washed with PBS, and detached with 0.05% Trypsin-EDTA; N/TERT-1 keratinocytes were resuspended in DMEM with 10% FCS to inactivate the enzyme, before being transferred to N/TERT-1 media.

3.3 Cell biology methods and cell stimulation

3.3.1 Cell stimulation

N/TERT-1 and HEK cells were plated at 5 x 10^4, 5 x 10^5, and 10^6 per 96-, 12-, and 6-well plates, respectively. For inflammasome activation, cells were stimulated with 6.5 µM Nigericin, 2 µM anisomycin, 2 µM Val-boroPro, or transfected with a mix of poly(I:C) and lipofectamine 2000 in Opti-MEM medium. For 96- and 12-well plates, the mix consisted of 200 ng of poly(I:C) and 0.3 µl lipofectamine in 50 µl Opti-MEM or 1.6 µg of poly(I:C) and 2.4 µl lipofectamine, respectively. For stimulations with other nucleic acids, the proportions were maintained as with poly(I:C) stimulation. For viral infections, cells were treated for an indicated amount of time and MOI with VACV or MVA, and stimuli or media were added on top without removing the inoculum. Independent experiments were conducted on different days or the same day using separately prepared stimuli.

3.3.2 HSV-1 propagation

WT HSV-1 was propagated in Vero cells, and dICP0 HSV-1 was propagated in U2OS cells. The cells were plated in 15 cm dishes. When fully confluent, they were infected with respective viruses at MOI of 0.001-0.01 in 5 ml of infection media (DMEM high glucose, 2% FCS, 20 mM HEPES). After 2 h incubation at 37°C, 8 ml of infection media were

added, and the cells were incubated until the cytopathic effect (CPE) was reached. The viral supernatant was harvested and centrifuged for 10 min at 1000 x *g*. The cell pellet was lysed by three cycles of freezing and thawing, centrifuged again, and the supernatant was added to the main stock. Next, the viral supernatant was filtered through a 0.45 µm filter, aliquoted, and frozen.

Cell titer of WT HSV-1 was determined by plaque assay. In detail, Vero cells were plated in a 12- or 6-well plate and cultured until 90-100% confluence. Ten-fold dilutions of the virus were prepared in infection media and incubated with the cells for 2 h. Next, methylcellulose solution was added to the final concentration of around 0.5% and cells were cultured at 37°C. When the plaques reached sufficient size, the overlay was removed, the cells were fixed for 15-45 min with 4% formaldehyde in PBS, and stained for 10-20min with a solution of 1% crystal violet and 20% ethanol in water. The stain was washed off with PBS or water, and the plaques were counted.

For experiments where WT HSV-1 was used with dICP0 HSV-1, the titer of both viruses was determined by TCID50 assay in U2OS cells. Briefly, the cells were plated at 4 x 10^4 per well in a 96-well plate, infected with a 10-fold dilution of viruses, and cultured until the CPE was reached. The wells showing CPE were counted and the viral titer was determined using the Spaerman-Kräber method.

3.3.3 HSV-1 ORF library screen

For viral ORF library screens, HEK cells constitutively expressing ASC tagged with mCherry (ASC-mCherry) and hsNLRP1 were used. The cells were transfected by inverse transfection; the transfection mix per one well consisted of 0.5 µl of GeneJuice, 175 ng of library or control plasmid (pcDNA3.1_mNeon), and 25ng of BFP (pcDNA3.1_NLS-BFP). In detail, 0.5 µl of GeneJuice was incubated at room temperature for 5 min. In the meantime, the plasmid mix was prepared in a 96-well plate, the GeneJuice mix was added and incubated at room temperature for 20-25 min. The cells were added on top of the mix at 5 x 10^4 cells per well in 100 µl. After 20-24 h incubation with the transfection mix, the cells were stimulated with 2 µM ANS and incubated for 4 h. Next,

the cells were detached with 2 mM EDTA in DMEM and transferred into a round-bottom plate. ASC specking was analyzed with BD LSRFortessa Cell Analyzer.

3.3.4 HEK293T transfection for flow cytometry analysis

For validation of ORF library screen hits, HEK cells were transfected as described in the screening procedure in 96-well format. The cells were stimulated as indicated, detached as in screen preparation, and analyzed with BD LSRFortessa Cell Analyser.

3.3.5 ASC specking in HSV-1- and MVA-infected HEK cells

HEK cells constitutively expressing hsNLRP1 and ASC-mCherry were plated in a 12-well plate at 5 x 10^5 cells per well and incubated overnight. The next day, the cells were infected and stimulated as indicated and detached with 2 mM EDTA in DMEM. ASC specking was analyzed with BD FACSMelody™ Cell Sorter.

3.3.6 Lentiviral and retroviral transduction

Lentiviruses and retroviruses were produced in HEK293T cells using PEI Max transfection. The PEI mix was prepared by diluting 31.8 µl PEI in 600 µl Opti-MEM and incubated at room temperature for 5 min. In the meantime, the DNA mix in 600 µl Opti-MEM was prepared. For lentivirus production, 3 µg of transfer plasmid, 4.5 µg of pMDL/pPRE, 1.5 µg of pRSV-rev, and 3 µg of pCMV-VSV-g plasmid were used. For retroviral production, 5.5 µg of transfer plasmid, 5.5 µg of GAG-Pol, and 2.2 µg of pCMV-VSV-g were used. PEI and DNA mixes were combined and incubated at room temperature for 25 min. HEK cells were seeded in a T-25 cell culture flask at 6 x 10^6 in 3 ml, and the transfection mix was added. Viral supernatants were collected after 48-72 h, centrifuged for 10 min at 1000 x *g*, and filtered through a 0.45 µm filter.

For transduction, 3 x 10^6 N/TERT-1 keratinocytes or HEK293T cells were seeded in a T-75 flask in 11 ml, and viral supernatant was added along with 8 µg/ml of polybrene. Cells were incubated overnight, the media was exchanged, and antibiotic selection was started 24-48 h post-transduction. The following concentrations of antibiotics were used: blasticidin S at 10 µg/ml for HEK293T and U2OS cells and 5 µg/ml for N/TERT-1

cells, hygromycin at 200 µg/ml hygromycin for HEK293T cells and 50 µg/ml for N/TERT-1 cells, puromycin at 5 µg/ml for HEK293T cells. N/TERT-1 keratinocytes stable for hsNLRP1 and hsNLRP3 were generated by Bauernfried et al (95).

3.3.7 Knock-out generation in N/TERT-1 cells

The knock-out N/TERT-1 keratinocytes were generated by Bauernfried et al (95). In detail, the cells were nucleofected with ribonucleoprotein (RNP) complexes consisting of recombinant Cas9 and guide RNA (gRNA), using two gRNAs per gene. Single guide RNA (sgRNA) was prepared by mixing 100 pmol of each CRISPR RNA (crRNA) with 200 pmol of transactivating CRISPR RNA (tracrRNA) and annealing the mix for 5 min at 95°C and for 20-30 min at room temperature. In the meantime, N/TERT-1 keratinocytes were washed with PBS and resuspended in 20 µl of P3 primary cell buffer at 10^6 cells per reaction. Next, 80 pmol of recombinant Cas9 was combined with the sgRNA mix, incubated for 10 min at room temperature, and added to the cells. The cells were incubated with the RNP complex for 5 min and electroporated using Lonza 4D-Nucleofector, program DS-138, after which they were transferred into a 6-well plate and expanded. Protein depletion was confirmed by western blotting and/or by PCR.

3.3.8 UV irradiation of MVA and HSV-1

HSV-1 and MVA were irradiated with UV-C using UVP Crosslinker CL-1000. Virus suspension was placed in the chamber in a 12-well plate (500 µl/well), the lid was removed, and the plate was irradiated for 1 min (0.3 J/cm^2), 2 min (0.8 J/cm^2), and 4 min (1.6 J/cm^2). Virus suspension was aliquoted and frozen for late use.

3.3.9 dsRNA staining

The procedure for dsRNA staining in N/TERT-1 keratinocytes was published by Bauernfried et al (95). In detail, the cells were infected as indicated, after which they were washed with PBS and fixed with 4% formaldehyde in PBS for 10 min at room temperature. Next, the cells were washed twice with PBS, permeabilized with 0.5% Triton X-100 in PBS, washed again, and blocked with 10% FCS in PBS for 30 min at room temperature. After blocking, the J2 antibody diluted 1:400 in blocking buffer was added

and incubated for at least one hour. Next, the cells were washed three times with PBS, and incubated in anti-mouse Alexa Fluor 488 diluted 1:500 in blocking buffer with 2 µg/ml Hoechst for at least one hour at room temperature. After incubation, the antibody was washed off with PBS and the cells were imaged with Leica DMi8 inverted microscope using HC PL FLUOTAR L 20X/o.40 DRY objective and ORCA-Flash4.0 LT+ Digital CMOS camera.

3.3.10 Live-cell imaging

For imaging ASC specking in N/TERT-1 keratinocytes, the cells were plated in 8 well µ-Slide (ibidi) at 4-5 x 10^4 cells per well and incubated overnight. The next day, the cells were infected with HSV-1 and MVA and stimulated as indicated. Two hours before the end of the stimulation, the cells were placed in the Incubator i8 (Pecon) set to 5% CO_2 37°C. At the end of the stimulation, the cells were imaged with Leica DMi8 inverted microscope using HC PL FLUOTAR L 20X/o.40 DRY objective and ORCA-Flash4.0 LT+ Digital CMOS camera.

3.3.11 LDH assay

LDH assays were performed using CyQUANT™ LDH Cytotoxicity Assay (Thermo Fisher Scientific) according to the manufacturer's instructions. In detail, cells were stimulated in a 96-well plate as indicated with the end volume of 150 µl. For positive full lysis control, lysis buffer was added to wells 10-30 min before the end of the experiment. Supernatants were harvested into a round-bottom 96-well plate, centrifuged for 5 min at 450 x *g*, and transferred into a fresh 96-well plate. For the LDH assay, 15 µl of the LDH substrate mix was mixed with 15 µl of the supernatant in a 384-well plate and incubated in the dark for 15-30 min at room temperature. The absorbance at 490 and 680 nm was measured using a Tecan Spark 20M microplate reader. LDH release was calculated with the following formula: % LDH release = (sample – unstimulated control)/(full lysis control – unstimulated control) * 100

3.3.12 CellTiter-Glo

CellTiter-Glo viability assay was conducted according to the manufacturer's instructions. In detail, the cells were infected with viruses in a 96-well plate, as indicated. The assay solution was added at 1:4 dilution, and the cells were incubated for 10-20 min in the dark at room temperature. Next, 15 µl of the lysate was transferred into a white 384-well plate (PerkinElmer). The luminescence was measured using a Tecan Spark 20M microplate reader.

3.3.13 ELISA

IL-1β release was measured using a homemade ELISA kit (Gevokizumab as capture antibody and biotinylated Canakinumab as detection antibody). IL-18 was measured using Human Total IL-18 DuoSet ELISA (R&D Systems). The samples for analysis were harvested as for LDH assay; the cells were stimulated in a 96-well plate with an end volume of 150 µl. The supernatant was harvested into a round-bottom 96-well plate, centrifuged for 5 min at 450 x *g*, and transferred into a fresh 96-well plate. High-binding ELISA plates were used for both cytokines. For IL-1β ELISA, the plates were coated with capture antibody diluted in ELISA coating buffer, and incubated for 2 h at room temperature, or overnight at 4°C. For IL-18 ELISA, the plates were coated with capture antibody diluted in PBS and incubated overnight at room temperature. Coated plates were used immediately or stored at 4°C. Next, the plates were washed three times and blocked for one hour at room temperature with PBS containing 10% FCS or 1% BSA for IL-1β and IL-18 ELISA, respectively. Supernatants and standards were diluted in respective blocking buffers. The blocking buffer was removed from the plates, and samples and standards were added and incubated for 2 h at room temperature. Next, the plates were washed five times, and the detection antibody diluted in a blocking buffer was added. After 1 h incubation at room temperature, the plates were washed again five times, and streptavidin-linked HRP diluted in blocking buffer was added and incubated for 30 min at room temperature. The plates were washed five to seven times and TMB Substrate Reagent mix was added and incubated in the dark for 5-15 min at room temperature. The reaction was stopped with 5% sulfuric acid solution, and the absorbance at 450 and 570 nm was measured using BioTek Gen5 Epoch microplate reader.

3.3.14 Western blotting

For western blot experiments, cells were stimulated in a 12-well plate; after stimulation, they were lysed directly in the well with 1x Laemmli buffer and boiled for 5-10 min at 95°C, shaking. Samples were separated on pre-cast Tris-Glycine or Bis-Tris gels with Tris-Glycine and MES buffer, respectively, at a constant voltage of 130-150 V until the dye front reached the bottom of the gel. Next, the samples were transferred onto 0.45 µm nitrocellulose membrane at 4°C, at a constant voltage of 100 V for 60-90 min using wet transfer system. The membranes were blocked in 3% milk in TBST for one hour at room temperature and incubated with primary antibodies overnight at 4°C or for 1-4 h at room temperature and in secondary antibodies for 1-4 h at room temperature. After each incubation with antibodies, the membranes were washed in TBST for 15 min at room temperature. Antibody solutions were prepared in 3% milk in TBST. Membranes were developed with Immobilon Forte or ECL Western Blot substrates using a Fusion Fx device.

3.3.15 Phos-tag gel electrophoresis

For Phos-tag gel, N/TERT-1 keratinocytes expressing NLRP1(PYD-DR)-mNeon were plated and stimulated as indicated in a 12-well plate. After stimulation, the cells were lysed directly in the well with 180 µl of Laemmli buffer and denatured for 5 min at 95°C, shaking. For analyzing phosphorylated ZAKα, 7.5% Phos-tag resolving gel was cast:

Acrylamide 30 w/v% (ml)	1.5
TrisHCl 1.5 M pH 8.8 (ml)	1.5
Phostag (µl)	36
$MnCl_2$ 10 mM (µl)	36
10% SDS (µl)	60
H_2O (ml)	2.83
TEMED (µl)	6
APS (µl)	30
Total volume (ml)	6

For analyzing phosphorylated NLRP1 DR, either 7.5% or 10% Phos-tag resolving gel was cast as above, changing the volume of acrylamide to 2 ml and of H_2O to 2.33 ml. The stacking gel was cast according to the following recipe:

Acrylamide 30 w/v% (ml)	1.65
TrisHCl 0.5 M pH 6.8 (ml)	1.5
10% SDS (µl)	60
H_2O (ml)	2.7
TEMED (µl)	6
APS (µl)	60
Total volume (ml)	6

A regular SDS PAGE was run in parallel to Phos-tag gel. For Phos-tag gel, an EDTA-free prestained Protein Marker was used. The gel was run on ice at the constant voltage of 120 V in EDTA-free MES running buffer. After protein separation, the gel was washed twice for 10 min in transfer buffer containing 10 mM EDTA and once for 10 min in transfer buffer with 0.1% SDS. Next, the proteins were transferred onto 0.45 µm nitrocellulose membrane at 4°C, at a constant voltage of 100 V for 60 min using wet transfer system with transfer buffer containing 1% SDS. After transfer, the membranes were blocked in 3% milk in TBST for one hour at room temperature and incubated in antibodies as described for the western blotting procedure.

3.3.16 Supernatant precipitation

For supernatant precipitation, the supernatant was harvested into an Eppendorf tube and centrifuged for 5 min at 450 x *g*. Next, 700 µl of the supernatant was transferred into a fresh tube, and 700 µl of methanol and 175 µl of chloroform were added, the tube was vortexed and centrifuged at 18 000 x *g* for 5 min. After centrifugation, the top layer was removed, and 700 µl of methanol was added. The tube was vortexed and centrifuged again. Next, the liquid was removed, 1x Laemmli buffer was added, and the samples were denatured for 10 min at 95°C.

3.3.17 DSS crosslinking

For DSS crosslinking experiments, N/TERT-1 keratinocytes were plated at 10^6 cells per well in a 6-well plate. The cells were infected and stimulated as indicated, after which

the supernatant was transferred into an Eppendorf tube and centrifuged for 5 min at 450 x *g* to collect the dead cells. In the meantime, the cells in the wells were detached with 0.05% Trypsin-EDTA. The supernatant was removed from the centrifuged cells, detached cells were added and washed twice with PBS (pH 8). The cells were resuspended in 200 µl PBS (pH 8) and split into two tubes. To one of the duplicates, DSS resuspended in DMSO was added to the final concentration of 4.4 mM, and the samples were incubated for 30 min at room temperature. After incubation, Laemmli buffer was added to the final concentration of 1x, and the samples were denatured for 10 min at 95°C.

3.4 Molecular biology methods

3.4.1 Competent bacteria

For cloning, the following *E. coli* strains were used: DH5alpha, One Shot TOP10, and STELLAR. Chemically competent bacteria were generated as described in the brochure 'Subcloning Notebooks' by Promega.

3.4.2 Polymerase chain reaction (PCR)

Primers for DNA amplification and Gibson assembly were designed using SnapGene. When possible, the melting temperature was 60°C. For Gibson assembly, homology arms were designed to have the melting temperature of 60°C. The DNA of interest was amplified from a plasmid using Phusion polymerase (Thermo Fisher Scientific). The reaction was prepared as follows:

GC buffer	12 µl
dNTPs (10 mM)	1.2 µl
Forward primer (100 µM)	0.3 µl
Reverse primer (100 µM)	0.3 µl
Phusion polymerase (2 U/µl)	0.6 µl
Template DNA (1 ng/µl)	10 µl
H_2O	35.6 µl

The following protocol was used for PCR:

Initial denaturation	98°C		
Denaturation	98°C	3 min	1x
Annealing	60-70°C	10 s	
Extension	72°C	30 s	30-32x
Final extension	72°C	30 s/1 kb	
Hold	12°C	7 min	1x
Lid	105°C		

3.4.3 Restriction digestion

The restriction digestion mix was prepared as follows:

Plasmid	8 µg
FD Green buffer	4 µl
Enzyme(s) (10 U/µl)	1 µl each
H_2O	to 40 µl

The sample was incubated for 3 h at 37°C, and the enzymes were inactivated for 5 min at 85°C.

3.4.4 Agarose gel electrophoresis

The products of PCR and restriction digestion were separated on agarose gel. In detail, 1% agarose solution in TAE buffer was prepared by heating. Next, Sybr Safe DNA Stain was added, and the gel was poured into an electrophoresis chamber and allowed to set. Samples and GeneRuler marker were loaded and run at 120-140 V for 30-60 min. The gel was imaged using the Gel Doc XR+ with Image Lab Software, and the backbones and inserts were cut out and purified using a QIAquick gel purification kit according to the manufacturer's instructions.

3.4.5 Ligation

For ligation, T4 DNA ligase was used according to the manufacturer's instructions. In short, 50 ng of the vector was mixed with inserts in a 20 µl reaction at the ratio of 1:3

with 1 U of the T4 enzyme, 2 µl of ligase buffer, and water. The samples were incubated for 2-16 h at room temperature.

3.4.6 Gibson assembly

Gibson assembly was prepared by mixing 10 µl of Gibson mix (MPI of Biochemistry Protein Production Core Facility) with 50 ng of the vector and inserts at the ratio of 1:3 and water to 20 µl. The sample was incubated at 50°C for 1 h 15 min.

3.4.7 Transformation of chemically competent E. coli

For *E. coli* transformation, 4 µl of Gibson assembly or ligation reaction were incubated with *E. coli* suspension on ice for 5-30 min. Next, bacteria were heat shocked by placing them on a heating block for 45 s at 42°C and transferring them back on ice for 2-5 min. Transformed bacteria were either directly streaked on LB-agar plates containing the appropriate antibiotic or incubated in antibiotic-free LB medium for 40 min at 36°C before streaking. Bacteria on the agar plate were incubated overnight at 37°C. The next day, colonies were picked, inoculated in LB medium containing antibiotic, and incubated in a shaking incubator for 8-16 h at 37°C, after which plasmids were isolated.

3.4.8 Plasmid isolation from E. coli

Plasmids were isolated from *E. coli* according to the QIAgen Spin Miniprep Kit protocol using homemade buffers. Plasmids were sequenced by Sanger sequencing, and colonies containing the correct insert were expanded for isolation of higher amounts of DNA with PureLink Maxiprep kit according to the manufacturer's instructions.

3.4.9 HSV-1 ORF library preparation

HSV-1 ORF library was a gift from Jan Rehwinkel (University of Oxford) and David Koelle (University of Washington, (139)). HSV-1 ORF library was transformed into chemically competent DH5alpha in a 96-well format as described earlier. Bacteria were streaked on agar plates with ampicillin and incubated overnight at 37°C, after which one colony per ORF was picked and grown overnight in LB medium with ampicillin. Plasmids were

isolated using the Promega PureYield Plasmid Miniprep System according to the manufacturer's instructions.

3.5 Data analysis and figure preparation

Data was plotted and statistically analyzed using GraphPad Prism. Flow cytometry data was analyzed using FlowJo. Cloning primers were designed using SnapGene. Illustrations of proteins and signaling pathways were prepared using BioRender.

4. Results

4.1 HSV-1 inhibits inflammasome activation

4.1.1 HSV-1 inhibits NLRP1 activation

To determine the effects of HSV-1 infection on NLRP1 inflammasome, we used N/TERT-1 immortalized keratinocytes. Those cells are often employed in the studies of NLRP1; they constitutively express all relevant inflammasome components and do not require priming for induction of pro-IL-1β expression. We infected the cells with HSV-1 and stimulated them with different NLRP1 inflammasome-activating stimuli: the DPP8/9 inhibitor, Val-boroPro (VbP), a synthetic analog of dsRNA, poly(I:C), and ribotoxic stress response (RSR)-inducing agent, anisomycin (ANS). Each of these stimuli activates the NLRP1 inflammasome by a different mechanism: VbP by inhibition of DPP9 which forms a complex with NLRP1, poly(I:C) by direct binding to NLRP1, and ANS by induction of RSR. Every activator induced IL-1β and IL-18 release from N/TERT-1 cells (Fig. 4.1.1A and B). Intriguingly, the release of both cytokines was strongly decreased by pre-treatment with HSV-1. In many of the subsequent experiments, we used ANS to activate NLRP1 as it displays the fastest kinetics, thus reducing the likelihood that the decrease in cytokine release is an unspecific effect of HSV-1 infection or caused by cell death. To exclude the possibility that decreased cytokine release after HSV-1 pre-treatment is caused by the downregulation of inflammasome components, we verified their expression by western blotting. We found no decrease in the expression of IL-1β or any of the other proteins involved in the NLRP1 signaling pathway (Fig. 4.1.1C). We further found that the inhibitory effect of HSV-1 was dose-dependent, as increasing the MOI decreased the ANS-stimulated IL-1β release (Fig. 4.1.1D).

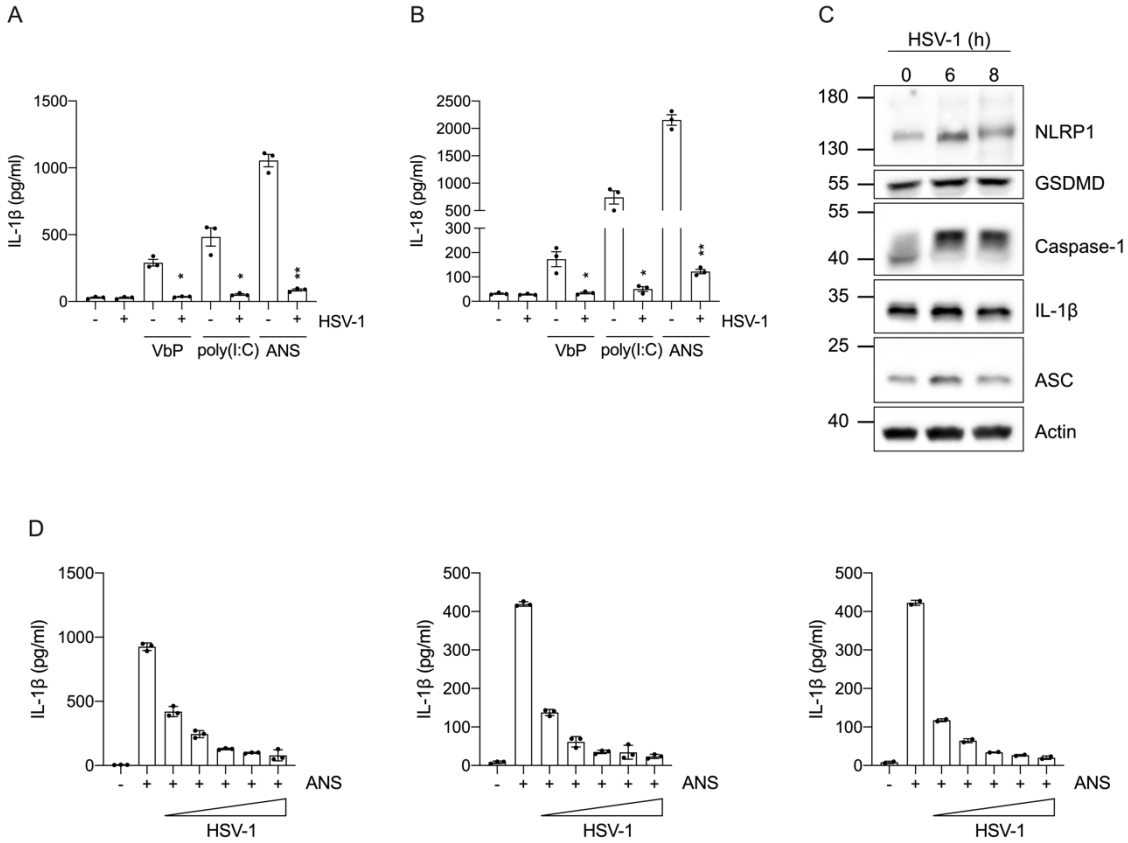

Fig. 4.1.1 (**A**) IL-1β and (**B**) IL-18 release from N/TERT-1 cells infected with HSV-1 at MOI 5 for 8 h, or pre-treated with HSV-1 for 1, 2, or 4 h and stimulated with VbP for 7 h, poly(I:C) for 6 h, or ANS for 2 h, respectively. Graphs represent mean ± SEM of 3 independent experiments. Data was analyzed by Holm-Sidak multiple paired t-tests comparing VbP/pIC/ANS-only to HSV-1 pre-treated cells (*p<0.05, **p<0.01). (**C**) N/TERT-1 cells were infected with HSV-1 at MOI 5 for the indicated time, and the expression of inflammasome components was determined by western blot. Depicted is one representative experiment of three. (**D**) IL-1β release from N/TERT-1 cells infected with HSV-1 at MOI 1 to 5 for 4 h and stimulated with ANS for 2 h. Each graph represents a separate experiment, bars represent mean ± SD of 2-3 biological replicates.

4.1.2 HSV-1 inhibits NLRP3 activation

To determine if the inhibitory effect of HSV-1 was specific to NLRP1 inflammasome, we generated NLRP1-deficient N/TERT-1 keratinocytes and complemented them with human NLRP1 (hsNLRP1) or hsNLRP3. We pre-treated the cells with HSV-1 for the indicated time and stimulated them with ANS or Nigericin, an NLRP3 activator

(Fig. 4.1.2A and B). The inflammasome activation was measured by the release of IL-1β and lactate dehydrogenase (LDH), a marker of pyroptotic cell death. We observed a significant decrease in NLRP1-mediated IL-1β and LDH release at 6 and 4 h pre-treatment. HSV-1 also reduced NLRP3 activation, although to a lesser extent. LDH release was not significantly decreased, whereas the IL-1β release was significantly decreased at all time points. Thus, HSV-1 inhibits both NLRP1 and NLRP3 inflammasome signaling.

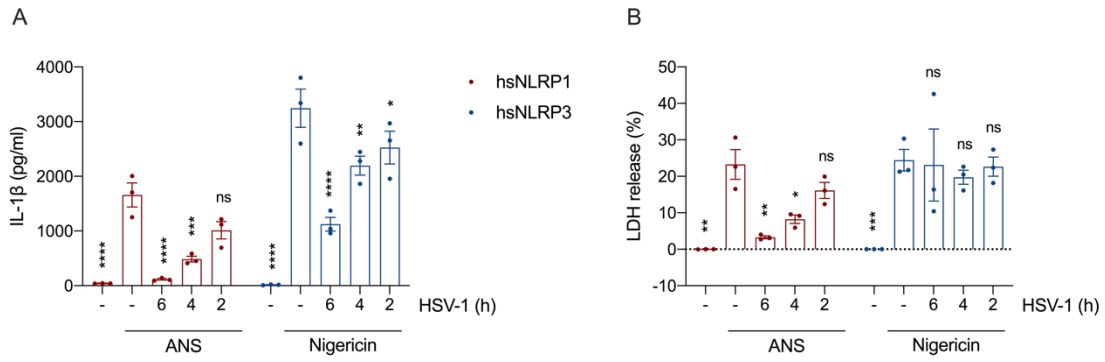

Fig. 4.1.2 (**A**) IL-1β and (**B**) LDH release from NLRP1-deficient N/TERT-1 cells complemented with hsNLRP1 or hsNLRP3 pre-treated with HSV-1 at MOI 5 for indicated time and stimulated with ANS or Nigericin for 2 h. Graphs represent mean ± SEM of 3 independent experiments. Data was analyzed by two-way ANOVA with Dunnett's multiple comparisons test comparing to Nigericin/ANS-stimulated cells (* p<0.05, **p<0.01, ***p<0.001, ****p<0.0001; ns, not significant).

4.1.3 HSV-1 infection prevents ASC polymerization

To verify which step of the inflammasome pathway is inhibited by HSV-1, we examined ASC polymerization; this step directly follows the sensor molecule oligomerization and is shared by the NLRP1 and NLRP3 pathways. First, we determined ASC dimerization by western blotting. To this end, we stimulated N/TERT-1 keratinocytes complemented with hsNLRP1 and hsNLRP3 with ANS or Nigericin, respectively, with or without HSV-1 pre-treatment. In DSS-crosslinked cells, ASC dimers were detectable after ANS and Nigericin stimulation, and pre-treatment with HSV-1 inhibited the dimerization in both cases (Fig. 4.1.3A). In addition, cleaved caspase-1, a hallmark of inflammasome

activation, was detectable in the supernatants of ANS- and Nigericin-stimulated cells but not in virus-infected cells (Fig. 4.1.3A). ASC polymerization can also be detected by microscopy and flow cytometry using ASC tagged with a fluorescent protein (96). In unstimulated cells, ASC is distributed across the cytoplasm, whereas upon stimulation, it forms specks. To this end, we generated HEK293T cells that constitutively express ASC tagged with mCherry (ASC-mCherry) and hsNLRP1 or hsNLRP3 (referred to as NLRP1-ASC and NLRP3-ASC HEKs, respectively). We stimulated the cells with ANS or Nigericin with or without HSV-1 pre-treatment. As expected, ANS caused ASC specking in NLRP1-ASC HEKs, which was reduced by HSV-1 pre-treatment. Nigericin caused specking in NLRP3-ASC HEKs, but surprisingly, it was not reduced by pre-treatment with HSV-1 (Fig. 4.1.3B). This lack of inhibition could have been caused by higher transgene expression in HEK cells than in N/TERT-1 cells. To examine ASC polymerization in keratinocytes, we used ASC-deficient N/TERT-1 cells complemented with ASC-mCherry. Stimulation with ANS or poly(I:C) caused the formation of ASC specks and pyroptotic cell death, characterized by balloon-like swelling. Pre-treatment with HSV-1 prevented the formation of ASC specks and decreased the number of pyroptotic cells (Fig. 4.1.3C). Overall, this data indicates that HSV-1 inhibits NLRP1 and NLRP3 inflammasomes at or upstream of ASC polymerization.

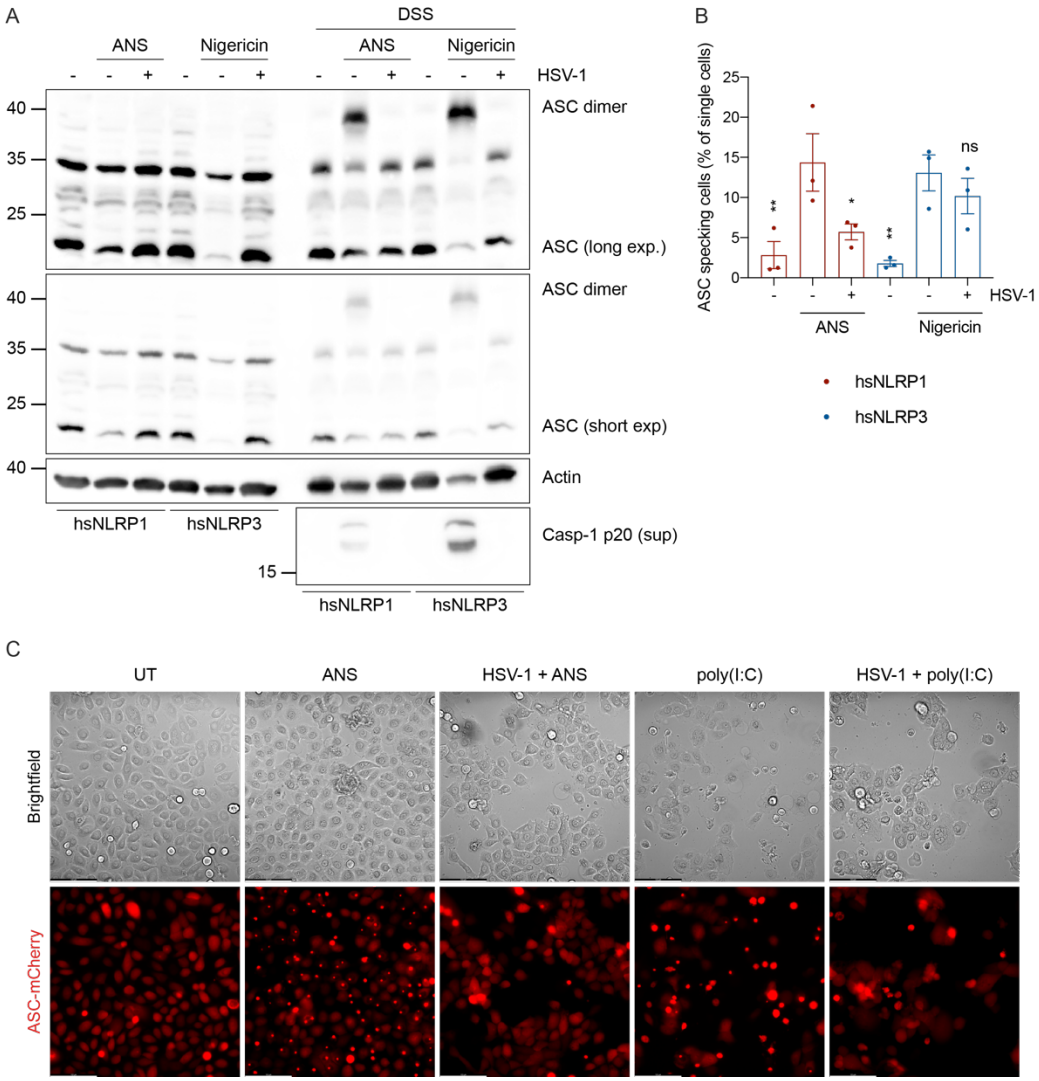

Fig. 4.1.3 (**A**) N/TERT-1 cells complemented as in Fig. 4.1.2 were infected with HSV-1 at MOI 5 for 4 h, stimulated with ANS or Nig for 2 h, and treated with DSS or left untreated. ASC dimerization was determined by western blotting. Depicted is one representative experiment out of two. (**B**) ASC specking in NLRP1-ASC and NLRP3-ASC HEKs pre-treated with HSV-1 at MOI 5 for 6 h and stimulated with ANS or Nigericin for 2 h. Bars represent mean ± SEM of three independent experiments. Data was analyzed by two-way ANOVA with Dunnett's multiple comparisons test comparing to ANS/Nigericin-stimulated cells (* $p<0.05$, ** $p<0.01$; ns, not significant). (**C**) ASC-deficient N/TERT-1 keratinocytes complemented with ASC-mCherry were pre-treated with HSV-1 for 2 h or 4h and stimulated with ANS for 2 h or poly(I:C) for 6 h, respectively. Bars represent 100 µm. Images are representative of three independent experiments.

4.2 Identification of HSV-1 ORF responsible for inhibiting NLRP1 inflammasome

4.2.1 NLRP1 is not inhibited by HSV-1 tegument protein

Next, we set out to identify the protein responsible for inflammasome inhibition. To verify if it is delivered within the viral tegument, we irradiated HSV-1 with UV light to prevent viral gene expression. To determine if the UV irradiation was successful, we measured the viability of HSV-1-infected keratinocytes. We reasoned that after prolonged stimulation, the untreated virus would cause cell death, and the irradiated virus would be unable to express genes necessary for replication and not cause cell death or changes in cell morphology. We found that untreated HSV-1 did not cause a decrease in viability; however, it changed keratinocyte morphology to clusters of rounded cells (Fig. 4.2.1A and B). Infection with the irradiated virus did not cause any changes in morphology, suggesting a disruption in viral gene expression. Upon infection of N/TERT-1 cells and stimulation with ANS, we observed that UV-irradiation decreased HSV-1's ability to inhibit NLRP1 inflammasome; irradiated HSV-1 did not reduce IL-1β release after ANS treatment. In contrast, the untreated virus decreased it almost to the baseline (Fig. 4.2.1C). Thus, these experiments suggested that the protein inhibiting NLRP1 is not part of the viral tegument.

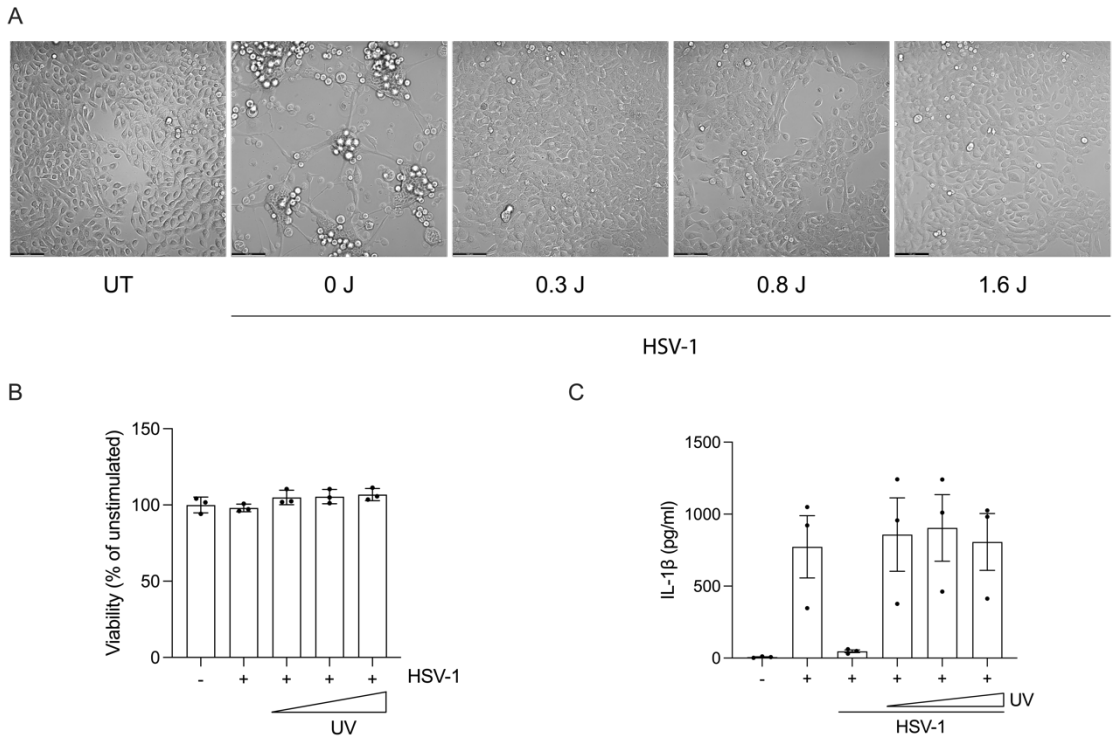

Fig. 4.2.1 (**A**) Images of N/TERT-1 cells infected with untreated or UV-irradiated HSV-1 at MOI 5 for 24 h. Bars represent 100 µm. Images are representative of one experiment. (**B**) Viability of N/TERT-1 cells infected as in (A). Bars represent mean ± SD of three biological replicates from one experiment. (**C**) IL-1β release from N/TERT-1 keratinocytes infected with untreated or UV-irradiated HSV-1 at MOI 5 for 4 h and stimulated with ANS for 2 h. Bars represent mean ± SEM of three independent

4.2.2 Screen of HSV-1 ORF library

To identify which HSV-1 open reading frame (ORF) encodes an NLRP1 inhibitor, we designed a screen of the HSV-1 ORF library. We turned to NLRP1-ASC HEKs as transfection of HEK cells is more efficient than N/TERT-1 keratinocytes. To screen the HSV-1 ORF library, we transfected NLRP1-ASC HEKs with two plasmids: one encoding BFP and the other encoding either a viral ORF or mNeon used as a control. To increase the sensitivity of our screen, we analyzed ASC specking only the BFP-positive population (Fig. 4.2.2A and B). We conducted three screens and identified four ORFs that decreased specking by more than 50% compared to mNeon in two or more screens: UL23 thymidine kinase, which came up in two screens, and UL26.5 capsid scaffolding protein, UL36A, and RL2-F2, which came up in three screens (Fig. 4.2.2C and D). Two of those - UL36A and RL2-F2 – had been previously reported to play a role in immune evasion. UL36A encodes a fragment of UL36 large tegument protein, which has deubiquitinating enzyme (DUB) activity (Fig. 4.2.3A). RL2-F2 is the second exon of the RL2 gene, which encodes the protein ICP0, an E3 ubiquitin ligase (Fig. 4.2.3B, details on the ORF library and splitting of UL36 and RL2 can be found in the Methods section).

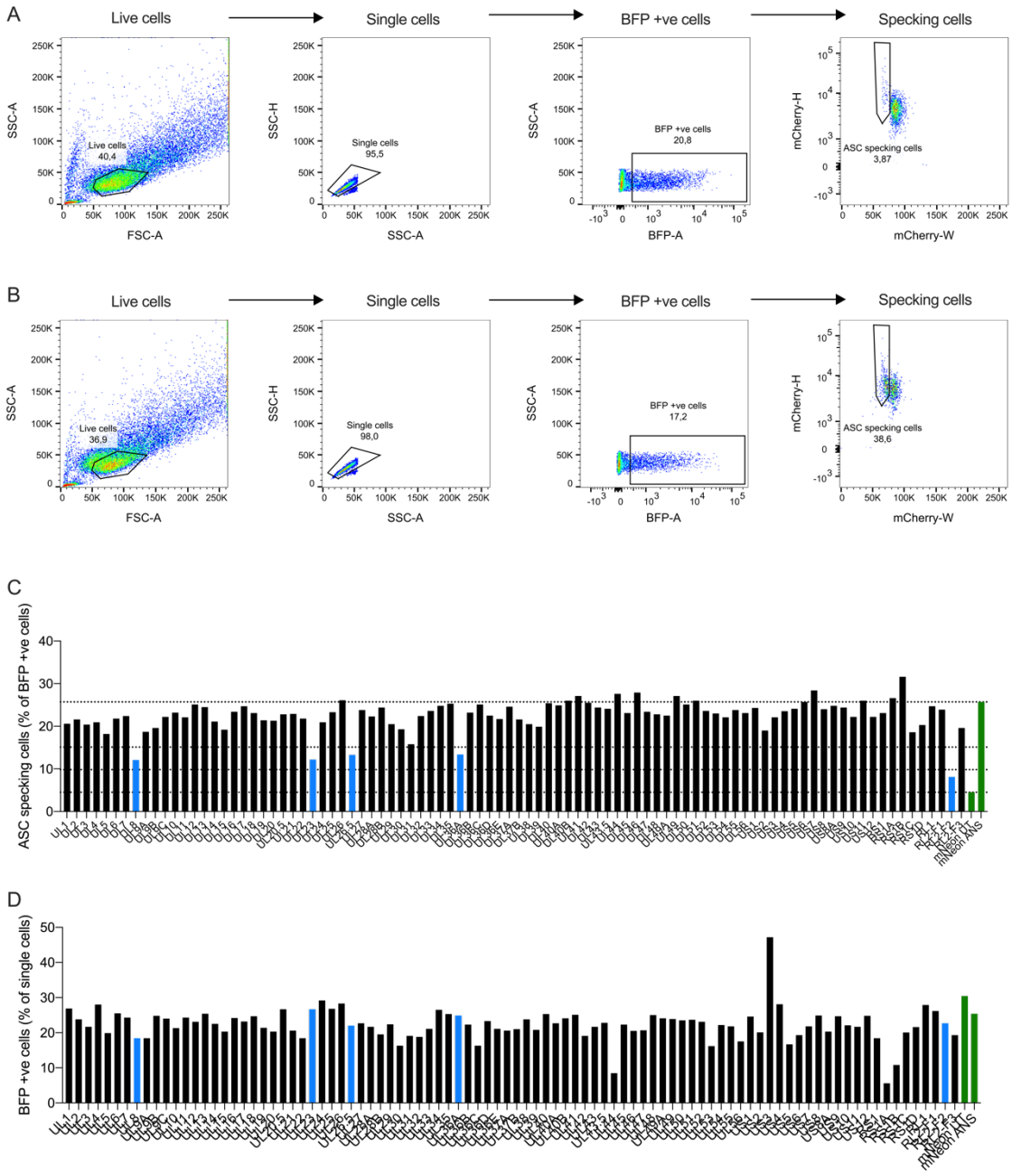

Fig. 4.2.2 Gating strategy for ORF library screens showing mNeon-transfected cells (**A**) left untreated or (**B**) stimulated with ANS for 4 h. The plots are representative of three screens. (**C**) Percentage of ASC specking and (**D**) BFP-positive NLRP1-ASC HEKs transfected with BFP and HSV-1 ORFs and stimulated with ANS for 4 h. Each bar represents cells from one well. Blue bars represent ORFs that decreased ASC specking by more than half, and green bars represent mNeon controls. Dotted lines represent specking of the ANS-stimulated and untreated control cells and 50% and 25% of the difference. The graphs are representative of three independent screens.

To validate our hits, we expressed these ORFs again in NLRP1-ASC HEKs. After stimulation with ANS, all ORFs reduced ASC specking; however, after stimulation with VbP, UL26.5 did not cause a significant decrease in specking. None of the ORFs caused a significant change in the proportion of BFP-positive cells (Fig. 4.2.3C). In addition, we examined mutant versions of UL36A and RL2-F2. UL36 is thought to be cleaved during the infection, generating an N-terminal fragment with DUB activity ($UL36^{USP}$, Fig. 4.2.3A). $UL36^{USP}$ length is estimated to be approximately 500 amino acids, which constitutes half of the UL36A library fragment (143,144). The DUB activity is abolished by the C40A mutation (Fig. 4.2.3A (143,144)). ICP0 contains multiple sites important for interactions with a variety of proteins. RL2-F2 corresponds to the second exon, which encompasses the RING domain and the phosphorylation site needed for the recruitment of a cellular ubiquitin ligase RNF8 (T67, Fig. 4.2.3B). We generated two RL2-F2 mutants: one with two mutations within the RING domain, C116G and C156A, which abolish ubiquitin ligase activity (RING finger mutant, FRm (145)), and one with T67A mutation, which impairs the interaction with RNF8 (146). Upon ANS stimulation, WT UL36A decreased the percentage of specking cells moderately but significantly, and the C40A mutation abolished the inhibitory effect (Fig. 4.2.3D). RL2-F2 was even more efficient in inhibiting ASC specking and decreased the proportion of specking cells to that of unstimulated cells. The T67A mutation did not affect the inhibition, whereas the RFm mutant could no longer inhibit specking. As in the previous experiment, the ORFs did not significantly change the proportion of BFP-positive cells. Overall, our data suggests that ICP0 and UL36 can inhibit NLRP1 inflammasome.

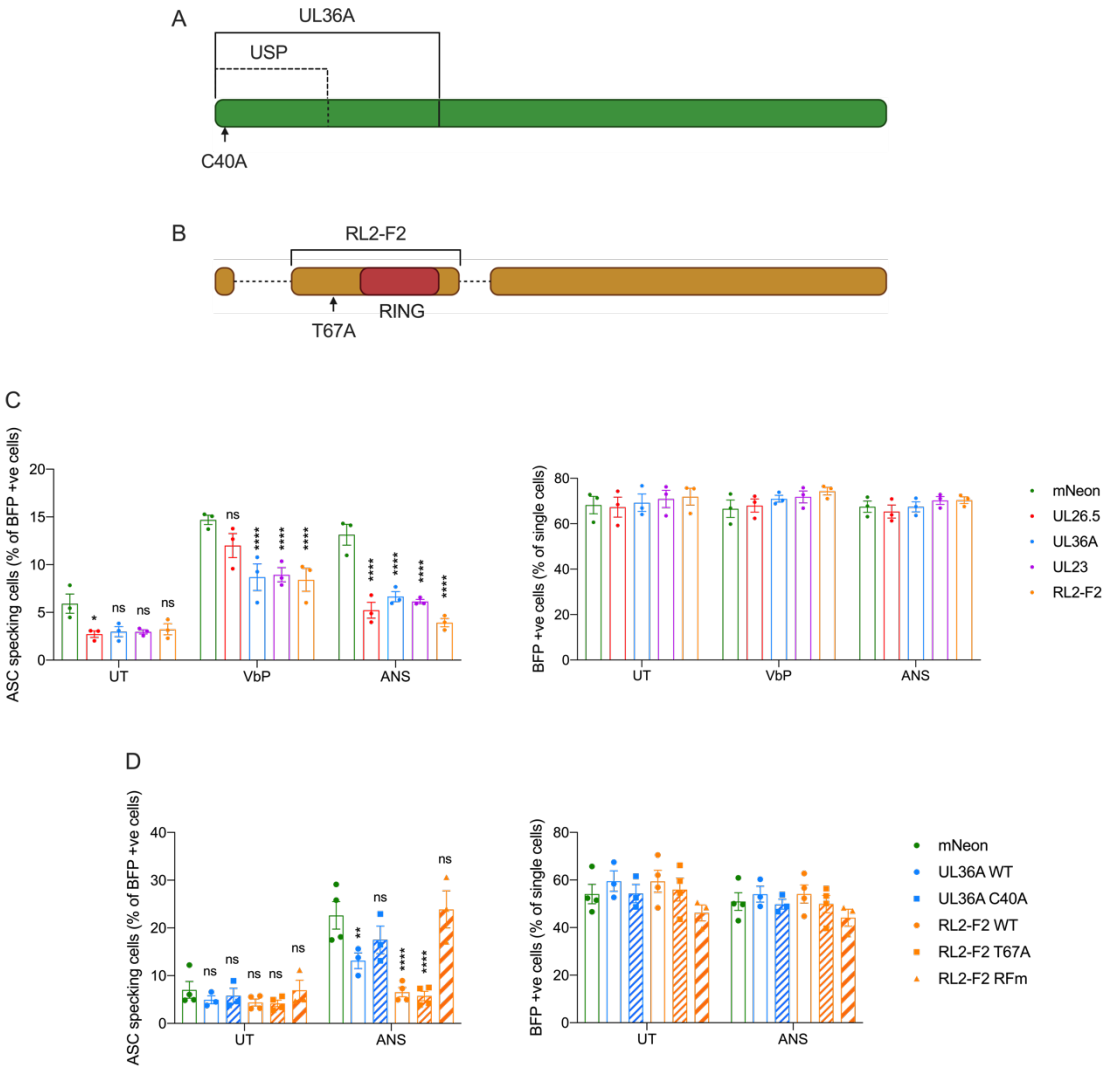

Fig. 4.2.3 (**A**) Schematic overview of UL36. UL36A corresponds to the library fragment, and USP corresponds to the UL36^{USP} fragment with DUB activity. The arrow indicates the mutation that abolishes DUB activity. (**B**) Schematic overview of ICP0 (adapted from Gu, 2016). The three fragments represent three exons. RL2-F2 is designated with a highlighted RING domain. The arrow indicates the mutation that abolishes the interaction with RNF8. The images in (A) and (B) are not to scale. (**C**) Percentage of ASC specking (left) and BFP-positive (right) NLRP1-ASC HEKs transfected with HSV-1 ORFs or mNeon and stimulated with VbP for 4 h or ANS for 2 h. (**D**) Percentage of ASC specking (left) and BFP-positive (right) NLRP1-ASC HEKs transfected with WT or mutant UL36A or RL2 or mNeon and stimulated with ANS for 2 h. Graphs in (C) and (D) represent mean ± SEM of 3-4 independent experiments. Data was analyzed by two-way ANOVA with Dunnett's multiple comparisons test comparing ORFs to mNeon control (* p<0.05, **p<0.01, ****p<0.0001; ns, not significant). There were no significant differences between the percentages of BFP-positive cells.

4.3 ICP0 inhibits the NLRP1 inflammasome

4.3.1 Expression of ICP0 prevents NLRP1 inflammasome activation

As ICP0 inhibited NLRP1-mediated ASC specking more strongly than UL36A, and the inhibition depended on the ubiquitin ligase activity, we chose to focus on it for more in-depth analysis. We expressed full-length WT ICP0 (encoded by the gene RL2) and ICP0 lacking the RING domain (RL2xE) in NLRP1-ASC HEKs and stimulated them with VbP or ANS (Fig. 4.3.1A). As expected, the full-length ICP0 reduced ANS-induced ASC specking almost to baseline, whereas ICP0 lacking the RING domain had no effect. We found that ICP0 was less efficient in decreasing VbP-induced ASC specking. However, the inhibition was significant and abolished by removing the RING domain. WT and mutated ICP0 did not affect transfection efficiency, measured by the percentage of BFP-positive cells (Fig. 4.3.1A).

To determine if ICP0 affects the activation of endogenously expressed NLRP1, we generated N/TERT-1 keratinocytes that express WT or RFm ICP0 under a doxycycline-inducible promoter. In line with the previous experiments in HEK cells, WT but not RFm ICP0 decreased ANS-induced IL-1β release (Fig. 4.3.1B). Furthermore, we validated the expression of ICP0 by western blotting. We found that the levels of RFm were a lot higher than those of WT ICP0, which was barely detectable (Fig. 4.3.1C). This difference is likely caused by autoubiquitination and increased degradation of WT ICP0 (147). Overall, these data demonstrated that expression of ICP0 in NLRP1-ASC HEKs and keratinocytes decreases ANS-induced ASC specking and IL-1β release.

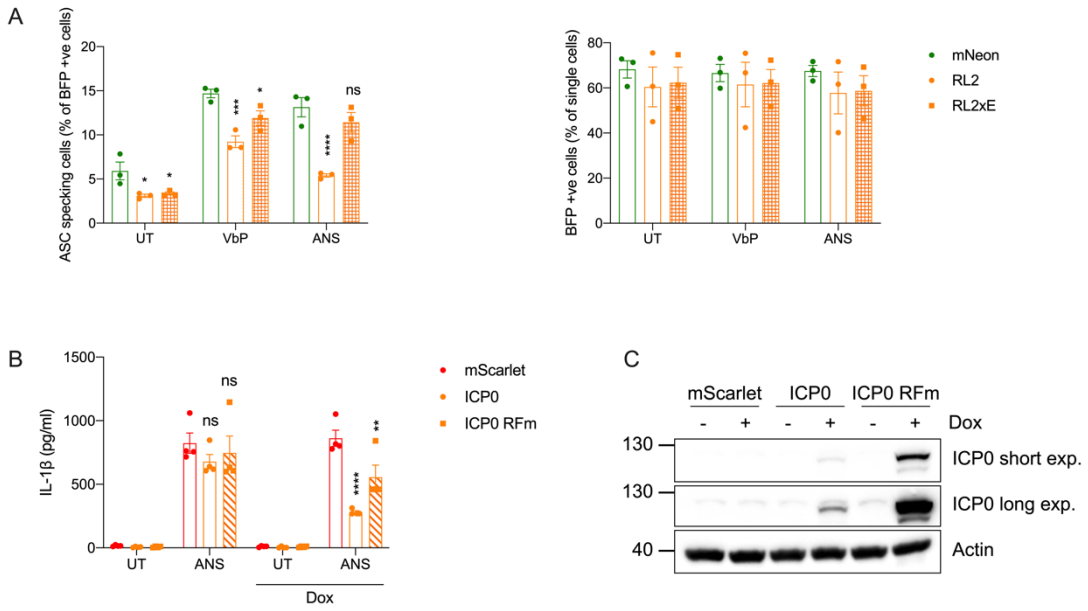

Fig. 4.3.1 (**A**) Percentage of ASC specking (left) and BFP-positive (right) NLRP1-ASC HEKs transfected with full-length ICP0 (RL2), ICP0 lacking RING domain (RL2xE) or mNeon and stimulated with VbP for 4 h or ANS for 2 h. Bars represent mean ± SEM of three independent experiments. The experiments were conducted with Fig. 4.2.3C and shown separately for clarity with the same mNeon control; statistical analysis was conducted separately. (**B**) IL-1β release from N/TERT-1 keratinocytes transgenic for doxycycline-inducible FLAG-mScarlet, ICP0 or ICP0 RFm incubated with doxycycline overnight and stimulated with ANS for 2 h. Bars represent mean ± SEM of four independent experiments. (**C**) ICP0 expression levels in transgenic N/TERT-1 keratinocytes from (B) after overnight incubation with doxycycline analyzed by western blotting. The data depicted is representative of three independent experiments. Data in (A) and (B) was analyzed by two-way ANOVA with Dunnett's multiple comparisons test comparing to mNeon (A) or FLAG-mScarlet control (* p<0.05, **p<0.01, ***p<0.001, ****p<0.0001; ns, not significant). There were no significant differences between the percentage of BFP-positive cells in (A).

4.3.2 ICP0 is required for NLRP1 inhibition during HSV-1 infection

To determine if ICP0 plays a role in NLRP1 signaling during HSV-1 infection, we used ICP0-deficient virus (dICP0). As expected, pre-treatment with WT HSV-1 decreased IL-1β release almost to baseline, whereas dICP0 HSV-1 reduced it mildly but significantly (Fig. 4.3.2A). To avoid the possibility that viral titers differ between genotypes and effectively different MOIs are used, we determined HSV-1 protein levels by western blotting.

Replication of the dICP0 HSV-1 is considerably reduced in many cell types, as ICP0 plays a role in the expression of other viral genes; therefore, we used U2OS cells, which support the replication of the dICP0 virus. We observed that the levels of the HSV-1 tegument protein ICP4 are similar between cells infected with WT and dICP0 HSV-1 (Fig. 4.3.2B). Thus, ICP0 expression during HSV-1 infection is needed for NLRP1 inhibition.

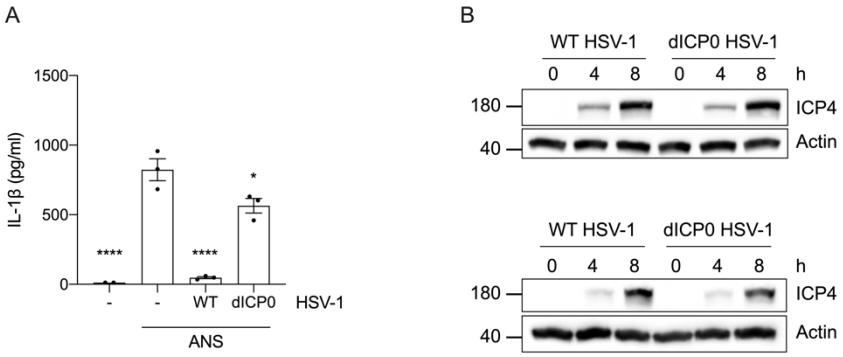

Fig. 4.3.2 (**A**) IL-1β release from N/TERT-1 keratinocytes pre-treated with WT or dICP0 HSV-1 at MOI 5 for 4 h and stimulated with ANS for 2 h. Bars represent mean ± SEM of three independent experiments. Data was analyzed by one-way ANOVA with Dunnett's multiple comparisons test comparing to ANS-stimulated cells (* $p<0.05$, ****$p<0.0001$). (**B**) Expression of ICP4 in U2OS cells infected with WT or dICP0 HSV-1 at MOI 1 for 4 or 8 h analyzed by western blotting. The blots represent two independent experiments.

4.4 ICP0-deficient HSV-1 does not activate NLRP1 inflammasome

Since HSV-1 developed a mechanism for inflammasome inhibition, we reasoned that the dICP0 virus would activate NLRP1. Unexpectedly, prolonged stimulation with dICP0 HSV-1 did not cause IL-1β release in N/TERT-1 keratinocytes (Fig. 4.4A). We hypothesized that HSV-1 could activate NLRP1 in one of two ways: by generation of dsRNA, which would directly bind to NLRP1, or by expression of a protein, which directly or indirectly would activate NLRP1. We speculated that ICP0 deficiency may decrease the generation of dsRNA or viral protein expression. To test the first hypothesis, we infected N/TERT-1 keratinocytes with WT HSV-1 to determine the generation of dsRNA. As a control, we used the Semliki Forest virus (SFV), which is known to produce dsRNA

and activate NLRP1 inflammasome (95). We detected dsRNA in SFV- but not HSV-1-infected cells (Fig. 4.4B). Therefore, NLRP1 could not be activated by dsRNA during HSV-1 infection.

The NLRP1 inflammasome is activated by the RSR, which leads to the ZAK kinase and mitogen-associated protein kinase (MAPK) pathway activation; this results in the hyperphosphorylation of the disordered region (DR) of NLRP1 and inflammasome assembly. The DR has phosphorylation sites for ZAKα and p38, a kinase from the MAPK pathway. To examine the effect of HSV-1 on the DR phosphorylation, we generated a construct consisting of the N-terminal PYD and DR, followed by mNeon. Due to a smaller size, phosphorylation of this construct can be detected more easily by western blotting than the full-length NLRP1. We expressed this construct in NLRP1-deficient N/TERT-1 cells, stimulated them with WT or dICP0 HSV-1 and ANS, and analyzed DR phosphorylation by western blotting after separation on Phos-tag gel (Fig. 4.4C and D). mNeon appeared in unstimulated cells as a double band, which is in line with the reports showing it is constitutively phosphorylated. As expected, ANS caused a robust shift, indicating phosphorylation of the construct. Intriguingly, stimulation with WT HSV-1 also led to a shift, although not as strong as ANS; in contrast, dICP0 HSV-1 did not cause a band shift, and the signal was comparable to that of untreated cells. The shift could also be observed after separation with regular SDS-PAGE. Furthermore, we found that both WT and dICP0 cause p38 phosphorylation, although weaker than ANS (Fig. 4.4A).

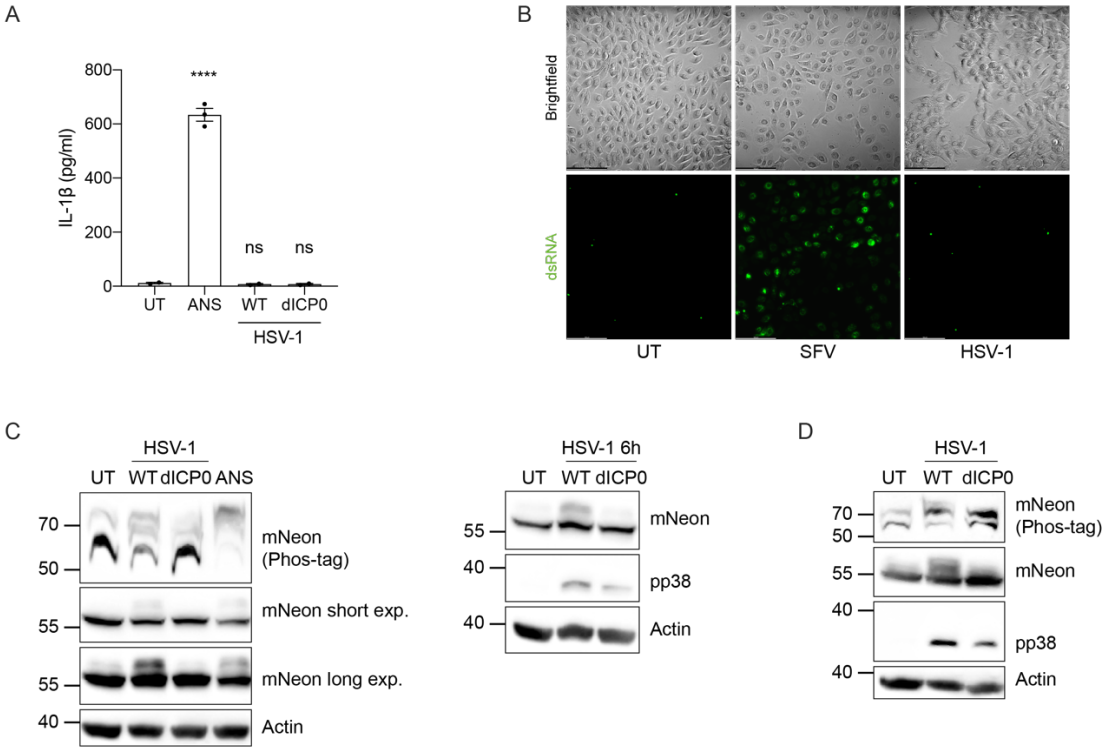

Fig. 4.4 (**A**) IL-1β release from N/TERT-1 keratinocytes stimulated with ANS for 2 h or infected with WT or dICP0 HSV-1 at MOI 10 for 22 h. The bars represent mean ± SEM of three independent experiments. Data was analyzed by one-way ANOVA with Dunnett's multiple comparisons comparing to untreated cells (****p<0.0001; ns, not significant). (**B**) N/TERT-1 cells were infected with SFV at MOI 5 for 7 h or with HSV-1 at MOI 5 for 6 h and stained for dsRNA. Bars represent 100 µm. Images are representative of two independent experiments. (**C** and **D**) NLRP1-deficient N/TERT-1 cells complemented with hsNLRP1(PYD-DR)-mNeon were infected with WT or dICP0 HSV-1 at MOI 5 for 6 h or stimulated with ANS for 2 h. Proteins were separated by Phos-tag (where indicated) or tris-glycine gel electrophoresis, and p38 and mNeon phosphorylation were analyzed by western blotting. Data in (C) and (D) depicts two independent experiments.

4.5 MVA inhibits inflammasome activation

4.5.1 MVA inhibits NLRP1 inflammasome

MVA is a dsDNA virus that can infect epithelial cells. Therefore, we hypothesized that it may affect NLRP1 inflammasome activation. To examine this, we turned again to the N/TERT-1 keratinocyte model. We pre-treated the cells with different MOIs of MVA before stimulating them with ANS. We found that with increasing MOI, MVA decreased

the release of IL-18 from keratinocytes (Fig. 4.5.1.A). IL-18 is another cytokine cleaved by caspase-1 upon inflammasome activation. We used it as a read-out for MVA studies instead of IL-1β, as we found that infection with MVA decreased the levels of pro-IL-1β (Fig. 4.5.1.B). Of note, MVA did not consistently cause the downregulation of any other component of the inflammasome signaling pathway, indicating that it inhibited inflammasome assembly.

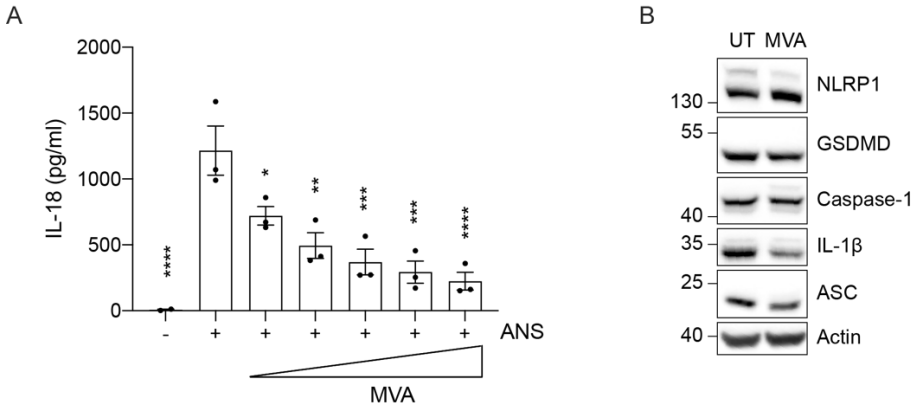

Fig. 4.5.1 (**A**) IL-18 release from N/TERT-1 keratinocytes infected with MVA at MOI 1 to 5 for 4 h and stimulated with ANS for 2 h. The bars represent mean ± SEM of 3 independent experiments. Data was analyzed by one-way ANOVA with Dunnett's multiple comparisons test comparing ANS-only-stimulated cells (* p<0.05, **p<0.01, ***p<0.001, ****p<0.0001; ns, not significant). (**B**) N/TERT-1 keratinocytes were infected with MVA at MOI 5 for 8 h, and the expression of inflammasome components was analyzed by western blotting. The data depicted is representative of three independent experiments.

4.5.2 MVA inhibits CARD8 but not NLRP3 inflammasome

Next, we set out to determine if MVA inhibition is specific for the NLRP1 inflammasome. We pre-treated NLRP1- and NLRP3-expressing N/TERT-1 cells with MVA for the indicated time and stimulated them with ANS or Nigericin (Fig. 4.5.2A and B). MVA decreased both IL-18 and LDH release upon NLRP1 activation, especially at 8 h pre-treatment, although the IL-18 decrease was not statistically significant. In contrast, the levels of NLRP3-mediated LDH and IL-18 release remained unchanged. CARD8 is an inflammasome sensor related to NLRP1, also activated by VbP but not by dsRNA or RSR

induction. N/TERT-1 cells do not express CARD8 endogenously; therefore, to examine the effect of MVA on CARD8 activation, we used NLRP1-deficient N/TERT-1 keratinocytes complemented with CARD8 or NLRP1. We infected the cells with different MOIs of MVA before stimulating them with VbP (Fig.4.5.2C). Surprisingly, we found that MVA decreased VbP-induced IL-18 release only in CARD8-expressing cells, while in NLRP1-expressing cells, the levels of IL-18 remained similar to VbP-only control. Overall, these results indicated that MVA inhibits NLRP1 activation induced by ANS but not VbP. In addition, it inhibits CARD8 but not NLRP3 inflammasome.

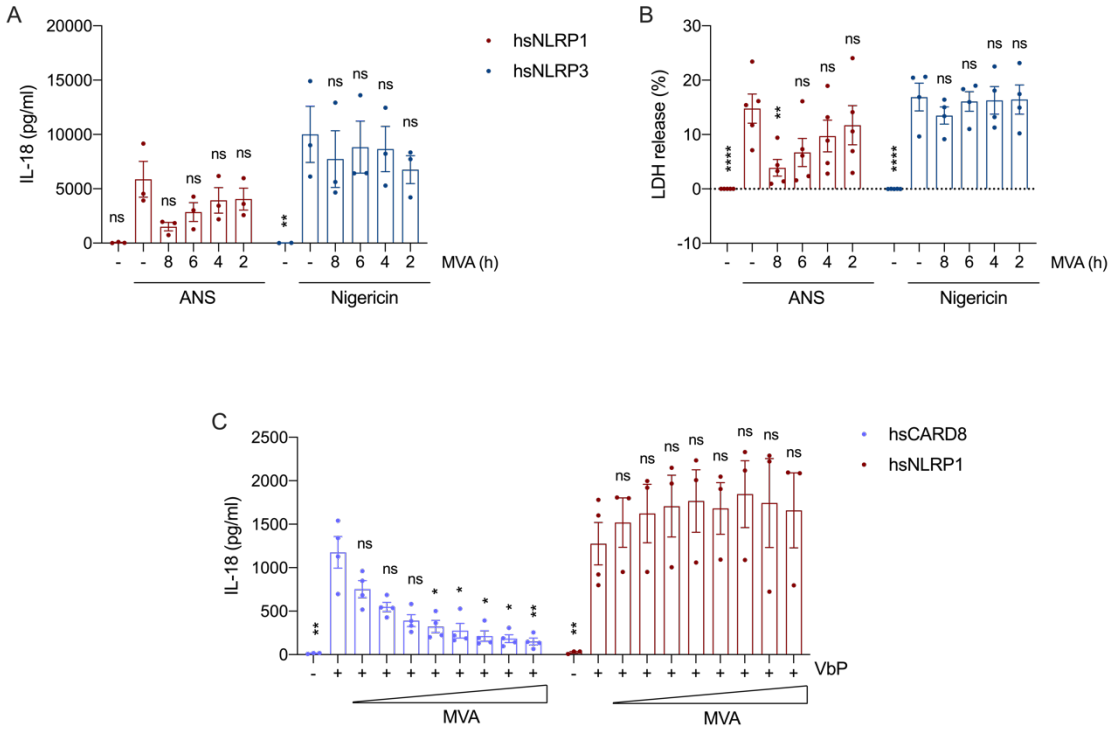

Fig. 4.5.2 (**A**) IL-18 and (**B**) LDH release from N/TERT-1 cells complemented as in Fig. 4.1.2 infected with MVA at MOI 5 for indicated time and stimulated with ANS or Nigericin for 2 h. The bars represent mean ± SEM of 3-5 independent experiments. (**C**) IL-18 release from NLRP1-deficient N/TERT-1 cells complemented with hsCARD8 or hsNLRP1 infected with MVA at MOI 1 to 8 for 2 h and stimulated with VbP for 4 h. The bars represent mean ± SEM of 3-4 independent experiments. The data was analyzed by two-way ANOVA with Sidak's multiple comparisons test comparing to ANS/Nigericin (A and B) or VbP (C) only-stimulated cells (* p<0.05, **p<0.01, ***p<0.001, ****p<0.0001; ns, not significant).

4.6 MVA inhibits NLRP1 inflammasome upstream of ASC polymerization

Our data suggested that the mechanism of MVA inhibition is different for CARD8 and NLRP1, and in subsequent experiments, we focused on the effect of MVA on NLRP1 inflammasome. First, we set out to determine which step of the signaling pathway is inhibited by MVA. We hypothesized that since MVA does not affect NLRP3 signaling, it inhibits NLRP1 inflammasome upstream of ASC polymerization. Indeed, pre-treatment with MVA prevented the formation of ASC dimers on western blot in NLRP1- but not in NLRP3-expressing cells stimulated with ANS or Nigericin, respectively. Furthermore, it inhibited ANS-induced release of cleaved caspase-1 (Fig. 4.6A). To corroborate this data, we turned again to NLRP1-ASC and NLRP3-ASC HEK cells; we infected them with MVA, followed by stimulation with ANS or Nigericin, and analyzed ASC specking by flow cytometry. As expected, MVA decreased the percentage of specking cells in NLRP1- but not in NLRP3-expressing cells (Fig. 4.6B). Next, we analyzed ASC specking and morphology of ASC-mCherry-expressing N/TERT-1 cells; we infected them with MVA and stimulated them with poly(I:C) or ANS. In line with the previous experiments, MVA pre-treatment decreased the number of specking cells after stimulation with poly(I:C) and ANS (Fig. 4.6C). Similarly to HSV-1, MVA prevented pyroptosis as fewer balloon-shaped cells were visible. Overall, these experiments showed that MVA inhibits NLRP1 inflammasome upstream of ASC polymerization.

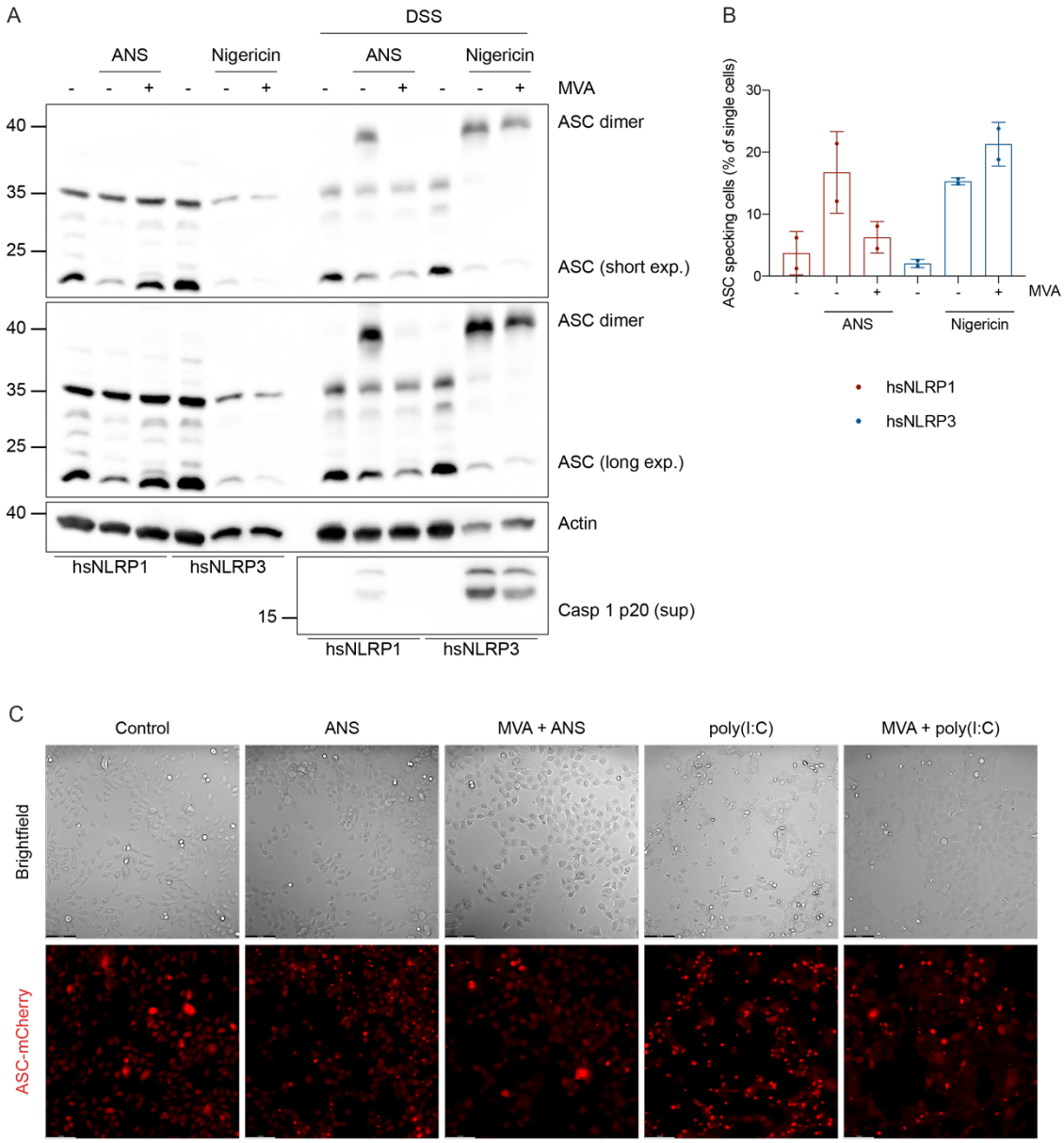

Fig. 4.6 (**A**) N/TERT-1 cells complemented as in Fig. 4.1.2 were infected with MVA at MOI 5 for 4 h, stimulated with ANS or Nigericin for 2 h, and treated with DSS or left untreated. ASC dimerization was determined by western blotting. Depicted is one representative experiment out of two. (**B**) ASC specking in NLRP1-ASC and NLRP3-ASC HEKs pre-treated with MVA at MOI 5 for 6 h and stimulated with ANS or Nigericin for 2 h. Bars represent mean ± SD of two independent experiments. (**C**) ASC-deficient N/TERT-1 keratinocytes complemented with ASC-mCherry were pre-treated with MVA for 2 h or 4h and stimulated with ANS for 2 h or poly(I:C) for 6 h, respectively. Bars represent 100 µm. Images are representative of three independent experiments. The experiments in (B) and (C) were conducted with Fig. 4.1.3B and C using the same controls; data was shown separately for clarity.

4.7 F1L inhibits NLRP1 but not CARD8

4.7.1 NLRP1 is not inhibited by a VACV virion protein or a late gene-encoded protein

To identify the MVA protein responsible for NLRP1 inhibition, we first irradiated MVA with UV light to prevent viral protein expression. Similarly to HSV-1 experiments, we first examined the viability of N/TERT-1 cells infected with UV-irradiated MVA. We found that untreated MVA caused a decrease in viability by more than 50%, and infected cells showed apoptotic-like morphology with membrane bubbles (Fig. 4.7.1A and B). UV-treated MVA did not cause any decrease in viability; some of the infected keratinocytes had pyroptotic morphology, but the majority looked similar to uninfected cells. We found that in N/TERT-1 keratinocytes, UV-irradiated MVA, in contrast to untreated virus, could no longer inhibit IL-18 release (Fig. 4.7.1C). Thus, the protein inhibiting NLRP1 is not a virion protein. To further characterize this protein, we co-stimulated MVA-infected cells with cytosine arabinoside (AraC), which inhibits DNA replication and, thereby, late gene expression. Treatment with AraC did not affect ANS-induced IL-18 release or MVA-mediated NLRP1 inhibition, suggesting that NLRP1 inhibitor is not encoded by a late gene (Fig. 4.7.1D).

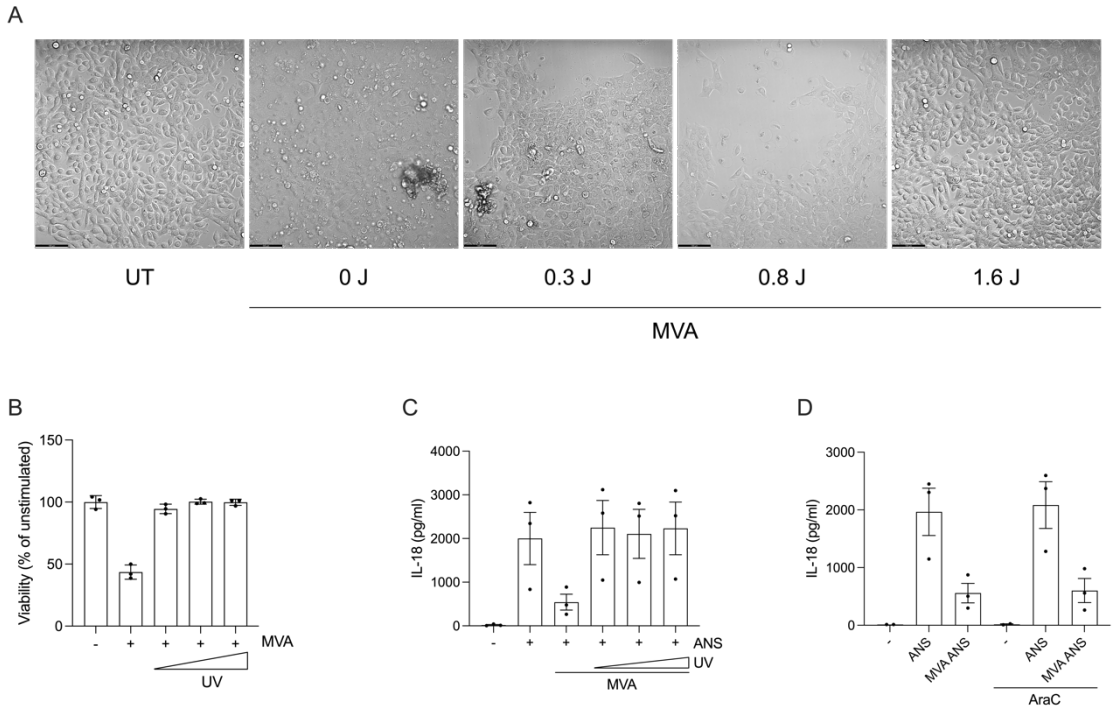

Fig. 4.7.1 (**A**) Images of N/TERT-1 cells infected with untreated or UV-irradiated MVA at MOI 5 for 24 h. Bars represent 100 µm. Images are representative of one experiment. (**B**) Viability of N/TERT-1 cells infected as in (A). Bars represent mean ± SD of three biological replicates from one experiment. The experiments in (A) and (B) were conducted with Fig. 4.2.1A and B using the same controls; data was shown separately for clarity. (**C**) IL-18 release from N/TERT-1 keratinocytes infected with untreated or UV-irradiated MVA at MOI 5 for 4 h and stimulated with ANS for 2 h. Bars represent mean ± SEM of three independent experiments. (**D**) IL-18 release from N/TERT-1 keratinocytes pre-treated with MVA at MOI 5, 10 µM AraC or MVA with AraC for 4 h and stimulated with ANS for 2 h. Bars represent mean ± SEM of three independent experiments. The experiments in (A) and (B) were conducted with Fig. 4.2.1A and B using the same controls; data was shown separately for clarity.

4.7.2 F1L is required for NLRP1 but not CARD8 inhibition during MVA infection

VACV was previously reported to inhibit NLRP1 inflammasome using the protein F1L. F1L is expressed early during infection, which is in line with our previous experiments. To determine if this protein plays a role in NLRP1 activation in keratinocytes, we pre-treated N/TERT-1 cells with WT MVA, F1L-deficient (dF1L) MVA, and dF1Lrev revertant virus, before ANS, VbP, and poly(I:C) stimulation. We observed a substantial decrease in ANS- and poly(I:C)-induced IL-18 release upon pre-treatment with WT and dF1Lrev but not dF1L MVA (Fig. 4.7.2A). Infection with MVA did not inhibit VbP-induced IL-18 release, and dF1L MVA greatly enhanced it. Since MVA also inhibits CARD8 inflammasome, we hypothesized that F1L can also interfere with CARD8 signaling; however, we found that dF1L virus still inhibited VbP-induced IL-18 release in CARD8-expressing cells (Fig. 4.7.2B).

To further examine the mechanism of NLRP1 inhibition, we cloned codon-optimized VACV F1L into a mammalian expression vector. First, we transiently expressed F1L in NLRP1-ASC HEKs. Expression of F1L did not decrease the percentage of BFP-positive ASC-specking cells; however, we found that the expression of F1L in HEK cells is very low, possibly accounting for the lack of inhibition. Overall, these results indicated that F1L-deficient MVA can no longer inhibit NLRP1 inflammasome activation in keratinocytes.

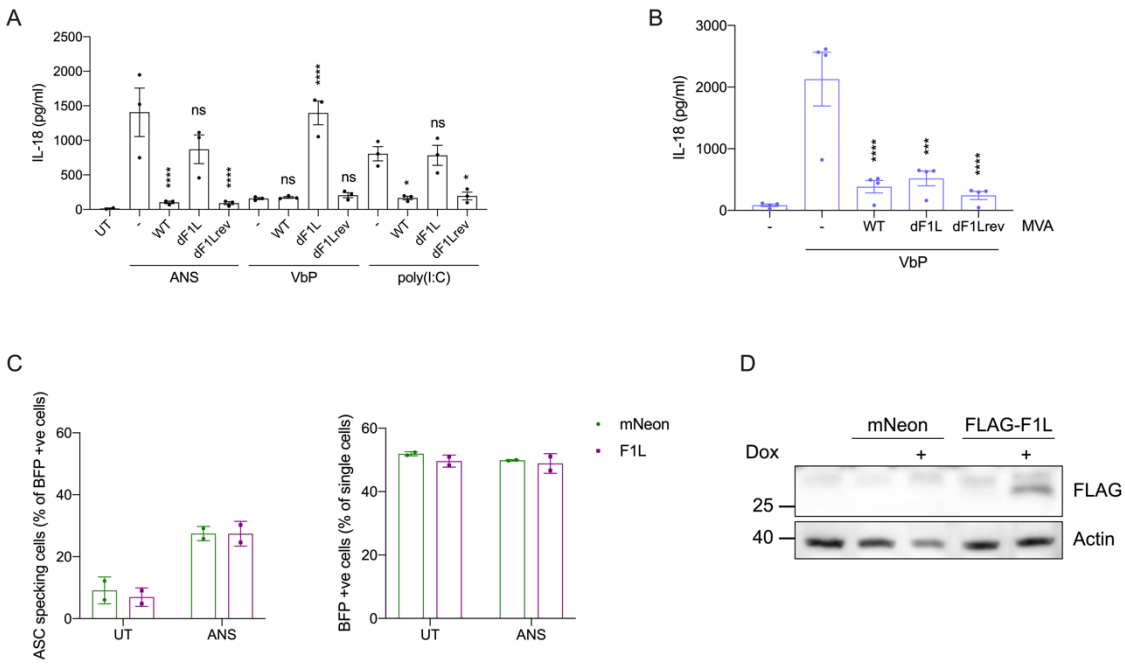

Fig. 4.7.2 (**A**) IL-18 release from N/TERT-1 keratinocytes pre-treated with WT/dF1L/dF1Lrev MVA at MOI 5 for 4, 1, or 2 h and stimulated with ANS for 2 h, VbP for 7 h, and poly(I:C) for 6 h, respectively. Bars represent mean ± SEM of three independent experiments. (**B**) IL-18 release from NLRP1-deficient N/TERT-1 keratinocytes complemented with hsCARD8 pre-treated with WT/dF1L/dF1Lrev MVA at MOI 5 for 2 h and stimulated with VbP for 4 h. Bars represent mean ± SEM of four independent experiments. (**C**) Percentage of ASC-specking (left) and BFP-positive (right) NLRP1-ASC HEK cells transfected with codon-optimized VACV F1L or mNeon in the presence of doxycycline and stimulated with ANS for 2 h. Bars represent mean ± SD of two independent experiments. The experiments were conducted with Fig. 4.2.3D and shown separately for clarity with the same mNeon control. (**D**) Expression of FLAG-F1L in HEK cells. The depicted blot represents one experiment. Data in (A) and (B) was analyzed by one-way ANOVA with Sidak's multiple comparisons test comparing ANS/VbP/poly(I:C)-only stimulated cells to respective MVA-pre-treated cells (* p<0.05, ***p<0.001, ****p<0.0001; ns, not significant).

4.8 dF1L MVA induces IL-18 release in keratinocytes

Our data suggested that VACV developed a mechanism for specific inhibition of NLRP1 inflammasome; therefore, we hypothesized that F1L-deficient MVA would trigger its assembly. To test this hypothesis, we infected N/TERT-1 cells with WT, dF1L, and

dF1Lrev MVA. We found that dF1L but not WT or revertant virus caused IL-18 release from keratinocytes (Fig. 4.8A); this was mediated by NLRP1 as NLRP1-deficient keratinocytes no longer secreted IL-18 after infection with dF1L MVA (Fig. 4.8B).

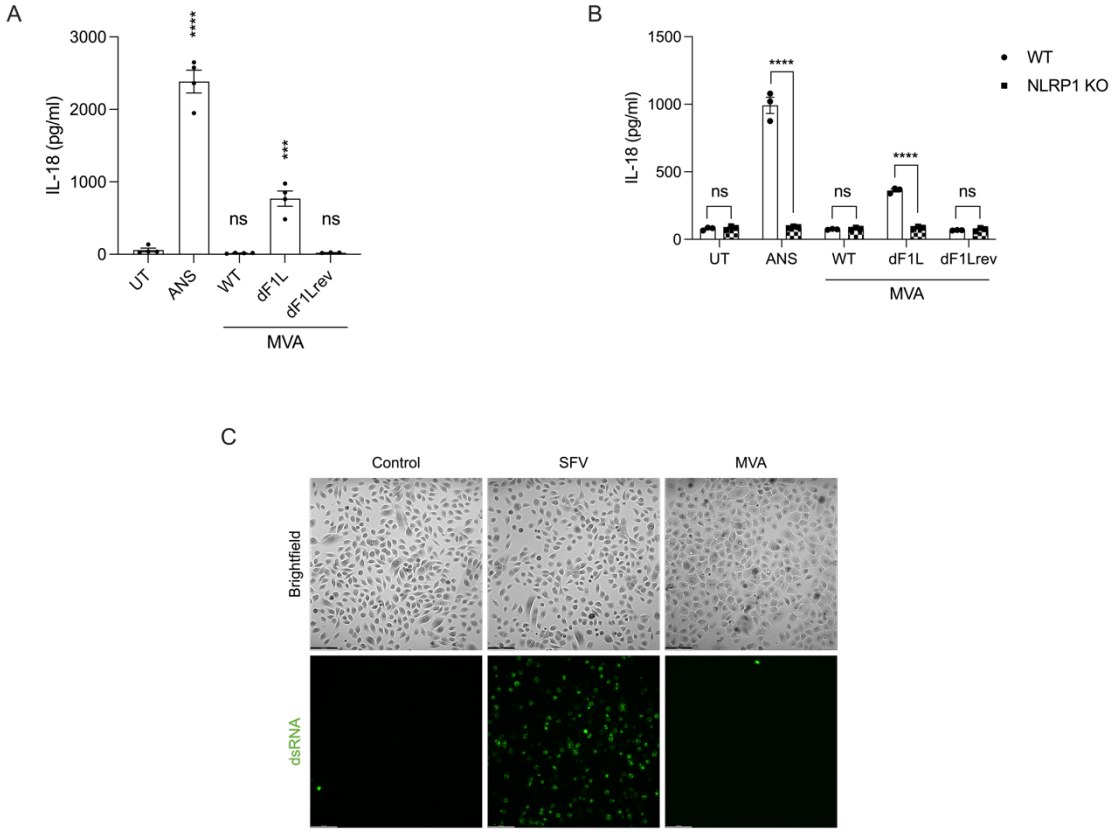

Fig. 4.8 (**A**) IL-18 release from N/TERT-1 keratinocytes infected with MVA at MOI 5 for 8h or stimulated with ANS for 2h. Bars represent mean ± SEM of four independent experiments. Some experiments were conducted together with Fig. 7.4.2A using the same controls. The data was shown separately for clarity. (**B**) IL-18 release from WT and NLRP1-deficient N/TERT-1 keratinocytes stimulated and infected as in (A). Bars represent mean ± SEM of three independent experiments. (**C**) N/TERT-1 cells were infected with SFV at MOI 5 for 7 h or with MVA at MOI 5 for 8 h and stained for dsRNA. Bars represent 100 µm. Images are representative of two independent experiments conducted with Fig. 4.4B and shown separately for clarity with the same controls. Data was analyzed with one-way (A) or two-way (B) ANOVA with Dunnett's multiple comparisons test comparing to untreated cells (A) or Sidak's multiple comparisons test comparing to WT (B, ***p<0.001, ****p<0.0001; ns, not significant).

VACV was reported to generate dsRNA, which activates NLRP1 inflammasome via the MAPK pathway (105). Therefore, we hypothesized that MVA could also generate dsRNA and thus trigger NLRP1; however, we could not detect any dsRNA in MVA-infected N/TERT-1 keratinocytes (Fig. 4.8C). Thus, our data suggest that dF1L MVA activates an inflammasome in N/TERT-1 cells, and this activation does not depend on the generation of dsRNA.

5. Discussion

5.1 HSV-1-mediated inflammasome inhibition

Inflammasomes play a critical role in pathogen clearance. NLRP1 was the first identified inflammasome, yet its activators were discovered only recently, and there are still many open questions about its activation mechanism. It was reported to be activated by multiple viruses, including SFV, Sindbis virus, rhinovirus, coxsackievirus, poliovirus, and SARS-CoV-2 (60,93,95,96); however, all those viruses activate NLRP1 by a different mechanism. SFV produces dsRNA, which binds to NLRP1, also triggering its ATPase activity. In addition, SFV and another alphavirus, Sindbis virus, were reported to activate NLRP1 by triggering the MAPK pathway. Rhinovirus, coxsackievirus, poliovirus, and SARS-CoV-2 encode proteases that cleave the N-terminus of NLRP1, leading to its degradation.

In our study, we examined how HSV-1 infection affects NLRP1 inflammasome signaling. HSV-1 was reported to generate dsRNA and activate the dsRNA sensor MDA5-MAVS, leading to interferon production (125,136). dsRNA is also a known NLRP1 ligand; however, HSV-1 infection does not activate NLRP1 inflammasome in keratinocytes (95). We thus hypothesized that the virus evolved a mechanism for NLRP1 inhibition. HSV-1 is a common human pathogen, and according to the WHO, over half of the world population is infected. HSV-1 infection is often asymptomatic but can also cause severe complications, such as encephalitis. HSV-1 has been extensively studied in the context of the immune response, primarily in immune cells, such as macrophages. Epithelial cells also play a role in HSV-1 infection, and although they are not professional immune cells, they express PRRs and are involved in pathogen detection. Skin is the first barrier many pathogens need to penetrate for successful infection; HSV-1 is transmitted during skin-to-skin contact, and entry occurs through a defect in the skin or other epithelial

barriers (122). Therefore, we chose to study the effects of HSV-1 infection on NLRP1 inflammasome in keratinocytes. They express NLRP1 and other inflammasome components and constitutively produce IL-1β, which eliminates the need for priming by stimulation of other PRRs. Furthermore, human keratinocytes express HVEM and nectin-1, the two receptors that mediate HSV-1 entry (148). Given the difficulty of culturing primary keratinocytes, we used N/TERT-1 immortalized human keratinocytes as a model. They have been used in many NLRP1 studies, are easy to manipulate with CRISPR/Cas9 technology, and can be made to express proteins using lentiviral transduction. The downside of using those cells is that they may not always respond like primary keratinocytes. For example, in primary keratinocytes, Nigericin activates NLRP1 through RSR induction, and in N/TERT-1 cells, it does not (104); this suggests differences in RSR or MAPK signaling between primary and N/TERT-1 keratinocytes, which may affect NLRP1 studies.

In the present work, we found that HSV-1 inhibits NLRP1 signaling in N/TERT-1 keratinocytes. We used three stimuli that trigger distinct mechanisms of NLRP1 activation: the DPP9 inhibitor Val-boroPro (VbP), dsRNA analog poly(I:C) (pIC), and RSR-inducing compound anisomycin (ANS). All those stimuli depend on proteasomal degradation of the NT fragment of NLRP1 but differ in the upstream mechanism: VbP-mediated activation relies on the inhibition of DPP9 and displacement of the CT fragment at the DPP9-NLRP1 complex, the activation by ANS depends on the RSR and MAPK pathway and hyperphosphorylation of the NLRP1 disordered region, and activation by dsRNA relies on its binding to the NT fragment of NLRP1, although the MAPK pathway may also play a role (36,95,96). We found that pre-treatment with HSV-1 inhibited all the mentioned pathways, suggesting that it interferes directly with NLRP1 or disrupts the downstream signaling. HSV-1 is known to interfere with host gene expression; therefore, we verified that it did not prevent the expression of NLRP1. Indeed, we found that HSV-1 infection did not change the levels of any of the proteins involved in inflammasome signaling, at least in the time frame studied.

However, we uncovered that HSV-1 also inhibited NLRP3 expressed in N/TERT-1 keratinocytes. NLRP1 and NLRP3 differ in their expression pattern and mechanism of

activation, but they share the steps downstream of sensor molecule oligomerization: ASC polymerization, caspase-1 activation, and IL-1β and GSDMD cleavage. We found that HSV-1 decreased NLRP3-mediated IL-1β and LDH release, although to a much lesser extent than in the case of NLRP1. Furthermore, HSV-1 also prevented NLRP1- and NLRP3-mediated ASC polymerization in N/TERT-1 keratinocytes, indicating that HSV-1 inhibited both inflammasomes. Surprisingly, HSV-1 did not inhibit NLRP3 activation in HEK cells. A possible reason could be higher levels of expression of inflammasome sensors in HEK cells than in keratinocytes. We considered the possibility that HSV-1 inhibited ASC polymerization directly, which would explain the inhibition of both inflammasomes. However, HSV-1 deficient for the AIM2-inhibiting protein VP22 activates AIM2 inflammasome, which is also ASC-dependent (121); this suggests that HSV-1 does not directly inhibit ASC polymerization. It is conceivable that HSV-1 developed a separate mechanism of inhibition of NLRP3 signaling.

HSV-1 causes a cytopathic effect in Vero cells; therefore, we considered that HSV-1-induced cell death could account for NLRP1 inhibition. We did not detect any decrease in the viability of HSV-1-infected N/TERT-1 keratinocytes over 24 h, although the infected cells clustered together, and we observed considerable changes in morphology with many cells rounded and detached. However, we also found that pre-treatment of N/TERT-1 keratinocytes with HSV-1 prevented ANS- and poly(I:C)-induced ASC specking and pyroptosis, as shown by a smaller number of balloon-shaped cells. In addition, we examined ASC specking in HSV-1-infected HEK cells by flow cytometry, gating for living cells only. At the same time after infection, ANS-stimulated HEK cells showed no specking, whereas Nigericin-induced specking was similar to that of uninfected cells; this suggests that at the time of analysis, the cells were still inflammasome-competent and cell death was not responsible the HSV-1-mediated inhibition.

5.2 ICP0 is responsible for HSV-1-mediated NLRP1 inhibition

HSV-1 encodes over 80 genes that are expressed during the infectious cycle; several of them encode proteins that are delivered into target cells in the viral tegument. Those proteins play a role in transporting the viral genetic material into the nucleus and in

immune evasion (120). To determine if the protein responsible for NLRP1 inhibition is in the tegument, we irradiated HSV-1 with UVC to prevent protein expression; we confirmed that irradiation was effective by infecting N/TERT-1 keratinocytes with irradiated virus and found that, in contrast to untreated HSV-1, it did not cause the cells to change morphology or detach. When we stimulated N/TERT-1 cells with ANS after infection with irradiated HSV-1, we discovered that it no longer prevented NLRP1-mediated IL-1β release.

To identify which of the HSV-1-encoded proteins inhibits NLRP1, we conducted a screen of HSV-1 open reading frames (ORFs). We turned to HEK cells that constitutively express NLRP1 and ASC tagged with mCherry, which allowed easy identification of cells where NLRP1 was activated by flow cytometry. We chose HEK cells over keratinocytes expressing endogenous NLRP1, as transfection of HEK cells is more efficient. To increase the screen sensitivity, we co-transfected a plasmid encoding BFP with a plasmid encoding a viral protein and analyzed only BFP-positive cells. We observed variability in the percentage of BFP-expressing cells between different conditions; this may have been caused by variable transfection efficiency and plasmid preparation impurities. The screen identified four viral ORFs that decreased ANS-induced ASC specking: UL23 encoding a thymidine kinase, UL26.5 encoding a capsid scaffolding protein, UL36A encoding a fragment of large tegument protein, and RL2-F2 encoding a fragment of E3 ubiquitin ligase ICP0.

Two of those four proteins were previously demonstrated to interfere with immune signaling: UL36 and ICP0. The N-terminus of UL36 has a deubiquitinating enzyme activity and was shown to disrupt interferon production by deubiquitinating TRAF3 downstream of RLR signaling (144). ICP0 has also been reported to inhibit multiple immune signaling pathways and, in contrast to UL36, it needs to be expressed during the infection; therefore, we chose to focus on it. In the library we used, ICP0 is split into three parts corresponding to its three exons. The fragment of ICP0 that came up in our screen is encoded by exon 2, which has the RING domain responsible for the E3 ligase activity of ICP0; thus, we hypothesized that the RING domain is critical for ICP0-mediated NLRP1 inhibition. We introduced point mutations to the RING domain, which

were previously shown to abolish the E3 ligase activity: C116G and C156A (RING finger mutant, RFm (145)), and we found that, indeed, RFm ICP0 no longer inhibited NLRP1-mediated specking; furthermore, full-length ICP0 but not ICP0 lacking RING domain decreased ASC specking in ANS-stimulated NLRP1-ASC HEK cells. To determine if ICP0 inhibited the activation of endogenous NLRP1 in keratinocytes, we expressed ICP0 along with the RFm in N/TERT-1 cells. Doing so, we found that WT ICP0, but not the mutant, decreased ANS-induced IL-1β release. To determine if ICP0 plays a role during HSV-1 infection, we pre-treated N/TERT-1 keratinocytes with ICP0-deficient virus and found that it only marginally reduced IL-1β release in ANS-stimulated cells. While we did not examine the effect of ICP0 on NLRP1 activation in keratinocytes by poly(I:C) and VbP, we demonstrated that ICP0 inhibits VbP-induced specking in HEK cells, so it most likely inhibits all modes of NLRP1 activation. Overall, we showed that ICP0 inhibits NLRP1 inflammasome when expressed in HEK cells and N/TERT-1 keratinocytes and during HSV-1 infection; this inhibition depends on the E3 ligase activity of ICP0.

In our study, we have not identified the mechanism of ICP0-mediated inhibition of NLRP1. ICP0 is a ubiquitin ligase, so it can be speculated that it induces ubiquitination and subsequent degradation of a protein participating in the NLRP1 signaling pathway. However, we found that HSV-1 infection did not cause a decrease in known NLRP1 inflammasome components. It is plausible that ICP0 targets a yet-to-be-identified component of the NLRP1 signaling. Analysis of changes in keratinocyte proteome after ICP0 expression could provide insights into the mechanism of ICP0-mediated inhibition. Since ICP0 significantly decreased ASC specking in NLRP1-expressing HEK cells stimulated with ANS and VbP, it can be hypothesized that ICP0 targets a signaling step shared by the two activation modes. One such step could be C-terminal oligomerization. Another characteristic shared between the two activation modes is their dependence on proteasomal function. N-terminal fragment degradation is necessary for NLRP1 activation, and proteasomal inhibition prevents inflammasome assembly. However, it is unclear whether NLRP1 is ubiquitinated and, if so, which ubiquitin ligase is responsible. HSV-1 was reported to target multiple cellular proteins, including ubiquitin ligases, such as USP7 or TRIM27, so it is plausible that it inhibits the degradation step in NLRP1 signaling (149).

5.3 ICP0-deficient HSV-1 does not activate NLRP1 inflammasome

Since ICP0 strongly inhibited NLRP1 activation in HEK cells and N/TERT-1 keratinocytes, we hypothesized that ICP0-deficient HSV-1 could activate NLRP1 inflammasome, either by the generation of dsRNA during its life cycle or by expression of a protein, which would activate NLRP1. Surprisingly, prolonged treatment with the dICP0 HSV-1 did not cause IL-1β release in N/TERT-1 cells. We speculated that ICP0 deficiency may inhibit dsRNA generation or the expression of the putative NLRP1-activating protein. ICP0 is not essential for viral replication, although the replication of ICP0-deficient HSV-1 is less efficient, depending on the cell type; it functions as a transactivator and influences the expression of other viral genes, including immediate early, early, and late genes (reviewed by (147,150)). Indeed, we found that the HSV-1-induced changes in morphology were delayed after the infection with dICP0 virus compared to the WT virus, indicating that the expression of other viral genes is delayed (data not shown).

HSV-1 was reported to produce dsRNA during infection; however, we did not detect any dsRNA in HSV-1-infected N/TERT-1 keratinocytes. We examined the presence of dsRNA at six hours post-infection, which is a shorter time than published literature. However, after prolonged HSV-1 infection, N/TERT-1 keratinocytes round up and detach, which makes examining the dsRNA production challenging. HSV-1 also developed a mechanism to prevent dsRNA accumulation by expressing virion host shutoff (vhs) RNase, which destabilizes mRNA (136).

Another possibility we considered was that NLRP1 is activated by an HSV-1-encoded protein whose expression is low or absent in the dICP0 virus. Opposing this hypothesis is that in our ORF library screen, we did not find an ORF that would increase NLRP1-mediated ASC specking; however, this does not exclude the possibility that such a protein exists. We used BFP to detect transfected cells, but we did not control the levels of HSV-1 proteins; as the library is not codon-optimized, the expression of some ORFs may be inefficient. In addition, there are interactions between different HSV-1 proteins, and individually expressed ORFs may not have the same effect as proteins expressed

during HSV-1 infection; for example, the protein encoded by UL26.5 is cleaved by the protease encoded by the UL26 gene (151).

While trying to determine which step of the NLRP1 signaling pathway is inhibited by HSV-1, we found that HSV-1 induced DR phosphorylation. We hypothesized that HSV-1 may encode a protein that phosphorylates NLRP1 directly or activates a signaling pathway that results in NLRP1 phosphorylation. In support of the second hypothesis, HSV-1 was reported to activate the MAPK pathway and induce p38 phosphorylation. An example of an HSV-1-encoded protein shown to activate p38 is the immediate early protein ICP27 (138,152). Indeed, we also observed p38 phosphorylation in keratinocytes treated with HSV-1; however, it was only marginally reduced after treatment with the dICP0 virus, whereas the NLRP1 DR phosphorylation was reduced to baseline, suggesting that the p38 phosphorylation by itself does not activate endogenous NLRP1 during HSV-1 infection. Alternatively, the phosphorylation could be mediated by ZAKα. The lack of NLRP1 activation by dICP0 virus could be attributed to the cell model we used. As mentioned before, there have been reported differences in RSR signaling between N/TERT-1 and primary keratinocytes (104). If HSV-1 induced RSR, the response in N/TERT-1 cells could be too weak to activate NLRP1 inflammasome, like in the case of Nigericin-induced RSR.

We also considered that ICP0 is redundant in the context of NLRP1 signaling. Our screens identified four ORFs that decreased ASC specking in HEK cells: RL2, UL36A, UL26.5, and UL23. UL36 large tegument protein was reported to inhibit immune signaling (144). We did not examine this protein in detail as it is delivered with the viral tegument, and if it played a role in NLRP1 inhibition, then UV-irradiated virus would still inhibit NLRP1. However, it is thought that UL36 needs to be cleaved to trigger its DUB activity. It is conceivable that the cleavage is performed by another viral protein expressed later during the infection. Supporting that hypothesis, the DUB activity in HSV-1 infected cells was only detectable 12 hours post-infection (143). As the N-terminus of NLRP1 needs to be degraded for activation, it could be speculated that UL36 prevents its ubiquitination and proteasomal degradation, thereby inhibiting inflammasome assembly. Another gene we found during our screen, UL26.5, encodes a

capsid scaffolding protein. However, it is a late protein, so its expression may be reduced in dICP0 HSV-1-infected cells. To exclude redundancy with a protein encoded by a late gene, late gene expression could be blocked during dICP0 HSV-1 infection. Undermining the potential role of UL26.5 is the fact that it is cleaved by the VP24 protease encoded by the UL26 gene, suggesting that its effect on NLRP1 may be non-specific (153). UL23 encodes a thymidine kinase primarily studied in the context of antiviral drug resistance. It is a tegument protein, which means it is not a likely candidate for NLRP1 inhibitor (154). It is worth noting that ICP0 was also detected in the tegument; however, it is a minor component, and its role there is not clear yet (154,155).

5.4 MVA-mediated inflammasome inhibition

Vaccinia virus (VACV) is known for being used as a vaccine to help with smallpox eradication. MVA is a strain of VACV generated by passaging VACV in chicken embryo fibroblasts over five hundred times, which resulted in deletions of parts of the viral genome. To this day, VACV and MVA are used for vaccine development and as a prototype poxvirus for virus-host interaction studies. VACV has been studied extensively in the context of the immune response. Similarly to HSV-1, it was shown to generate dsRNA that activates the MDA5-MAVS signaling pathway (132). More recently, dsRNA generated during VACV infection was reported to activate NLRP1 inflammasome in keratinocytes (105). VACV also inhibits immune signaling pathways; for example, it encodes several proteins that inhibit NF-kB and IRF3 signaling (156). In addition, it expresses a protein called F1L, which was reported to inhibit NLRP1 inflammasome; however, the studies of VACV and F1L in the context of NLRP1 signaling have been conducted mainly in THP-1 monocytes, which, to our knowledge, do not endogenously express NLRP1 (95,135). Human NLRP1 is primarily expressed in epithelial cells, including keratinocytes; therefore, we aimed to examine the effect of VACV on NLRP1 singling in keratinocytes.

We first verified if VACV inhibits endogenous NLRP1 in N/TERT-1 keratinocytes. As MVA also expresses F1L, the reported NLRP1 inhibitor, we used it instead of VACV for safety

reasons. We found that pre-treatment of N/TERT-1 keratinocytes with MVA at increasing MOI caused a dose-dependent decrease in the ANS-induced IL-18 release. We used IL-18 as a read-out of inflammasome activation as we found that MVA infection reduced the expression of pro-IL-1β; however, it did not consistently decrease the levels of any other component of the NLRP1 signaling pathway.

To examine the specificity of MVA-mediated inflammasome inhibition, we infected N/TERT-1 cells complemented with NLRP3. We found that the virus did not inhibit NLRP3 inflammasome, suggesting it inhibits a signaling step upstream of ASC polymerization. In line with this hypothesis, MVA prevented ASC dimerization in NLRP1- but not NLRP3-expressing cells; it also decreased ANS- and poly(I:C)-induced ASC specking in transgenic NLRP1-ASC HEK cells and N/TERT-1 keratinocytes expressing ASC-mCherry. We found that the decrease in IL-18 release in N/TERT-1 cells complemented with hsNLRP1 was not significant; this could be attributed to the large variability of data, as even IL-18 release by untreated cells is not significantly different from ANS-stimulated cells. The variability could be caused by a decrease in transgene expression over time.

We found that prolonged infection with MVA decreased N/TERT-1 cell viability; however, we think it is unlikely that MVA-mediated inhibition relies on cell death induction. Pre-treatment with MVA did not affect NLRP3 inflammasome activation, suggesting the cells were still inflammasome-competent. In addition, we observed a decrease in specking of NLRP1-ASC but not NLRP3-ASC HEKs analyzed by flow cytometry and gated for living cells. Furthermore, MVA infection decreased the number of pyroptotic keratinocytes. Overall, we demonstrated that MVA inhibits endogenous NLRP1 inflammasome upstream of ASC polymerization.

5.5 F1L inhibits NLRP1 inflammasome

F1L was reported to inhibit NLRP1 inflammasome in THP-1 cells (135); therefore, we investigated whether it also plays a role in the NLRP1 activation in keratinocytes. As F1L is produced early during infection (157), we first excluded that a virion protein or a

protein encoded by a late gene mediates the inhibition. To this end, we infected the cells with UV-irradiated MVA or co-treated them with MVA and AraC, a compound inhibiting late gene expression. We found that UV irradiation abolished the inhibition, whereas AraC had no effect. This data indicated that the protein encoded by an early or intermediate gene is responsible for NLRP1 inhibition.

To determine the role of F1L during MVA infection, we pre-treated cells with MVA deficient in F1L (dF1L (158)). We found that it no longer inhibited ANS- and pIC-induced NLRP1 activation. The inhibition was restored in the revertant virus (dF1Lrev). Neither WT nor dF1Lrev affected VbP-induced NLRP1 activation, and the dF1L virus greatly potentiated it. These results suggested that F1L does not inhibit NLRP1 directly by, for example, inhibiting C-terminal oligomerization but may interfere with the RSR pathway or the binding of dsRNA.

In NLRP1-ASC HEK cells, transient expression of F1L did not decrease ANS-induced ASC specking; however, the expression levels of F1L were low, which likely accounts for the lack of inhibition. We could not express sufficient levels of F1L despite designing a codon-optimized sequence; other groups studying F1L protein also had problems expressing it in mammalian cells (159). We have found that F1L from the MVA strain is expressed more strongly than from strain Copenhagen (data not shown). In addition, we observed a higher expression of F1L in HEK cells when cloned into the Clontech pEYFP-C3 vector. Transient expression of F1L in this vector was sufficient for NLRP1 inhibition in HEK cells (data not shown).

Due to the poor expression of F1L in mammalian cells, we could not investigate the mechanism of F1L-mediated NLRP1 inhibition. It was previously suggested that it inhibits NLRP1 by binding to its LRR region (135). We find it unlikely that the binding disrupts NLRP1 N-terminal degradation as it would also cause inhibition of VbP-induced inflammasome assembly; however, we speculate that the binding could impair the binding of dsRNA (95). The LRR has no known function in ANS-mediated NLRP1 activation, but F1L binding could impair DR phosphorylation. Alternatively, F1L could interfere with upstream signaling components instead of directly binding to NLRP1.

RSR- and dsRNA-mediated NLRP1 assembly could require a not-yet-identified protein, which is dispensable for VbP-mediated activation, and this putative protein could be the target of F1L.

5.6 F1L-deficient MVA activates NLRP1 inflammasome

Considering that VACV developed a specific mechanism for NLRP1 inhibition, we hypothesized that F1L-deficient MVA would activate NLRP1; indeed, we found that stimulation of N/TERT-1 keratinocytes with dF1L MVA induced NLRP1-dependent IL-18 release and potentiated VbP-induced IL-18 release. Since MVA blocks RSR- and dsRNA-induced NLRP1 activation, we speculated that F1L-deficient MVA could activate it by induction of RSR or production of dsRNA. Indeed, VACV was shown to trigger MAPK signaling and, in particular, p38 phosphorylation (160). A recent publication reported that dsRNA derived from VACV-infected cells activates NLRP1 in keratinocytes, possibly in a ZAKα-dependent manner (105); however, we did not detect dsRNA in N/TERT-1 cells infected with MVA. The same study also demonstrated that F1L-deficient VACV causes only a minor activation of NLRP1 in keratinocytes; therefore, the authors speculated that VACV encodes another protein inhibiting NLRP1 signaling. This difference in NLRP1 activation could be attributable to the read-out. We found that in addition to inhibiting NLRP1, MVA decreases the levels of pro-IL-1β; therefore, we examined only IL-18 release. However, we could not exclude that VACV encodes additional inflammasome inhibitors, which are absent in MVA.

5.7 MVA inhibits CARD8 inflammasome independently of F1L

As NLRP1 and CARD8 are related sensors, we also tested the effect of MVA on CARD8 signaling. Both sensors are kept in check by DPP9, and VbP binding to the active site of DPP9 disrupts this complex and leads to the accumulation of the free CT fragment in the cytosol. We found that MVA inhibited VbP-induced IL-18 release in CARD8-expressing cells but did not affect NLRP1-expressing cells. This result was unexpected as the mechanism for VbP-mediated NLRP1 and CARD8 activation are thought to be similar. We also found that the deletion of F1L did not affect the inhibition of CARD8.

These data strongly suggest that the mechanism of CARD8 inhibition is different from that of NLRP1 inhibition.

5.8 The physiological relevance of viral inhibition of NLRP1 inflammasome

In our study, we demonstrated that HSV-1 and MVA developed a mechanism for specific inhibition of NLRP1 inflammasome. Both viruses are also known to inhibit immune signaling pathways to avoid detection by the immune system. Identifying the viral proteins responsible for the inhibition may help disease prevention and treatment. Inhibition of viral proteins blocking the immune signaling could potentiate immune response.

In addition, finding the mechanism of F1L- and ICP0-mediated NLRP1 inhibition could improve our understanding of NLRP1 signaling. Our data suggest that the two proteins do not interact with NLRP1 directly. Instead, they could be inhibiting one or more proteins upstream of NLRP1 activation, which has not yet been identified. In summary, our work helped elucidate the effect of MVA and HSV-1 on NLRP1 inflammasome signaling, highlighting its importance in antiviral immunity.

6. Summary

NLRP1 is an inflammasome-forming protein known to play a role in antiviral immunity. HSV-1 and VACV are dsDNA viruses that were reported to generate dsRNA during their life cycles. dsRNA is a known activator of NLRP1 inflammasome; however, neither virus activates NLRP1 in human keratinocytes (95). Both viruses are often used in studies of virus-host interactions, particularly in the context of antiviral immunity and viral evasion of immune response. In our study, we demonstrated that HSV-1 and MVA developed a mechanism for specific inhibition of NLRP1 inflammasome.

We showed that HSV-1 inhibited ANS-, poly(I:C)-, and VbP-induced NLRP1 activation without causing downregulation of any of the inflammasome components. It inhibited ASC dimerization on Western blot and ASC specking in N/TERT keratinocytes and transgenic HEK cells. Our screen of the HSV-1 ORF library identified the E3 ubiquitin ligase ICP0 as the protein that inhibits NLRP1 activation. We confirmed this finding by expressing ICP0 in N/TERT-1 cells, where it decreased ANS-induced IL-1β release, and by infection of keratinocytes with ICP0-deficient HSV-1, which could no longer inhibit NLRP1. Furthermore, we found that ICP0-mediated inhibition depends on its ubiquitin ligase activity, as introducing point mutations into the RING domain abolished the inhibition. In addition, we showed that HSV-1 caused phosphorylation of NLRP1, although we did not observe NLRP1 activation by ICP0-deficient HSV-1.

We also demonstrated that MVA inhibited ANS- and pIC- but not VbP-induced NLRP1 assembly. Similarly to HSV-1, it inhibited ASC dimerization on Western blot and specking in N/TERT keratinocytes and transgenic HEK cells. As VACV F1L protein was previously reported to inhibit NLRP1, we examined the effect of F1L-deficient MVA on NLRP1 signaling. We found that dF1L MVA no longer inhibited NLRP1 signaling; furthermore, it induced NLRP1-dependent IL-18 release from keratinocytes. Our data suggest that this

activation is not mediated by dsRNA production, although the exact mechanism remained elusive.

7. Bibliography

1. Murphy K, Weaver C, Janeway C. Janeway's immunobiology. 9th ed. 2017.
2. Marshall JS, Warrington R, Watson W, Kim HL. An introduction to immunology and immunopathology. Vol. 14, Allergy, Asthma and Clinical Immunology. BioMed Central Ltd.; 2018.
3. Li D, Wu M. Pattern recognition receptors in health and diseases. Vol. 6, Signal Transduction and Targeted Therapy. Springer Nature; 2021.
4. Roh JS, Sohn DH. Damage-Associated Molecular Patterns in Inflammatory Diseases. Immune Netw. 2018;18(4).
5. Parkin J, Cohen B. An overview of the immune system. The Lancet. 2001;357:1777–89.
6. Merad M, Sathe P, Helft J, Miller J, Mortha A. The Dendritic Cell Lineage: Ontogeny and Function of Dendritic Cells and Their Subsets in the Steady State and the Inflamed Setting. Annu Rev Immunol. 2013 Mar 21;31(1):563–604.
7. Nguyen A V., Soulika AM. The dynamics of the skin's immune system. Vol. 20, International Journal of Molecular Sciences. MDPI AG; 2019.
8. Larsen SB, Cowley CJ, Fuchs E. Epithelial cells: liaisons of immunity. Vol. 62, Current Opinion in Immunology. Elsevier Ltd; 2020. p. 45–53.
9. Chessa C, Bodet C, Jousselin C, Wehbe M, Lévêque N, Garcia M. Antiviral and Immunomodulatory Properties of Antimicrobial Peptides Produced by Human Keratinocytes. Front Microbiol. 2020 Jun 3;11.
10. Medzhitov R. The spectrum of inflammatory responses. Science (1979) [Internet]. 2021;374. Available from: https://www.science.org
11. Netea MG, Balkwill F, Chonchol M, Cominelli F, Donath MY, Giamarellos-Bourboulis EJ, et al. A guiding map for inflammation. Vol. 18, Nature Immunology. Nature Publishing Group; 2017. p. 826–31.

12. Janeway CA. Approaching the asymptote? Evolution and revolution in immunology. In: Cold Spring Harbor Symposia on Quantitative Biology. 1989. p. 1–13.
13. Bertani B, Ruiz N. Function and Biogenesis of Lipopolysaccharides. EcoSal Plus. 2018 Feb 8;8(1).
14. Fitzgerald KA, Kagan JC. Toll-like Receptors and the Control of Immunity. Vol. 180, Cell. Cell Press; 2020. p. 1044–66.
15. Lemaitre B, Nicolas E, Michaut L. The Dorsoventral Regulatory Gene Cassette spä tzle/Toll/cactus Controls the Potent Antifungal Response in Drosophila Adults. Vol. 86, Cell. 1996.
16. Medzhitov R, Preston-Hurlburt P, Janeway CA. A human homologue of the Drosophila Toll protein signals activation of adaptive immunity. Nature. 1997;388:394–7.
17. Poltorak A, He X, Smirnova I, Liu MY, Huffel C Van, Du X, et al. Defective LPS Signaling in C3H/HeJ and C57BL/10ScCr Mice: Mutations in Tlr4 Gene. Science (1979). 1998 Dec 11;282(5396):2085–8.
18. Hornung V, Hartmann R, Ablasser A, Hopfner KP. OAS proteins and cGAS: Unifying concepts in sensing and responding to cytosolic nucleic acids. Nat Rev Immunol. 2014;14(8):521–8.
19. Broz P, Dixit VM. Inflammasomes: Mechanism of assembly, regulation and signalling. Vol. 16, Nature Reviews Immunology. Nature Publishing Group; 2016. p. 407–20.
20. Greulich W, Wagner M, Gaidt MM, Stafford C, Cheng Y, Linder A, et al. TLR8 Is a Sensor of RNase T2 Degradation Products. Cell. 2019 Nov;179(6):1264-1275.e13.
21. Takeuchi O, Akira S. Pattern Recognition Receptors and Inflammation. Vol. 140, Cell. 2010.
22. Heinz LX, Lee J, Kapoor U, Kartnig F, Sedlyarov V, Papakostas K, et al. TASL is the SLC15A4-associated adaptor for IRF5 activation by TLR7–9. Nature. 2020 May 21;581(7808):316–22.
23. Geijtenbeek TBH, Gringhuis SI. Signalling through C-type lectin receptors: shaping immune responses. Nat Rev Immunol. 2009 Jul;9(7):465–79.

24. Rehwinkel J, Gack MU. RIG-I-like receptors: their regulation and roles in RNA sensing. Nat Rev Immunol. 2020 Sep 13;20(9):537–51.
25. Lamkanfi M, Dixit VM. Mechanisms and functions of inflammasomes. Vol. 157, Cell. Elsevier B.V.; 2014. p. 1013–22.
26. Stafford CA, Gassauer AM, de Oliveira Mann CC, Tanzer MC, Fessler E, Wefers B, et al. Phosphorylation of muramyl peptides by NAGK is required for NOD2 activation. Nature. 2022 Sep 15;609(7927):590–6.
27. Trindade BC, Chen GY. NOD1 and NOD2 in inflammatory and infectious diseases. Immunol Rev. 2020 Sep 17;297(1):139–61.
28. Hopfner KP, Hornung V. Molecular mechanisms and cellular functions of cGAS–STING signalling. Nat Rev Mol Cell Biol. 2020 Sep 18;21(9):501–21.
29. Tanaka T, Narazaki M, Kishimoto T. IL-6 in Inflammation, Immunity, and Disease. Cold Spring Harb Perspect Biol. 2014 Oct 1;6(10):a016295–a016295.
30. Garlanda C, Dinarello CA, Mantovani A. The Interleukin-1 Family: Back to the Future. Vol. 39, Immunity. 2013. p. 1003–18.
31. Oberst A, Green DR. It cuts both ways: reconciling the dual roles of caspase 8 in cell death and survival. Nat Rev Mol Cell Biol. 2011 Nov 21;12(11):757–63.
32. Schoggins JW. Interferon-Stimulated Genes: What Do They All Do? Annu Rev Virol. 2019 Sep 29;6(1):567–84.
33. Johnson DC, Taabazuing CY, Okondo MC, Chui AJ, Rao SD, Brown FC, et al. DPP8/DPP9 inhibitor-induced pyroptosis for treatment of acute myeloid leukemia. Nat Med. 2018 Aug 1;24(8):1151–6.
34. Martinon F, Burns K, Rg Tschopp J. The Inflammasome: A Molecular Platform Triggering Activation of Inflammatory Caspases and Processing of proIL-b. Mol Cell. 2002;10:417–26.
35. Bauernfried S, Hornung V. Human NLRP1: From the shadows to center stage. Journal of Experimental Medicine. 2021 Dec 15;219(1).
36. Robinson KS, Toh GA, Rozario P, Chua R, Bauernfried S, Sun Z, et al. ZAKa-driven ribotoxic stress response activates the human NLRP1 inflammasome. Science (1979) [Internet]. 2022;377:328–35. Available from: https://www.science.org

37. Groß CJ, Mishra R, Schneider KS, Médard G, Wettmarshausen J, Dittlein DC, et al. K + Efflux-Independent NLRP3 Inflammasome Activation by Small Molecules Targeting Mitochondria. Immunity. 2016 Oct;45(4):761–73.
38. Muñoz-Planillo R, Kuffa P, Martínez-Colón G, Smith BL, Rajendiran TM, Núñez G. K+ Efflux Is the Common Trigger of NLRP3 Inflammasome Activation by Bacterial Toxins and Particulate Matter. Immunity. 2013 Jun;38(6):1142–53.
39. Chen J, Chen ZJ. PtdIns4P on dispersed trans-Golgi network mediates NLRP3 inflammasome activation. Nature. 2018 Dec 28;564(7734):71–6.
40. Swanson K V., Deng M, Ting JPY. The NLRP3 inflammasome: molecular activation and regulation to therapeutics. Nat Rev Immunol. 2019 Aug 29;19(8):477–89.
41. Kofoed EM, Vance RE. Innate immune recognition of bacterial ligands by NAIPs determines inflammasome specificity. Nature. 2011 Sep 29;477(7366):592–7.
42. Rayamajhi M, Zak DE, Chavarria-Smith J, Vance RE, Miao EA. Cutting Edge: Mouse NAIP1 Detects the Type III Secretion System Needle Protein. The Journal of Immunology. 2013 Oct 15;191(8):3986–9.
43. Valeria MRR, Ramirez J, Naseer N, Palacio NM, Siddarthan IJ, Yan BM, et al. Broad detection of bacterial type III secretion system and flagellin proteins by the human NAIP/NLRC4 inflammasome. Proc Natl Acad Sci U S A. 2017 Dec 12;114(50):13242–7.
44. Wang Q, Gao H, Clark KM, Mugisha CS, Davis K, Tang JP, et al. CARD8 is an inflammasome sensor for HIV-1 protease activity. Science (1979). 2021 Mar 19;371(6535).
45. Hornung V, Ablasser A, Charrel-Dennis M, Bauernfeind F, Horvath G, Caffrey DanielR, et al. AIM2 recognizes cytosolic dsDNA and forms a caspase-1-activating inflammasome with ASC. Nature. 2009 Mar 26;458(7237):514–8.
46. Heilig R, Broz P. Function and mechanism of the pyrin inflammasome. Eur J Immunol. 2018 Feb;48(2):230–8.
47. Angosto-Bazarra D, Molina-López C, Pelegrín P. Physiological and pathophysiological functions of NLRP6: pro- and anti-inflammatory roles. Vol. 5, Communications Biology. Nature Research; 2022.

48. Zheng D, Liwinski T, Elinav E. Inflammasome activation and regulation: toward a better understanding of complex mechanisms. Vol. 6, Cell Discovery. Springer Nature; 2020.
49. Próchnicki T, Vasconcelos MB, Robinson KS, Mangan MSJ, De Graaf D, Shkarina K, et al. Mitochondrial damage activates the NLRP10 inflammasome. Nat Immunol. 2023 Apr 20;24(4):595–603.
50. Hoffman HM, Mueller JL, Broide DH, Wanderer AA, Kolodner RD. Mutation of a new gene encoding a putative pyrin-like protein causes familial cold autoinflammatory syndrome and Muckle-Wells syndrome. Nat Genet. 2001;29(3):301–5.
51. Aksentijevich I, Centola M, Deng Z, Sood R, Balow JE, Wood G, et al. Ancient Missense Mutations in a New Member of the RoRet Gene Family Are Likely to Cause Familial Mediterranean Fever The International FMF Consortium* Introduction Group 4. Vol. 90, Cell. 1997.
52. Zhong FL, Mamaï O, Sborgi L, Boussofara L, Hopkins R, Robinson K, et al. Germline NLRP1 Mutations Cause Skin Inflammatory and Cancer Susceptibility Syndromes via Inflammasome Activation. Cell. 2016 Sep 22;167(1):187-202.e17.
53. Van Opdenbosch N, Lamkanfi M. Caspases in Cell Death, Inflammation, and Disease. Vol. 50, Immunity. Cell Press; 2019. p. 1352–64.
54. Lu A, Magupalli VG, Ruan J, Yin Q, Atianand MK, Vos MR, et al. Unified polymerization mechanism for the assembly of asc-dependent inflammasomes. Cell. 2014 Mar 13;156(6):1193–206.
55. Thornberry NA, Lazebnik Y. Caspases: Enemies Within. Science (1979). 1998 Aug 28;281(5381):1312–6.
56. Shi J, Zhao Y, Wang K, Shi X, Wang Y, Huang H, et al. Cleavage of GSDMD by inflammatory caspases determines pyroptotic cell death. Nature. 2015 Oct 29;526(7575):660–5.
57. Taabazuing CY, Okondo MC, Bachovchin DA. Pyroptosis and Apoptosis Pathways Engage in Bidirectional Crosstalk in Monocytes and Macrophages. Cell Chem Biol. 2017 Apr 20;24(4):507-514.e4.

58. Broz P, Von Moltke J, Jones JW, Vance RE, Monack DM. Differential requirement for caspase-1 autoproteolysis in pathogen-induced cell death and cytokine processing. Cell Host Microbe. 2010 Dec 16;8(6):471–83.
59. Wen J, Xuan B, Liu Y, Wang L, He L, Meng X, et al. Updating the NLRC4 Inflammasome: from Bacterial Infections to Autoimmunity and Cancer. Vol. 12, Frontiers in Immunology. Frontiers Media S.A.; 2021.
60. Robinson KS, Teo DET, Tan K Sen, Toh GA, Ong HH, Lim CK, et al. Enteroviral 3C protease activates the human NLRP1 inflammasome in airway epithelia. Science (1979). 2020 Dec 4;370(6521).
61. Okondo MC, Johnson DC, Sridharan R, Go E Bin, Chui AJ, Wang MS, et al. DPP8 and DPP9 inhibition induces pro-caspase-1-dependent monocyte and macrophage pyroptosis. Nat Chem Biol. 2017 Jan 1;13(1):46–53.
62. Ball DP, Taabazuing CY, Griswold AR, Orth EL, Rao SD, Kotliar IB, et al. Caspase-1 interdomain linker cleavage is required for pyroptosis. Life Sci Alliance. 2020;3(3).
63. Ding J, Wang K, Liu W, She Y, Sun Q, Shi J, et al. Pore-forming activity and structural autoinhibition of the gasdermin family. Nature. 2016 Jul 6;535(7610):111–6.
64. Devant P, Kagan JC. Molecular mechanisms of gasdermin D pore-forming activity. Nature Immunology. Nature Research; 2023.
65. Xia S, Zhang Z, Magupalli VG, Pablo JL, Dong Y, Vora SM, et al. Gasdermin D pore structure reveals preferential release of mature interleukin-1. Nature. 2021 May 27;593(7860):607–11.
66. Broz P, Pelegrín P, Shao F. The gasdermins, a protein family executing cell death and inflammation. Nat Rev Immunol [Internet]. 2020;20. Available from: https://doi.org/10.1038/s41577-
67. Kayagaki N, Kornfeld OS, Lee BL, Stowe IB, O'Rourke K, Li Q, et al. NINJ1 mediates plasma membrane rupture during lytic cell death. Nature. 2021 Mar 4;591(7848):131–6.
68. Gaidt MM, Ebert TS, Chauhan D, Schmidt T, Schmid-Burgk JL, Rapino F, et al. Human Monocytes Engage an Alternative Inflammasome Pathway. Immunity. 2016 Apr 19;44(4):833–46.

69. Dinarello CA, Renfer L, Wolff SM. Human leukocytic pyrogen: Purification and development of a radioimmunoassay. Proc Natl Acad Sci U S A [Internet]. 1977;74(10):4624–7. Available from: https://www.pnas.org

70. Sand J, Haertel E, Biedermann T, Contassot E, Reichmann E, French LE, et al. Expression of inflammasome proteins and inflammasome activation occurs in human, but not in murine keratinocytes article. Cell Death Dis. 2018 Feb 1;9(2).

71. Dinarello CA. Overview of the IL-1 family in innate inflammation and acquired immunity. Vol. 281, Immunological Reviews. Blackwell Publishing Ltd; 2018. p. 8–27.

72. Evans SS, Repasky EA, Fisher DT. Fever and the thermal regulation of immunity: The immune system feels the heat. Vol. 15, Nature Reviews Immunology. Nature Publishing Group; 2015. p. 335–49.

73. Deets KA, Vance RE. Inflammasomes and adaptive immune responses. Vol. 22, Nature Immunology. Nature Research; 2021. p. 412–22.

74. Kaneko N, Kurata M, Yamamoto T, Morikawa S, Masumoto J. The role of interleukin-1 in general pathology. Vol. 39, Inflammation and Regeneration. BioMed Central Ltd.; 2019.

75. Ridker PM, Everett BM, Thuren T, MacFadyen JG, Chang WH, Ballantyne C, et al. Antiinflammatory Therapy with Canakinumab for Atherosclerotic Disease. New England Journal of Medicine. 2017 Sep 21;377(12):1119–31.

76. Ridker PM, MacFadyen JG, Thuren T, Everett BM, Libby P, Glynn RJ, et al. Effect of interleukin-1β inhibition with canakinumab on incident lung cancer in patients with atherosclerosis: exploratory results from a randomised, double-blind, placebo-controlled trial. The Lancet. 2017 Oct;390(10105):1833–42.

77. Boyden ED, Dietrich WF. Nalp1b controls mouse macrophage susceptibility to anthrax lethal toxin. Nat Genet. 2006 Feb;38(2):240–4.

78. Lilue J, Doran AG, Fiddes IT, Abrudan M, Armstrong J, Bennett R, et al. Sixteen diverse laboratory mouse reference genomes define strain-specific haplotypes and novel functional loci. Nat Genet. 2018 Nov 1;50(11):1574–83.

79. Gai K, Okondo MC, Rao SD, Chui AJ, Ball DP, Johnson DC, et al. DPP8/9 inhibitors are universal activators of functional NLRP1 alleles. Cell Death Dis. 2019 Aug 5;10(8):587.

80. Sandstrom A, Mitchell PS, Goers L, Mu EW, Lesser CF, Vance RE. Functional degradation: A mechanism of NLRP1 inflammasome activation by diverse pathogen enzymes. Science (1979). 2019 Apr 5;364(6435).

81. Hollingsworth LR, Sharif H, Griswold AR, Fontana P, Mintseris J, Dagbay KB, et al. DPP9 sequesters the C terminus of NLRP1 to repress inflammasome activation. Nature. 2021 Apr 29;592(7856):778–83.

82. Finger JN, Lich JD, Dare LC, Cook MN, Brown KK, Duraiswamis C, et al. Autolytic proteolysis within the function to find domain (FIIND) is required for NLRP1 inflammasome activity. Journal of Biological Chemistry. 2012 Jul 20;287(30):25030–7.

83. D'Osualdo A, Weichenberger CX, Wagner RN, Godzik A, Wooley J, Reed JC. CARD8 and NLRP1 undergo autoproteolytic processing through a ZU5-like domain. PLoS One. 2011 Nov 8;6(11).

84. Robert Hollingsworth L, David L, Li Y, Griswold AR, Ruan J, Sharif H, et al. Mechanism of filament formation in UPA-promoted CARD8 and NLRP1 inflammasomes. Nat Commun. 2021 Dec 1;12(1).

85. Gong Q, Robinson K, Xu C, Huynh PT, Chong KHC, Tan EYJ, et al. Structural basis for distinct inflammasome complex assembly by human NLRP1 and CARD8. Nat Commun. 2021 Dec 1;12(1).

86. Jun Y, Mailloux CM, Gowan K, Riccardi SL, LaBerge G, Bennet DC, et al. NALP1 in Vitiligo-Associated Multiple Autoimmune Disease. N Engl J Med [Internet]. 2007;356:1216–41. Available from: www.nejm.org

87. Drutman SB, Haerynck F, Zhong FL, Hum D, Hernandez NJ, Belkaya S, et al. Homozygous NLRP1 gain-of-function mutation in siblings with a syndromic form of recurrent respiratory papillomatosis. Proc Natl Acad Sci U S A. 2019 Sep 17;116(38):19055–63.

88. Chui AJ, Okondo MC, Rao SD, Gai K, Griswold AR, Johnson DC, et al. N-terminal degradation activates the NLRP1B inflammasome [Internet]. Vol. 364, Science. 2019. Available from: http://science.sciencemag.org/

89. Okondo MC, Rao SD, Taabazuing CY, Chui AJ, Poplawski SE, Johnson DC, et al. Inhibition of Dpp8/9 Activates the Nlrp1b Inflammasome. Cell Chem Biol. 2018 Mar 15;25(3):262-267.e5.

90. Zhong FL, Robinson K, Teo DET, Tan KY, Lim C, Harapas CR, et al. Human DPP9 represses NLRP1 inflammasome and protects against autoinflammatory diseases via both peptidase activity and FIIND domain binding. Journal of Biological Chemistry. 2018 Dec 7;293(49):18864–78.
91. Harapas CR, Robinson KS, Lay K, Wong J, Traspas RM, Nabavizadeh N, et al. DPP9 deficiency: An inflammasomopathy that can be rescued by lowering NLRP1/IL-1 signaling. Sci Immunol [Internet]. 2022;7(75). Available from: https://www.science.org
92. Faustin B, Lartigue L, Bruey JM, Luciano F, Sergienko E, Bailly-Maitre B, et al. Reconstituted NALP1 Inflammasome Reveals Two-Step Mechanism of Caspase-1 Activation. Mol Cell. 2007 Mar 9;25(5):713–24.
93. Tsu B V., Beierschmitt C, Ryan AP, Agarwal R, Mitchell PS, Daugherty MD. Diverse viral proteases activate the nlrp1 inflammasome. Elife. 2021 Jan 1;10:1–76.
94. Planès R, Pinilla M, Santoni K, Hessel A, Passemar C, Lay K, et al. Human NLRP1 is a sensor of pathogenic coronavirus 3CL proteases in lung epithelial cells. Mol Cell. 2022 Jul 7;82(13):2385-2400.e9.
95. Bauernfried S, Scherr MJ, Pichlmair A, Duderstadt KE, Hornung V. Human NLRP1 is a sensor for double-stranded RNA. Science (1979). 2021 Jan 29;371(6528).
96. Jenster LM, Lange KE, Normann S, Vom Hemdt A, Wuerth JD, Schiffelers LDJ, et al. P38 kinases mediate NLRP1 inflammasome activation after ribotoxic stress response and virus infection. Journal of Experimental Medicine. 2023 Jan 2;220(1).
97. Tang Z, Tong X, Huang J, Liu L, Wang D, Yang S. Research progress of keratinocyte-programmed cell death in UV-induced Skin photodamage. Vol. 37, Photodermatology Photoimmunology and Photomedicine. John Wiley and Sons Inc; 2021. p. 442–8.
98. Wu CCC, Peterson A, Zinshteyn B, Regot S, Green R. Ribosome Collisions Trigger General Stress Responses to Regulate Cell Fate. Cell. 2020 Jul 23;182(2):404-416.e14.
99. Fenini G, Grossi S, Contassot E, Biedermann T, Reichmann E, French LE, et al. Genome Editing of Human Primary Keratinocytes by CRISPR/Cas9 Reveals an

Essential Role of the NLRP1 Inflammasome in UVB Sensing. Journal of Investigative Dermatology. 2018 Dec 1;138(12):2644–52.

100. Fenini G, Grossi S, Gehrke S, Beer HD, Satoh TK, Contassot E, et al. The p38 Mitogen-Activated Protein Kinase Critically Regulates Human Keratinocyte Inflammasome Activation. Journal of Investigative Dermatology. 2018 Jun 1;138(6):1380–90.

101. Robinson KS, Toh GA, Rozario P, Bayat S, Sun Z, Bauernfried S, et al. Human NLRP1 is activated by ZAKα-driven ribotoxic stress response. bioRxiv [Internet]. 2022; Available from: https://doi.org/10.1101/2022.01.24.477516

102. Robinson KS, Toh GA, Firdaus MJ, Khek Chian T, Rozario P, Lim C, et al. Corynebacterium diphtheriae causes keratinocyte-intrinsic ribotoxic stress and NLRP1 inflammasome activation in a model of cutaneous diphtheria. bioRxiv [Internet]. 2023; Available from: https://doi.org/10.1101/2023.01.16.524188

103. Pinilla M, Mazars R, Vergé R, Gorse L, Santoni K, Robinson S, et al. EEF2-inactivating toxins engage the NLRP1 inflammasome and. bioRxiv [Internet]. 2023; Available from: https://doi.org/10.1101/2023.01.16.524164

104. Rozario P, Pinilla M, Vind AC, Robinson KS, Toh GA, Firdaus MJ, et al. Mechanistic basis for nigericin-induced NLRP1 inflammasome activation in human epithelial cells. bioRxiv [Internet]. 2023; Available from: https://doi.org/10.1101/2023.06.23.546021

105. Zhou JY, Sarkar MK, Okamura K, Harris JE, Gudjonsson JE, Fitzgerald KA. Activation of the NLRP1 inflammasome in human keratinocytes by the dsDNA mimetic poly(dA:dT). Proc Natl Acad Sci U S A. 2023 Jan 31;120(5).

106. Orth-He EL, Huang HC, Rao SD, Wang Q, Chen Q, O'Mara CM, et al. Protein folding stress potentiates NLRP1 and CARD8 inflammasome activation. Cell Rep. 2023 Jan 31;42(1).

107. Rao SD, Chen Q, Wang Q, Orth-He EL, Saoi M, Griswold AR, et al. M24B aminopeptidase inhibitors selectively activate the CARD8 inflammasome. Nat Chem Biol. 2022 May 1;18(5):565–74.

108. Ball DP, Tsamouri LP, Wang AE, Huang HC, Warren CD, Wang Q, et al. Oxidized thioredoxin-1 restrains the NLRP1 inflammasome. Sci Immunol [Internet]. 2022;7. Available from: https://www.science.org

109. Wang Q, Hsiao JC, Yardeny N, Huang HC, O'Mara CM, Orth-He EL, et al. The NLRP1 and CARD8 inflammasomes detect reductive stress. Cell Rep. 2023 Jan 31;42(1).
110. Yang X, Zhou J, Liu C, Qu Y, Wang W, Xiao MZX, et al. KSHV-encoded ORF45 activates human NLRP1 inflammasome. Nat Immunol. 2022 Jun 1;23(6):916–26.
111. Sharif H, Hollingsworth LR, Griswold AR, Hsiao JC, Wang Q, Bachovchin DA, et al. Dipeptidyl peptidase 9 sets a threshold for CARD8 inflammasome formation by sequestering its active C-terminal fragment. Immunity. 2021 Jul 13;54(7):1392-1404.e10.
112. Johnson DC, Taabazuing CY, Okondo MC, Chui AJ, Rao SD, Brown FC, et al. DPP8/DPP9 inhibitor-induced pyroptosis for treatment of acute myeloid leukemia. Nat Med. 2018 Aug 1;24(8):1151–6.
113. Johnson DC, Okondo MC, Orth EL, Rao SD, Huang HC, Ball DP, et al. DPP8/9 inhibitors activate the CARD8 inflammasome in resting lymphocytes. Cell Death Dis. 2020 Aug 1;11(8).
114. Linder A, Bauernfried S, Cheng Y, Albanese M, Jung C, Keppler OT, et al. CARD8 inflammasome activation triggers pyroptosis in human T cells. EMBO J. 2020 Oct;39(19).
115. Chui AJ, Griswold AR, Taabazuing CY, Orth EL, Gai K, Rao SD, et al. Activation of the CARD8 Inflammasome Requires a Disordered Region. Cell Rep. 2020 Oct 13;33(2).
116. Hsiao JC, Neugroschl AR, Chui AJ, Taabazuing CY, Griswold AR, Wang Q, et al. A ubiquitin-independent proteasome pathway controls activation of the CARD8 inflammasome. Journal of Biological Chemistry. 2022 Jul 1;298(7).
117. Tsu B V., Agarwal R, Gokhale NS, Kulsuptrakul J, Ryan AP, Fay EJ, et al. Host-specific sensing of coronaviruses and picornaviruses by the CARD8 inflammasome. PLoS Biol. 2023 Jun 8;21(6):e3002144.
118. Nadkarni R, Chu WC, Lee CQE, Mohamud Y, Yap L, Toh GA, et al. Viral proteases activate the CARD8 inflammasome in the human cardiovascular system. Journal of Experimental Medicine. 2022 Oct 3;219(10).
119. Diefenbach RJ, Fraefel C. Herpes Simplex Virus Methods and Protocols [Internet]. Second. Humana Press; 2020. Available from: http://www.springer.com/series/7651

120. Ibáñez FJ, Farías MA, Gonzalez-Troncoso MP, Corrales N, Duarte LF, Retamal-Díaz A, et al. Experimental Dissection of the Lytic Replication Cycles of Herpes Simplex Viruses in vitro. Front Microbiol. 2018 Oct 11;9.
121. Maruzuru Y, Ichinohe T, Sato R, Miyake K, Okano T, Suzuki T, et al. Herpes Simplex Virus 1 VP22 Inhibits AIM2-Dependent Inflammasome Activation to Enable Efficient Viral Replication. Cell Host Microbe. 2018 Feb 14;23(2):254-265.e7.
122. Plewig G, French L, Ruzicka T, Kaufmann R, Hertl M. Braun-Falco's Dermatology. 4th ed. 2022.
123. Heath JR, Dembowski JA. Fashionably late: Temporal regulation of HSV-1 late gene transcription. PLoS Pathog. 2022 Jun 1;18(6).
124. Paludan SR, Bowie AG, Horan KA, Fitzgerald KA. Recognition of herpesviruses by the innate immune system. Vol. 11, Nature Reviews Immunology. Nature Publishing Group; 2011. p. 143–54.
125. Melchjorsen J, Rintahaka J, Søby S, Horan KA, Poltajainen A, Østergaard L, et al. Early Innate Recognition of Herpes Simplex Virus in Human Primary Macrophages Is Mediated via the MDA5/MAVS-Dependent and MDA5/MAVS/RNA Polymerase III-Independent Pathways. J Virol. 2010 Nov;84(21):11350–8.
126. Melchjorsen J, Sirén J, Julkunen I, Paludan SR, Matikainen S. Induction of cytokine expression by herpes simplex virus in human monocyte-derived macrophages and dendritic cells is dependent on virus replication and is counteracted by ICP27 targeting NF-κB and IRF-3. Journal of General Virology. 2006 May;87(5):1099–108.
127. Wang S, Wang K, Li J, Zheng C. Herpes Simplex Virus 1 Ubiquitin-Specific Protease UL36 Inhibits Beta Interferon Production by Deubiquitinating TRAF3. J Virol. 2013 Nov;87(21):11851–60.
128. Su C, Zhan G, Zheng C. Evasion of host antiviral innate immunity by HSV-1, an update. Virol J. 2016 Dec 8;13(1):38.
129. Volz A, Sutter G. Modified Vaccinia Virus Ankara: History, Value in Basic Research, and Current Perspectives for Vaccine Development. Adv Virus Res. 2017;97:187–243.

130. Kaynarcalidan O, Moreno Mascaraque S, Drexler I. Vaccinia Virus: From Crude Smallpox Vaccines to Elaborate Viral Vector Vaccine Design. Biomedicines. 2021 Nov 26;9(12):1780.
131. Li XD, Wu J, Gao D, Wang H, Sun L, Chen ZJ. Pivotal Roles of cGAS-cGAMP Signaling in Antiviral Defense and Immune Adjuvant Effects. Science (1979). 2013 Sep 20;341(6152):1390–4.
132. Pichlmair A, Schulz O, Tan CP, Rehwinkel J, Kato H, Takeuchi O, et al. Activation of MDA5 Requires Higher-Order RNA Structures Generated during Virus Infection. J Virol. 2009 Oct 15;83(20):10761–9.
133. Smith GL, Benfield CTO, Maluquer de Motes C, Mazzon M, Ember SWJ, Ferguson BJ, et al. Vaccinia virus immune evasion: mechanisms, virulence and immunogenicity. Journal of General Virology. 2013 Nov 1;94(11):2367–92.
134. Kettle S, Khanna A, Alcamv≠ A, Jassoy C, Ehret R, Smith GL. Vaccinia virus serpin B13R (SPI-2) inhibits interleukin-1beta-converting enzyme and protects virus-infected cells from TNF- and Fas-mediated apoptosis, but does not prevent IL-1beta-induced fever. Journal of General Virology. 1997 Mar 1;78(3):677–85.
135. Gerlic M, Faustin B, Postigo A, Yu ECW, Proell M, Gombosuren N, et al. Vaccinia virus F1L protein promotes virulence by inhibiting inflammasome activation. Proceedings of the National Academy of Sciences. 2013 May 7;110(19):7808–13.
136. Dauber B, Saffran HA, Smiley JR. The herpes simplex virus host shutoff (vhs) RNase limits accumulation of double stranded RNA in infected cells: Evidence for accelerated decay of duplex RNA. PLoS Pathog. 2019 Oct 18;15(10):e1008111.
137. de Magalhães JC, Andrade AA, Silva PNG, Sousa LP, Ropert C, Ferreira PCP, et al. A Mitogenic Signal Triggered at an Early Stage of Vaccinia Virus Infection. Journal of Biological Chemistry. 2001 Oct;276(42):38353–60.
138. Hargett D, McLean T, Bachenheimer SL. Herpes Simplex Virus ICP27 Activation of Stress Kinases JNK and p38. J Virol. 2005 Jul;79(13):8348–60.
139. Jing L, Haas J, Chong TM, Bruckner JJ, Dann GC, Dong L, et al. Cross-presentation and genome-wide screening reveal candidate T cells antigens for a herpes simplex virus type 1 vaccine. Journal of Clinical Investigation. 2012 Feb 1;122(2):654–73.

140. Schmid-Burgk JL, Höning K, Ebert TS, Hornung V. CRISPaint allows modular base-specific gene tagging using a ligase-4-dependent mechanism. Nat Commun. 2016 Jul 28;7(1):12338.
141. Gaidt MM, Morrow A, Fairgrieve MR, Karr JP, Yosef N, Vance RE. Self-guarding of MORC3 enables virulence factor-triggered immunity. Nature. 2021 Dec 2;600(7887):138–42.
142. Dickson MA, Hahn WC, Ino Y, Ronfard V, Wu JY, Weinberg RA, et al. Human Keratinocytes That Express hTERT and Also Bypass a p16 INK4a-Enforced Mechanism That Limits Life Span Become Immortal yet Retain Normal Growth and Differentiation Characteristics. Mol Cell Biol. 2000 Feb 1;20(4):1436–47.
143. Kattenhorn LM, Korbel GA, Kessler BM, Spooner E, Ploegh HL. A Deubiquitinating Enzyme Encoded by HSV-1 Belongs to a Family of Cysteine Proteases that Is Conserved across the Family Herpesviridae. Mol Cell. 2005 Aug;19(4):547–57.
144. Wang S, Wang K, Li J, Zheng C. Herpes Simplex Virus 1 Ubiquitin-Specific Protease UL36 Inhibits Beta Interferon Production by Deubiquitinating TRAF3. J Virol. 2013 Nov;87(21):11851–60.
145. Orzalli MH, DeLuca NA, Knipe DM. Nuclear IFI16 induction of IRF-3 signaling during herpesviral infection and degradation of IFI16 by the viral ICP0 protein. Proceedings of the National Academy of Sciences. 2012 Oct 30;109(44).
146. Chaurushiya MS, Lilley CE, Aslanian A, Meisenhelder J, Scott DC, Landry S, et al. Viral E3 Ubiquitin Ligase-Mediated Degradation of a Cellular E3: Viral Mimicry of a Cellular Phosphorylation Mark Targets the RNF8 FHA Domain. Mol Cell. 2012 Apr;46(1):79–90.
147. Smith MC, Boutell C, Davido DJ. HSV-1 ICP0: paving the way for viral replication. Future Virol. 2011 Apr;6(4):421–9.
148. Sayers CL, Elliott G. Herpes Simplex Virus 1 Enters Human Keratinocytes by a Nectin-1-Dependent, Rapid Plasma Membrane Fusion Pathway That Functions at Low Temperature. J Virol. 2016 Nov 15;90(22):10379–89.
149. Conwell SE, White AE, Harper JW, Knipe DM. Identification of TRIM27 as a Novel Degradation Target of Herpes Simplex Virus 1 ICP0. J Virol. 2015 Jan;89(1):220–9.

150. Rodríguez MC, Dybas JM, Hughes J, Weitzman MD, Boutell C. The HSV-1 ubiquitin ligase ICP0: Modifying the cellular proteome to promote infection. Virus Res. 2020 Aug;285:198015.
151. Preston VG, Al-Kobaisi MF, McDougall IM, Rixon FJ. The herpes simplex virus gene UL26 proteinase in the presence of the UL26.5 gene product promotes the formation of scaffold-like structures. Journal of General Virology. 1994 Sep 1;75(9):2355–66.
152. Gillis PA, Okagaki LH, Rice SA. Herpes Simplex Virus Type 1 ICP27 Induces p38 Mitogen-Activated Protein Kinase Signaling and Apoptosis in HeLa Cells. J Virol. 2009 Feb 15;83(4):1767–77.
153. Preston VG, Al-Kobaisi MF, McDougall IM, Rixon FJ. The herpes simplex virus gene UL26 proteinase in the presence of the UL26.5 gene product promotes the formation of scaffold-like structures. Journal of General Virology. 1994 Sep 1;75(9):2355–66.
154. Loret S, Guay G, Lippé R. Comprehensive Characterization of Extracellular Herpes Simplex Virus Type 1 Virions. J Virol. 2008 Sep;82(17):8605–18.
155. Boutell C, Everett RD. Regulation of alphaherpesvirus infections by the ICP0 family of proteins. Journal of General Virology. 2013 Mar 1;94(3):465–81.
156. Albarnaz J, Torres A, Smith G. Modulating Vaccinia Virus Immunomodulators to Improve Immunological Memory. Viruses. 2018 Feb 28;10(3):101.
157. Fischer SF, Ludwig H, Holzapfel J, Kvansakul M, Chen L, Huang DCS, et al. Modified vaccinia virus Ankara protein F1L is a novel BH3-domain-binding protein and acts together with the early viral protein E3L to block virus-associated apoptosis. Cell Death Differ. 2006 Jan 1;13(1):109–18.
158. Volz A, Jany S, Freudenstein A, Lantermann M, Ludwig H, Sutter G. E3L and F1L Gene Functions Modulate the Protective Capacity of Modified Vaccinia Virus Ankara Immunization in Murine Model of Human Smallpox. Viruses. 2018 Jan 4;10(1):21.
159. Kvansakul M, Yang H, Fairlie WD, Czabotar PE, Fischer SF, Perugini MA, et al. Vaccinia virus anti-apoptotic F1L is a novel Bcl-2-like domain-swapped dimer that binds a highly selective subset of BH3-containing death ligands. Cell Death Differ. 2008 Oct 13;15(10):1564–71.

160. Park C, Walsh D. RACK1 Regulates Poxvirus Protein Synthesis Independently of Its Role in Ribosome-Based Stress Signaling. J Virol. 2022 Sep 28;96(18).
161. Gu H. Infected cell protein 0 functional domains and their coordination in herpes simplex virus replication. World J Virol. 2016;5(1):1.

8. List of abbreviations

3CL	3C-like (protease)
AIM2	absent in melanoma 2
ALRs	AIM2-like receptors
ANS	anisomycin
AP-1	activating protein-1
APC	antigen-presenting cell
APP	acute phase protein
AraC	cytosine arabinoside
ASC	apoptosis-associated speck-like protein containing a CARD
ATP	Adenosine triphosphate
BCR	B cell receptor
CARD	caspase activation and recruitment domain
CARD8	caspase recruitment domain-containing protein 8
CD4/8	cluster of differentiation 4/8
cGAMP	cyclic GMP-AMP [G(2',5')pA(3',5')p]
cGAS	cyclic GMP-AMP synthase
CLR	C-type lectin receptor
CRISPR	clustered regularly interspaced short palindromic repeats
CRP	C-reactive protein
CT	C-terminal
DAMP	damage-associated molecular pattern
DC	dendritic cell
DED	death effector domain
DNA	deoxyribonucleic acid
DPP8/9	dipeptidyl peptidase 8/9
DR	disordered region
dsDNA	double-stranded DNA
dsRNA	double-stranded RNA
DSS	disuccinimidyl suberate
E. coli	Escherichia coli
EEF2	eucaryotic elongation factor 2
EGF	Epidermal growth factor
ER	endoplasmic reticulum
FIIND	function-to-find domain

gRNA	guide RNA
GSDMD	gasdermin D
HIV-1	human immunodeficiency virus type 1
HMGB1	high mobility group box 1
HSV-1/2	herpes simplex virus 1/2
HVEM	Herpes Virus Entry Mediator
ICP	infected cell protein
IFN	interferon
IFNAR	interferon-α/β receptor
IL	interleukin
IL-1Ra	IL-1 receptor antagonist
IRF	interferon regulatory factor
ISG	IFN-stimulated genes
JAK1	Janus kinase 1
JNK	c-Jun N-terminal kinases
KSHV	Kaposi's sarcoma associated virus
LF	lethal factor
LGP2	laboratory of genetics and physiology 2
LPS	lipopolysaccharide
LRR	leucin-rich repeat
LTA	lipoteichoic acid
MAPK	mitogen-activated protein kinase
MAPKKK	mitogen-activated protein kinase kinase kinase
MAVS	mitochondrial antiviral-signaling protein
MDA5	melanoma differentiation-associated gene 5
MDP	muramyl dipeptide
MeBs	bestatin methyl ester
MHC	major histocompatibility complex
MPXV	monkeypox virus
MVA	modified vaccinia Ankara virus
MyD88	myeloid differentiation primary response gene 88
NACHT	NAIP, CIITA, HET-E, and TP-1
NAIP	NLR family apoptosis inhibitory protein
NF-κB	nuclear factor kappa-light-chain-enhancer of activated B cells
NK	natural killer
NLR	NOD-like receptor
NLRC4	NLR family CARD domain containing 4
NLRP	nucleotide-binding oligomerization domain, Leucine rich Repeat and Pyrin domain containing
NOD	nucleotide oligomerization domain
NT	N-terminal
PAMP	pathogen-associated molecular pattern

PGE2	prostaglandin E2
poly(dA:dT)	poly(deoxyadenylic-deoxythymidylic) acid sodium salt
poly(I:C)	polyinosinic-polycytidylic acid
PRR	pattern recognition receptor
PYD	pyrin domain
RIG-I	retinoic acid-inducible gene I
RLR	RIG-I-like receptor
RNA	ribonucleic acid
RSR	ribotoxic stress response
SAPK	stress activated protein kinase
SARS-CoV-2	severe acute respiratory syndrome coronavirus 2
SFV	Semliki Forest virus
STING	stimulator of interferon genes
T3SS	type 3 secretion system
TCR	T cell receptor
TGN	*trans*-Golgi network
Th cell	T helper cell
TIR	Toll/Interleukin-1 (domain)
TLR	toll-like receptors
TNFα	tumor necrosis factor α
TRAF3	TNF receptor-associated factor 3
TRIF	TIR domain-containing adaptor protein inducing interferon beta
TRX1	thioredoxin-1
UVB	ultraviolet B
VACV	vaccinia virus
VARV	variola virus
VbP	Val-boroPro
vhs	virion host shutoff
VZV	varicella zoster virus
WT	wild type
ZAK	sterile alpha motif and leucine zipper containing kinase AZK

9. Gene sequences

9.1 NLS-BFP

Sequence of NLS-BFP from pcDNA3.1_NFL-BFP with NLS and BFP sequences color-coded.

NLS

TagBFP

ATGCCAGCAGCGAAGAAAAAGAAGCTGGATAGCGAGCTGATTAAGGAGAACATGCACATGA
AGCTCTATATGGAGGGCACCGTGGACAACCATCACTTCAAGTGCACATCCGAGGGCGAAGGC
AAGCCCTACGAGGGCACCCAGACCATGAGAATCAAGGTGGTCGAGGGCGGCCCTCTCCCCTT
CGCCTTCGACATCCTGGCTACTAGCTTCCTCTACGGCAGCAAGACCTTCATCAACCACACCCAG
GGCATCCCCGACTTCTTCAAGCAGTCCTTCCCTGAGGGCTTCACATGGGAGAGAGTCACCACA
TACGAAGACGGGGGCGTGCTGACCGCTACCCAGGACACCAGCCTCCAGGACGGCTGCCTCAT
CTACAACGTCAAGATCAGAGGGGTGAACTTCACATCCAACGGCCCTGTGATGCAGAAGAAAA
CACTCGGCTGGGAGGCCTTCACCGAGACGCTGTACCCCGCTGACGGCGGCCTGGAAGGCAG
AAACGACATGGCCCTGAAGCTCGTGGGCGGGAGCCATCTGATCGCAAACATCAAGACCACAT
ATAGATCCAAGAAACCCGCTAAGAACCTCAAGATGCCTGGCGTCTACTATGTGGACTACAGA
CTGGAAAGAATCAAGGAGGCCAACAACGAGACCTACGTCGAGCAGCACGAGGTGGCAGTGG
CCAGATACTGCGACCTCCCTAGCAAACTGGGGCACAAACTTAATTGA

9.2 hsNLRP1(PYD-DR)-mNeon

Sequence of hsNLRP1(PYD-DR)-mNeon from pFUGW_hsNLRP1(PYD-DR)-mNeon_Blast with hsNLRP1 and mNeon sequences color-coded.

hsNLRP1

mNeonGreen

ATGGCTGGCGGAGCCTGGGGCCGCCTGGCCTGTTACTTGGAGTTCCTGAAGAAGGAGGAGC
TGAAGGAGTTCCAGCTTCTGCTCGCCAATAAAGCGCACTCCAGGAGCTCTTCCGGTGAGACA
CCCGCTCAGCCAGAGAAGACGAGTGGCATGGAGGTGGCCTCGTACCTGGTGGCTCAGTATG

GGGAGCAGCGGGCCTGGGACCTAGCCCTCCATACCTGGGAGCAGATGGGGCTGAGGTCACT
GTGCGCCCAAGCCCAGGAAGGGGCAGGCCACTCTCCCTCATTCCCCTACAGCCCAAGTGAAC
CCCACCTGGGGTCTCCCAGCCAACCCACCTCCACCGCAGTGCTAATGCCCTGGATCCATGAAT
TGCCGGCGGGGTGCACCCAGGGCTCAGAGAGAAGGGTTTTGAGACAGCTGCCTGACACATC
TGGACGCCGCTGGAGAGAAATCTCTGCCTCACTCCTCTACCAAGCTCTTCCAAGCTCCCCAGA
CCATGAGTCTCCAAGCCAGGAGTCACCCAACGCCCCCACATCCACAGCAGTGCTGGGGAGCT
GGGGATCCCCACCTCAGCCCAGCCTAGCACCCAGAGAGCAGGAGGCTCCTGGGACCCAATG
GCCTCTGGATGAAACGTCAGGAATTTACTACACAGAAATCAGAGAAAGAGAGAGAGAGAAA
TCAGAGAAAGGCAGGCCCCCATGGGCAGCGGTGGTAGGAACGCCCCCACAGGCGCACACCA
GCCTACAGCCCCACCACCACCCAGTGAGCAAGGGCGAGGAGGATAACGCCTCTCTCCCAGCG
ACACATGAGTTACACATCTTTGGCTCCATCAACGGTGTGGACTTTGACATGGTGGGTCAGGGC
ACCGGCAATCCAAATGATGGTTATGAGGAGTTAAACCTGAAGTCCACCAAGGGTGACCTCCA
GTTCTCCCCCTGGATTCTGGTCCCTCATATCGGGTATGGCTTCCATCAGTACCTGCCCTACCCT
GACGGGATGTCGCCTTTCCAGGCCGCCATGGTAGATGGCTCCGGATACCAAGTCCATCGCAC
AATGCAGTTTGAAGATGGTGCCTCCCTTACTGTTAACTACCGCTACACCTACGAGGGAAGCCA
CATCAAAGGAGAGGCCCAGGTGAAGGGGACTGGTTTCCCTGCTGACGGTCCTGTGATGACCA
ACTCGCTGACCGCTGCGGACTGGTGCAGGTCGAAGAAGACTTACCCCAACGACAAAACCATC
ATCAGTACCTTTAAGTGGAGTTACACCACTGGAAATGGCAAGCGCTACCGGAGCACTGCGCG
GACCACCTACACCTTTGCCAAGCCAATGGCGGCTAACTATCTGAAGAACCAGCCGATGTACGT
GTTCCGTAAGACGGAGCTCAAGCACTCCAAGACCGAGCTCAACTTCAAGGAGTGGCAAAAGG
CCTTTACCGATGTGATGGGCATGGACGAGCTGTACAAGTGA

9.3 FLAG-mScarlet

Sequence of mScarlet with an N-terminal FLAG tag from pLI_FLAG-mScarlet_Blast with FLAG, linker, and mScarlet sequences color-coded.

FLAG

Linker

mScarlet

ATGGCGGACTACAAGGATGATGATGATAAGGGTGGGGGGAGTGTGTCAAAAGGCGAGGCC
GTGATCAAAGAGTTCATGCGGTTCAAGGTGCACATGGAAGGCAGCATGAACGGCCACGAGT
TTGAGATCGAAGGCGAAGGCGAGGGCAGACCTTATGAGGGAACACAGACCGCCAAGCTGAA

AGTGACCAAAGGCGGACCCCTGCCTTTCAGCTGGGACATTCTGAGCCCTCAGTTTATGTACGG
CAGCCGGGCCTTCACAAAGCACCCTGCCGATATTCCCGACTACTACAAGCAGAGCTTCCCCGA
GGGCTTCAAGTGGGAGAGAGTGATGAACTTCGAGGACGGCGGAGCCGTGACCGTGACACA
GGATACAAGCCTGGAAGATGGCACCCTGATCTACAAAGTGAAGCTGCGGGGCACCAACTTTC
CACCTGATGGCCCCGTGATGCAGAAAAAGACCATGGGCTGGGAAGCCAGCACCGAGAGACT
GTATCCTGAGGACGGGGTCCTGAAGGGCGACATCAAAATGGCCCTGCGGCTGAAAGACGGC
GGCAGATACCTGGCCGATTTCAAGACCACCTACAAGGCCAAGAAACCCGTGCAGATGCCTGG
CGCCTACAACGTGGACAGAAAGCTGGACATCACCAGCCACAACGAGGACTACACCGTGGTG
GAACAGTACGAGCGGAGCGAAGGCAGACACTCTACAGGCGGAATGGACGAGCTGTACAAAT
GA

9.4 FLAG-VACV-F1L-codopt

Sequence of codon-optimized F1L with an N-terminal FLAG tag from pLI_FLAG-VACV-F1L_Blast with FLAG, linker, and F1L sequences color-coded.

FLAG

Linker

VACV-F1L

ATGGATTACAAGGACGACGATGACAAGGGCGGCGGCAGCATGCTGTCAATGTTCATGTGCA
ATAACATTGTTGATTATGTTGACGACATTGACAACGGTATAGTGCAAGATATCGAGGACGAA
GCATCAAACAATGTGGATCATGACTATGTGTATCCGTTGCCCGAAAATATGGTTTACCGCTTC
GATAAGAGCACCAATATCCTCGACTATTTGTCCACGGAGAGAGACCACGTAATGATGGCAGT
CCGGTATTATATGTCCAAACAACGACTTGATGATTTGTATCGACAACTTCCAACAAAGACTCG
AAGCTACATTGATATTATCAACATTTACTGCGATAAAGTGTCCAACGACTATAACCGGGATAT
GAATATCATGTACGATATGGCATCTACAAAGTCTTTCACAGTCTACGACATCAATAATGAGGT
GAATACTATCTTGATGGACAACAAAGGGCTGGGTGTAAGGCTCGCCACGATAAGTTTTATTA
CCGAACTTGGCCGACGGTGTATGAACCCAGTCAAAACCATCAAAATGTTTACTCTTCTTTCCCA
TACGATCTGCGACGACTGCTTCGTCGATTACATAACGGACATCAGTCCGCCAGACAACACAAT
CCCGAATACCAGTACCAGGGAATACCTTAAACTGATTGGAATAACTGCAATAATGTTTGCGAC
GTACAAGACCCTGAAGTATATGATAGGTTAA

10. Acknowledgments

‘What is life, after all if not dancing on graves?’
Olga Tokarczuk, *The Books of Jacob*

Thank you to my parents for their support and to my friend Lukasz for his enthusiasm and conversation.

I want to thank Prof. Veit Hornung for the opportunity to do my PhD in his group and all the lab members for their suggestions, support, and technical help.

I want to thank my collaborators: Prof. Gerd Sutter and Dr Alina Tscherne for MVA viruses, Prof. Lars Dölken and Prof. Andreas Pichlmair for HSV-1, Prof. Jan Rehwinkel and Prof. David Koelle for sharing the HSV-1 ORF library, Stefan for sharing all the protocols, plasmids, knock-out and transgenic cells, Moritz for sharing the ICP0 plasmid.